Fault Detection and Isolation for Lateral Control of an Autonomous Vehicle

A Model Based Approach

C.J. van der Ploeg

Master of Science Thesis

TU Delft Delft University of Technology

Delft Center for Systems and Control

Fault Detection and Isolation for Lateral Control of an Autonomous Vehicle

A Model Based Approach

Master of Science Thesis

For the degree of Master of Science in Systems and Control at Delft University of Technology

C.J. van der Ploeg

November 21, 2018

Faculty of Mechanical, Maritime and Materials Engineering (3mE) · Delft University of Technology

The work in this thesis was supported by TNO Automotive, department Integrated Vehicle Safety. Their cooperation is hereby gratefully acknowledged.

Delft University of Technology
Department of
Delft Center for Systems and Control (dcsc)

The undersigned hereby certify that they have read and recommend to the Faculty of Mechanical, Maritime and Materials Engineering (3mE) for acceptance a thesis entitled

Fault Detection and Isolation for Lateral Control of an Autonomous Vehicle

by

C.J. van der Ploeg

in partial fulfillment of the requirements for the degree of

Master of Science Systems and Control

Dated: November 21, 2018

Supervisor(s):

prof.dr.ir. N. van de Wouw

dr. M. Alirezaei

dr. P. Mohajerin Esfahani

Reader(s):

dr. ir. R. Happee

Abstract

Over the past years, the automotive industry has seen a constantly increasing level of automation of automotive vehicles. This increasing level of automation contributes to an increasing safety in traffic and a reduction of traffic congestions due tio faster response times and higher reliability, with respect to the human driver. The automation of a vehicle over the longitudinal and lateral degree of freedom requires additional safety measures to ensure safety of the passengers during automated maneuvers. In a lateral control scenario, the fault detection and isolation of faults occuring in the steering system belongs to these set of safety measures. By detecting and isolating faults of interest in this system, a decision process follows which will, for example, either compensate for the acting fault or bring the vehicle to a safe standstil in the case that the fault surpasses a non-acceptable threshold.

This work presents a set of novel methods for fault detection and isolation for a generalized set of linear time-invariant and parameter-varying systems. The faults under investigation comprise of an additive fault acting as an offset on the system and a multiplicative fault acting non-linearly on a set of known signals. Furthermore, the system is subjected to exogenous disturbances. The first challenge imposed is the lack of isolability of the additive and multiplicative fault using conventional linear estimation techniques. The second challenge imposed is the design of a fault detection mechanism for linear parameter-varying systems subject to exogenous faults and disturbances.

The first contribution of this research is a moving least-squares based approach as an extension to an existing nullspace computation based parity-space fault detection filter. This novel combination allows a decoupled estimation of the additive and multiplicative fault. The second contribution is an extension to the first contribution by attacking one of the largest sources of error: the dynamical content of the parity-space filter. The estimation performance of the combined fault detection and isolation filter of both contributions is provided with a guaranteed performance bound, providing not only an intuitive tool to push down the estimation error, but also shows possible trajectories for future work. The third and final theoretical contribution is the adaption of the linear time-invariant parity space method for a linear parameter-varying environment. A convex quadratic optimization problem is used

which has an exact analytical solution for approximately rejecting the parameter-varying effects of the system.

A contribution of the more practical aspect of this thesis, is a demonstration of the applicability of the developed framework on real-life problems, both in a simulation setting and an experimental setting. The theoretical framework has been applied in a practical case study in fault detection and isolation for lateral control of autonomous vehicles. After having proven out the theoretical framework in a linearized simulation environment, a systematic approach is given for applying the developed theoretical tools in an experimental setting on an autonomous vehicle. The experimental results confirm the theorems, showing that the faults can be detected and isolated both in theory and in practice.

Glossary

List of Acronyms

ADAS	Advanced Driver Assistance Systems
CACC	Cooperative Adaptive Cruise Control
CAN	Controller Area Network
DAE	Differential-Algebraic Equation
EPS	Electrical Power Steering
FD	Fault Detection
FDI	Fault Detection and Isolation
FI	Fault Isolation
HMI	Human Machine Interface
LP	Linear Programming
LPV	Linear Parameter-Varying
LTI	Linear Time-Invariant
MPC	Model Predictive Control
QP	Quadratic Programming
RCP	Rapid Control Prototyping
RHS	Right-hand side
SAE	Society of Automotive Engineers
SDP	Semidefinite Programming
VAF	Variance Accounted For

Contents

List of Figures

Acknowledgements

This report represents not only the work I have done during the past nine months, it represents a summary of all the knowledge and motivation gained during my university degree. It has been the most colourful experience I could have wished for.

First of all, I would like to thank my daily supervisors, Peyman Mohajerin Esfahani and Mohsen Alirezaei. Peyman, thank you for allowing me to storm into your office for eternally lasting intellectual discussions, even at the most inconvenient times. Mohsen, thank you for the down-to-earth and practically insightful discussions at the university, at TNO and in the train from Eindhoven to Delft. I would also like to thank my supervising professor Nathan van de Wouw for his critical and helpful attitude towards my work and his advice on facing theoretical problems in a more systematic approach.

A special thank you goes to TNO department Integrated Vehicle Safety for allowing me to graduate under their wings. Thanks to you, the valuable theorems and simulations have been filled up with experimental results, showing that the contributions not only have a value in theory but also in practice.

I would like to thank my family for their support throughout my university degrees, I am forever grateful for you allowing me to always take the path I was most passionate about. Furthermore, I wouldn't have ended on this level of motivation if it wasn't for all my friends from Systems and Control and Formula Student Team Delft. You have set the bar for me and hopefully I have, and will be able to return this favor to you.

Finally I want to thank my girlfriend Manon for her ever-lasting support and love throughout my university degree, no matter which path, activity or even country I decided to shift my focus on.

Delft, University of Technology — C.J. van der Ploeg
November 21, 2018

"Either I will find a way, or I will make one."
— *Philip Sidney*

Chapter 1

Introduction

Over the past century the road network has seen a constantly increasing number of automotive vehicles. The growth rate of the number of vehicles, together with a decreasing space to expand the road network results in many societal problems. Belonging to these problems is the vastly increasing vehicle count together with a limited road capacity which as a result increases the fuel consumption, traffic congestions, but above all the safety risks [1].

Following these observations, the focus is shifted towards the biggest uncertainty in road safety and vehicle emissions: the human driver in charge of controlling the vehicle to its destination. Cognitive and physical limitations of the human being have been a motivating factor to increase automation in human transport [2]. Slow response times and signs of fatigue have resulted in over 25 thousand traffic related fatalities in the European Union in 2017 alone [3]. These numbers motivate the need of action towards a safer and more efficient road network.

Advanced Driver Assistance Systems (ADAS) have been developed to aid the driver in safely controlling the vehicle. Recent developments of these ADAS systems show a constantly increasing level of automation. This increasing level of automation in ADAS systems is motivated by a potential increase in traffic safety and reduction of fuel consumption. For example, a main motivating factor for the use of Cooperative Adaptive Cruise Control (CACC) was given to be the reduction of traffic related accidents, traffic congestions and thus as a result fuel consumption [4]. The next step towards a more efficient and safer road network is the progression towards fully autonomous capabilities of personal and commercial vehicles, a progression which is well captured in Figure 1-1.

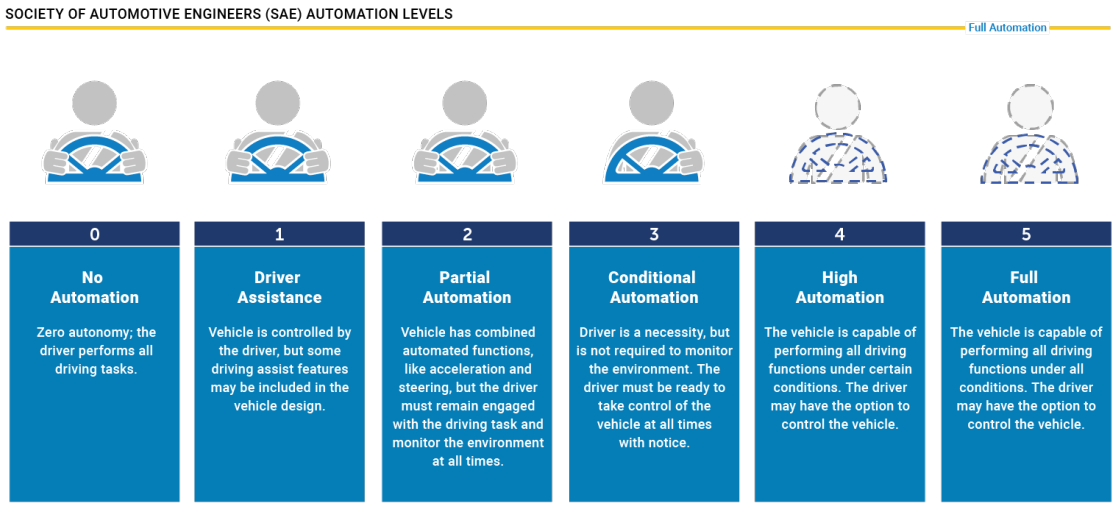

Figure 1-1: SAE Vehicle automation taxonomy, adopted from [5].

The Society of Automotive Engineers (SAE) has defined a taxonomy for levels of automation [6] (see Figure 1-1). The levels in this taxonomy range from level 0 (no driving automation) to level 5 (full driving automation). From level 3 onwards, the attention of the human driver is no longer required, unless requested by the vehicle. For the levels 0, 1 and 2, the driver is always in control of the vehicle. Automation level 3 and onward impose challenging conditions. For these levels, the human driver is no longer expected to monitor the environment, which introduces higher demands on the safety logic of the vehicles controllers.

Undesired behavior caused by faulty system components is usually easily detected by the human driver. The driver is usually aware of abnormal behavior of the vehicle and ensures that either the vehicle is controlled to a safe stop, or the abnormal behavior is mitigated by alternative control action. However, in an automation level where no human assistance is required unless requested, the vehicle's controller has to detect this fault or abnormal behavior and as a result, act accordingly. What follows is a decision making process which, based on the severity of the fault, results in either a compensation in control action or an activation of a limp home mode to bring the car to a standstill into a safe scenario.

1-1 Fault detection in lateral control

This research specifically focusses on a case study on the lateral control of an autonomous vehicle for highway lane-keeping and vehicle-following. The area of lateral control is a thoroughly studied domain. Automated lateral control of the vehicle provides, together with the earlier mentioned CACC-controllers, a unifying controller combination for fully automated vehicle platoons. The goal of the lateral controller is to steer the vehicle to the center of the reference-trajectory. This reference trajectory is generated either by the lane-marking for lane-keeping or for example by the trajectory of the ego-vehicle for vehicle-following controllers. The main control actuator for the lateral controller is the steering actuator, which must

ensure that the lateral position and heading of the vehicle corresponds to the generated trajectory. More often than not, the action for controlling the vehicle to the desired trajectory is calculated by using a-priori knowledge of the lateral dynamics of the vehicle [7, 8], combined with a set of measurements capturing the dynamical behavior of the vehicle and its relative position with respect to the desired trajectory.

The use of model-based lateral control methods is often compromised once faults are acting in the system. Often, the model-knowledge does not take into account behavior of the system in faulty scenarios. In these scenarios, faults acting on the system can cause a deviation of the system model behaviour from reality. As a result of this model-mismatch, the lateral controller could cause a deviation from the desired trajectory or in the worst case cause unstable behavior of the vehicle [9]. In light of the before mentioned SAE automation levels [6], it is also important to be aware of the faults as to be able to compensate for them; excessive faults could require additional action such as a request for driver take-over or a switch to a limp home mode to bring the car to a safe standstill.

In this research, a distinction is made between two types of faults occuring from the steering input of the lateral controller to the actual lateral behavior of the vehicle. Both of these faults have represent a different physical effect and require different actions from the decision making process when such a fault occurs. The first fault is considered to be an offset of the true steering angle δ with respect to the steering-angle setpoint δ_{set}. This fault can present itself as being an offset in the mechanical rack and pinion of the steering system, an angular offset of the steering sensor with respect to the steering axle or for example an angular misalignment of the wheels with respect to the steering system. This fault can simply be modeled as a constant offset f_a with respect to the steering angle setpoint δ_{set} from the lateral controller:

$$\delta = \delta_{set} + f_a. \tag{1.1}$$

The second fault considered is a proportional gain f_m on the steering angle setpoint δ_{set} from the lateral controller. In a faultless scenario, the value of this proportional gain is equal to one as it results in a direct throughput of the steering angle setpoint to the vehicle. An increase or decrease of this fault can be caused by for example a compliance in the steering system excited by the lateral force and yaw moment, or a change in tyre pressure resulting in a higher or respectively lower cornering stiffness. This fault can be modeled with respect to the steering input δ_{set} and true steering angle δ as

$$\delta = f_m \delta_{set}. \tag{1.2}$$

The two before mentioned faults f_a (1.1) and f_m (1.2) result in the total input-output fault model which has been adopted more often in literature [10], and is given as

$$\delta = f_m \delta_{set} + f_a. \tag{1.3}$$

The main challenge imposed by this fault model is as follows: the transfer function from $f_m \delta_{set}$ to the system outputs is identical to the transfer function from f_a to the system outputs, leading to a case of input unobservabillity. This challenge is formalized in a more general setting in Chapter 2 and will be taken into consideration as a requirement in the following section. In the following section, the concept of fault detection and isolation is introduced combined with the current state-of-the-art of model-based methods.

1-2 Fault detection and isolation, a brief overview

Generally, the function of fault diagnosis in control applications is to be aware of an undesirable fault acting on the system. The main concept of detectability is shown in Figure 1-2.

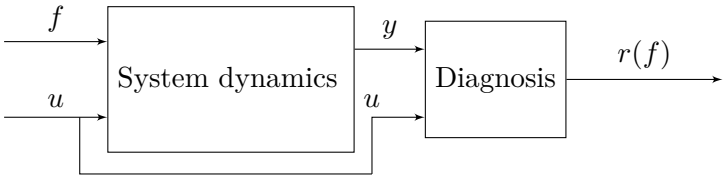

Figure 1-2: A schematical representation for fault detection.

When a system is affected by an unknown fault, f, it is the purpose of fault detection to find a mapping from the fault to a diagnosis signal, $r(f)$, by use of the known inputs (u) and outputs (y). This signal, $r(f)$, is called the residual. For fault detection, the demands on the residual are simple: if no fault is present, r should be equal to zero and if a fault is present the residual r should be non-zero.

The notion of isolation is an extension to the definition of detection. It might be of interest to detect a specific fault while rejecting other faults or disturbances that are not of interest. Figure 1-3 depicts the intuition behind fault isolation, where f_1 and f_2 represent specific fault signals of interest and d represents the unkown disturbances. The purpose of fault detection and isolaton in this case is to decouple or isolate the detection of the faults. It is to provide a signal $r(f_1)$, which is only dependent on a non-zero f_1, and a signal $r(f_2)$, which is only dependent on the faulty behavior f_2. As a result, both residuals are decoupled from other faults and/or disturbances d.

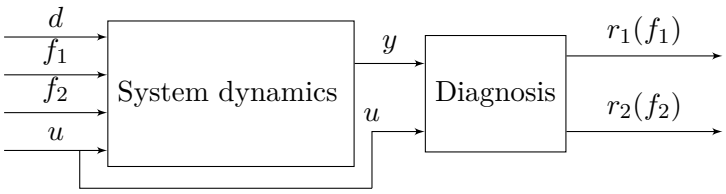

Figure 1-3: A schematical representation for fault isolation.

Isermann [11, 12] describes the current state-of-the-art in the area of fault diagnosis. A distinction can be made between methods that use knowledge about the system and its processes, or more heuristic methods such as statistical classification or fuzzy logic. This thesis project is focussed on the domain of model-based fault diagnosis methods as model knowledge is assumed to be available, resulting in more reliable estimates. Referring back to Figure 1-2 and Figure 1-3, the diagnosis block therefore consists of a model-based diagnosis method. Generally three different linear approaches in fault diagnosis exist: observer-based methods, parameter-estimation methods and parity-space methods. After discussing these three main pillars, other methods will be discussed which are formed by a combination of the before mentioned methods.

The main concept of linear observer-based methods is to apply classical observer theory on a known model. An estimation error between the outputs of the real plant and the outputs of the observer provides a residual from which the magnitude of model mismatch can be determined. This model mismatch can consecutively be linked to the presence of a fault. In the case of a single fault acting on the system and having exact knowledge of the mathematical model of the system, this can yield good results. Although in the case of several unknown inputs acting on the system, i.e., disturbances, the problem itself becomes difficult to solve. In this work, we do not assume to have knowledge on the dynamical behavior of the disturbance signals and therefore we can not assume that the disturbance acting on our vehicles have a low frequency content. Due to this assumption, linear observer techniques that enable fault compensation by an augmented state observer, such as [13], can not be applied. Using this method would increase the chance of false alarms, due to inaccurate disturbance estimation. In [14, 15], methods are described to minimize the effect of the disturbance on the fault residual in a linear observer by posing it as a Semidefinite Programming (SDP) optimization problem. However, perfect decoupling is not guaranteed and additionally it requires a trade-off between fault sensitivity and disturbance sensitivity. Beard [16] describes a method where a full-order observer employs a directional gain to tune the sensitivity for a specific fault of interest, given that the faults of interest are isolable, although a clear systematic approach is missing.

A different method for fault detection and isolation is parameter estimation. Parameter estimation methods employ a type of system identification to identify the system parameters of the system under consideration. A deviation in these system parameters can lead to the conclusion of a faulty system as emphasized in [12]. The estimated parameters can either represent physical parameters or parameters of a different realization. As opposed to the observer and parity-space methods, a parameter estimation method can easily detect the non-linearly acting multiplicative parameter and the linearly acting additive parameter, given conditions on the persistency of excitation. An example of fault detection demonstrating the recursive tracking of a fault parameter, is given by [17]. A large downside of these parameter estimation techniques has been highlighted in [18] and [19]: the parameter estimation algorithm is weakly robust for external disturbances. Parameter estimation techniques rely on the availability of measurable inputs and outputs. Therefore, additonal methods have to be applied to allow disturbance decoupling.

In [20], a parity-space solution is decribed which fully decouples the unmeasured disturbances from the fault residuals using an algebraic null-space approach (provided the necessary and sufficient conditions are fulfilled). This approach ensures, given the detectability and isolability conditions and full knowledge on the dynamic appearance of the disturbances, that the disturbances can be fully decoupled from the fault residual using efficient computation techniques. This method does not allow direct application for our requirements as it assumed that the faults are observable, which is an assumption that does not hold for our fault model (see Section 2-3 for a more detailled description of this challenge). In [21], an extension to this method is provided and two relevant contributions are emphasized. Furthermore, the linear disturbance decoupling problem can be posed as a numerically efficient convex optimization problem, but next to that the filter can be trained to reject the undesirable effect of non-linearities in the system (requiring training the filter for a finite set of non-linear disturbances). A different extension from [20] is given by [22], in which a feasible extension for Linear

Parameter-Varying (LPV) systems is given for the detection of additive faults or multiplicative faults modelled as additive faults. However, it imposes a high computational complexity due to the non-convex optimization problem. Similar as in the observer techniques, a variant of detectability is assumed in [23]. This is not applicable given our background information, since the faults are inseperable due to a lack of observability (see Section 2-3 for a more detailled description of this challenge), hence we can only detect the presence of a fault and not necessarily isolate the presence of a specific fault.

An extension for the detection and isolation of multiplicative and additive faults is given by [24], where a class of continuous- and discrete-time adaptive observers is introduced. These techniques are formed as a combination of the linear observer techniques combined with parameter estimation methods. Parameter estimation methods provide an online estimation of uncertain dynamical parameters and subsequently these estimated parameters are used to estimate the state or unknown input. An adaptive observer is applied in [25], showing that the multiplicative fault can be modelled in the unknown state input matrix and the additive fault as an exogenous signal. The same shortcoming of the regular linear observer applies to these methods. It is difficult to decouple unmeasurable disturbances, hence resulting in poor performance of the parameter estimation method due to acting disturbances. Although good results can be obtained using this method, the absense of a systematic design method makes its use cumbersome.

The state of the art of the case study, fault detection in lateral control of autonomous vehicles, is composed from methods discussed in this section. The method proposed in [26] find its closest similarity to the problem description in this thesis. A similar fault model is used and an adaptive observer (i.e., a Luenberger with parameter estimation) is used to estimate the additive and multiplicative faults. However, the rejection of disturbances has not systematically been taken into account, residual evaluation using thresholds is proposed to increase robustness of the method for unmeasured disturbances. Other works are primarily focussed on estimation of the steering offset or the additive fault. The work of [27] employs a Luenberger observer with a gain that maximizes robustness against model uncertainties, such as the varying longitudinal velocity, though its purpose is only to estimate the additive fault and the presence of a multiplicative fault is neglected. The methods in [28, 29] employ a sliding mode observer to increase robustness for unknown disturbances, while estimating multiplicative and additive faults, where the multiplicative faults appear in the state dynamics. The method however does not allow for estimation of an additive and multiplicative fault acting on the same signal.

1-3 Research goal and contributions

The objective of this thesis research is to develop a method for fault detection and isolation of faults occuring in the steering system of an autonomous vehicle. The main research goals posed by this problem are twofold. The first goal is the development of a fault detection mechanism for a fault in the system, demanding the rejection of modeled disturbances and the detection of the fault for a linear time-invariant and parameter-varying system model.

The second research goal is the development of a method which can split the residual from the detection mechanism into the two specific (slowly time-varying) faults of interest. The combination of the two goals provide a total goal to detect and isolate the two faults of interest for both linear time-invariant and parameter-varying systems. Following the goals, the contributions of this thesis work are listed below:

- A methodology for a non-linear isolation filter is proposed which can isolate the additive and the multiplicative fault from the residual of a fault detection filter. The filter is provided with a guaranteed performance bound which provides a tool to expose the main strengths and weaknesses of the method.
- The main source of error in the non-linear isolation filter is incorporated in the design of the isolation filter using the pre-filter. This extension shows that the dynamical effect of the detection filter can be fully decoupled in a constant fault scenario. Again, a guaranteed performance bound is given, showing the main strengths and weaknesses of the extension in certain conditions.
- A tractable synthesis approach for a parameter-varying fault detection mechanism is proposed. Given that the parameter-variations are measurable, the outcome is a detection filter which can decouple the parameter-varying effect of the model from the detection residual.
- The theoretical framework of the developed fault detection and isolation methods is applied on a case study in the lateral control of autonomous vehicles. The case study shows the applicability and the systematic approach of applying the methods on the single-track lateral model.
- The theoretical framework is applied in an experimental setting: a real autonomous vehicle in a lane-keeping maneuver. Application of the methods in a real-life setting shows the effectiveness and robustness of the provided methods, not only in simulation, but also in reality.

1-4 Notation

Before introducing the outline of the thesis, a few notational definitions are introduced that will be used throughout the theoretical framework of this research.

Notation. The symbols $\mathbb{Z}$ and $\mathbb{R}$ represent the set of integers and real numbers and the symbols $\mathbb{Z}_+$ and $\mathbb{R}_+$ represent the set of non-negative integers and real numbers, respectively. The operators $\mu_n[x](k) \in \mathbb{R}$, $\sigma_n^2[x](k) \in \mathbb{R}_+$, $V_n[x](k) \in \mathbb{R}_+$ represent the first moment $\mu_n[x](k) \coloneqq \frac{1}{n}\sum_{i=0}^{n-1} x(k-i)$, the second moment $\sigma_n^2[x](k) \coloneqq \frac{1}{n}\sum_{i=0}^{n-1} x^2(k-i)$ and finally the variance $V_n[x](k) \coloneqq \sigma_n^2[x](k) - \mu_n^2[x](k)$ of the signal $x(\cdot)$. Let a concatenated signal $x(\cdot)$ over n horizon be defined as $x_n(k) \coloneqq \Big[x(k), x(k-1), \ldots, x(k-n+1)\Big]^\intercal$ and can be written in a diagonal matrix using the operator $x_n^{\square}(k) = I_n \cdot (1_n^\intercal \otimes x_n(k))$ where the operation $\otimes$ represents the Kronecker product. The p-norm for signal $x_n(k)$ is defined as $\|x_n(k)\|_p$, this notation can be redefined by a n-restricted vector p-norm for a signal $x(\cdot)$ as $\|x\|_{\mathscr{L}_{np}}(k)$. For $p = 2$ we find the n-restricted Euclidean norm as $\|x\|_{\mathscr{L}_{n2}}(k) \coloneqq \sqrt{\sum_{i=0}^{n-1} |x(k-i)|^2}$ and

the n-restricted ∞-norm (p=∞) is defined as $\|x_n(k)\|_{\mathscr{L}_{n\infty}}(k) \coloneqq \max_{0\leq i\leq n-1}|x(k-i)|$. Let $A \in \mathbb{R}^{n\times m}$ be a matrix with real values, $A^\intercal \in \mathbb{R}^{m\times n}$ be its transpose. let $\|A\|_2 \coloneqq \overline{\sigma}(A) \coloneqq \sqrt{\overline{\lambda}(A^\intercal A)}$ be its induced 2-norm, where $\overline{\sigma}$ represents the largest singular value and $\overline{\lambda}$, $\underline{\lambda}$ represent the maximum and minimum eigenvalue, respectively. The symbol q represents the shift operator, i.e., $q[x(k)] = x(k+1)$.

1-5 Outline of the thesis

The structure of the thesis is outlined as below:

Chapter 2: Problem description and outline of the proposed approach

Chapter 2 introduces a generalized set of models to which the model of the case study belongs. A motivating example illustrates the applicability of the set of models by converting it to a state-space set of equations. Next, the problem statement and challenges of the method for the generalized setting are introduced. Finally, a short outline of the theoretical contributions is discussed as a prequel to Chapter 3.

Chapter 3: Main results

Chapter 3 provides the theoretical framework of the novel methods developed during this thesis. These methods present the non-linear isolation filter and an extension to the non-linear isolation filter with the purpose to improve the estimation results. Finally, an extension to the fault detection method to deal with the linear parameter-varying nature of the system is proposed.

Chapter 4: An Application to the Lateral Control of Autonomous Vehicles

Chapter 4 provides an in-depth analysis of application of the developed theorems to the case study mentioned in the introduction. Furthermore, it is shown that for the linearized system the methods provide desired performance. Subsequently, a sensitivity analysis is performed to show the applicability of the problem in scenarios with a larger parametric uncertainty.

Chapter 5: Experimental results

Chapter 5 provides experimental results for the tests applied on a real autonomous vehicle. The testing methods and location are introduced. Subsequently, an elaborate analysis of the results is given along with a methodology to adapt the methods to real-life scenarios.

Chapter 6: Conclusion, discussion and future work

Finally, Chapter 6 provides a conclusion on how the work of this thesis solves the original problem statement. To conclude, a set of propositions is given for future work that have been shortly explored throughout this thesis, but lie outside of its scope to be fully worked out at this time.

Chapter 2

Problem Description and Outline of the Proposed Approach

In this chapter, a formal description of the generic model class used in this thesis is given. The basic principles of the initial Fault Detection and Isolation (FDI) method are proposed and shortcomings of this method are explained. Subsequently, a motivating example is given showing that the proposed methodology can be applied to a broad spectrum of faulty systems. Finally, the challenges of developing such an FDI method are introduced, followed by an outline of the proposed novel extension of the FDI design method to provide a solution to these challenges.

2-1 Model Description and Problem Statement

In this section, a class of non-linear models is introduced. This class encompasses the systems dynamics throughout this thesis. Consider the following discrete-time non-linear Differential-Algebraic Equation (DAE) model

$$H(q)[x] + L(q)[z] + F(q)[f_a] + F(q)[E(z)f_m] = 0, \tag{2.1}$$

where the functions x, z, f represent discrete-time signals taking values in $\mathbb{R}^{n_x}, \mathbb{R}^{n_z}, \mathbb{R}^{n_f}$, respectively, and $E : \mathbb{R}^{n_z} \to \mathbb{R}^{n_E}$ is a continuous mapping. The matrices $H(q)$, $L(q)$, $F(q)$ are polynomial functions with appropriate dimensions in the variable q, which is viewed as the shift operator, and thus they may be cast as linear operators in the space of discrete-time signals. The function x contains all unknown signals in the DAE system, typically representing the internal states and unknown exogenous disturbances. The function z is composed of all known signals including the control inputs u and the output measurements y. The signal f_a is considered an additive fault, while the signal f_m is considered to be a multiplicative fault or intrusion which interacts non-linearly with the signal $E(z)$.

In absence of the fault signals f_a, f_m, all possible z-trajectories of the system can be characterized as

$$\mathcal{M} \coloneqq \{z : \mathbb{Z} \to \mathbb{R}^{n_z} | \, \exists x : \mathbb{Z} \to \mathbb{R}^{n_x} : \quad H(q)[x] + L(q)[z] = 0\}, \tag{2.2}$$

which is called the behavior of the system. The goal for the fault detection and isolation filter is to design a proper and stable filter whose input is the the known signal z and the respective output, also referred to as the filter residual, is zero for all $z \in \mathcal{M}$. Note that throughout this study we assume that the initial conditions of the system, as well as the FDI filter, is equal to zero. In the absence of zero initial conditions, the above definition of the residual is relaxed to satisfy the condition only once the filter has settled from its initial condition. The second condition for our residual generator is concerned with the fault sensitivity. For any particular fault of interest, f_a or f_m, we require that the transfer function from that particular fault to the residual is non-zero. In previous approaches [21, 20], a residual generator has been designed via the use of a polynomial matrix $N_H(q)$ ensuring that the behavior of the system (2.2), by multiplication of this matrix $N_H(q)$, can be recast as

$$\begin{aligned} \mathcal{M} =& \{z : \mathbb{Z} \to \mathbb{R}^{n_z} | \underbrace{N_H H(q)}_{=0}[x] + N_H(q)L(q)[z] = 0\}, \\ =& \{z : \mathbb{Z} \to \mathbb{R}^{n_z} | N_H(q)L(q)[z] = 0\}, \end{aligned} \tag{2.3}$$

where $N_H(q)$ represents an irreducible polynomial basis for the nullspace of $H(q)$. A linear combination of this basis $N(q) = \gamma(q)N_H(q)$ can be taken such that a Fault Detection (FD)-filter $N(q)L(q)$ can be applied on the known signal z, resulting in the behavior (2.3). This operation creates the following conditions of a filter applied on the DAE model (2.1)

$$N(q)H(q) = 0, \tag{2.4a}$$
$$N(q)F(q) \neq 0. \tag{2.4b}$$

The first condition (2.4a) ensures rejection of the disturbances and the unknown states in the residual r. The second condition (2.4b) ensures a non-zero response when the fault is non-zero.

Assumption 2-1.1 (Detectability)**.** *Following [21] (Fact 4.4), a solution $N(q)$ can be found for* (2.4) *iff*

$$Rank\Big(\begin{bmatrix} H(q) & F(q) \end{bmatrix}\Big) > Rank(H(q)). \tag{2.5}$$

It is assumed throughout the remainder of this research that this condition is fulfilled. Additionally, for the sake of simplicity and to avoid clutter, it is assumed throughout the remainder of this work that $F(q)$ is a polynomial column vector. The latter implies that $n_E, n_{f_a}, n_{f_m} = 1$. Extension of the main results for n_E, n_{f_a}, $n_{f_m} > 1$ can be made, hence the latter assumption is made without loss of generality.

Following Assumption 2-1.1, a proper Linear Time-Invariant (LTI) FD-filter can be designed fulfilling (2.3) and (2.4) by use of the following residual generator:

$$r = d^{-1}(q)N(q)L(q)[z], \tag{2.6}$$

where the stable transfer function $d^{-1}(q)$ is intended to make the residual generator strictly proper and stable. Note, that the LTI transfer function from the faults f_a and f_m, to the residual r, as a result of applying filter (2.6) on (2.1) (which satisfies (2.4)), results in

$$r = \underbrace{-\frac{N(q)F(q)}{d(q)}}_{G(q)}[E(z)f_m + f_a]. \tag{2.7}$$

Using the theorem from [21] (Lemma 4.2), this filter can be found by solving a linear programming feasibility problem. The following lemma provides a framework for finding such a solution.

Lemma 2-1.2. *Under Assumption 2-1.1, let $N(q)$ be a feasible polynomial of degree d_N for the following feasible solution to the set of conditions in* (2.4)

$$d^{-1}(q)N(q)H(q) = 0, \tag{2.8a}$$
$$d^{-1}(1)N(1)F(1) = -1, \tag{2.8b}$$

where the transfer matrices can be decomposed as

$$H(q) \coloneqq \sum_{i=0}^{d_H} H_i q^i, \qquad F(q) \coloneqq \sum_{i=0}^{d_F} F_i q^i,$$
$$N(q) \coloneqq \sum_{i=0}^{d_N} N_i q^i, \qquad d(q) \coloneqq \sum_{i=0}^{d_d} d_i q^i,$$

where d_H, d_F, d_N and d_d represent the maximum degree of matrices $H(q)$, $F(q)$, $N(q)$ and $d(q)$ respectively. Note, that (2.8b) *describes a necessary condition on the DC-gain of the fault mapping* (2.7)*. Let the polynomial matrices $\bar{N}$, $\bar{H}$, $\bar{F}$, $\bar{d}$ be given as*

$$\bar{N} \coloneqq \begin{bmatrix} N_0 & N_1 & \dots & N_{d_N} \end{bmatrix},$$
$$\bar{H} \coloneqq \begin{bmatrix} H_0 & H_1 & \dots & H_{d_H} & 0 & \dots & 0 \\ 0 & H_0 & H_1 & \dots & H_{d_H} & 0 & \vdots \\ \vdots & & \ddots & \ddots & & \ddots & 0 \\ 0 & \dots & 0 & H_0 & H_1 & \dots & H_{d_H} \end{bmatrix},$$
$$\bar{F} \coloneqq \begin{bmatrix} F_0 & F_1 & \dots & F_{d_F} & 0 & \dots & 0 \\ 0 & F_0 & F_1 & \dots & F_{d_F} & 0 & \vdots \\ \vdots & & \ddots & \ddots & & \ddots & 0 \\ 0 & \dots & 0 & F_0 & F_1 & \dots & F_{d_F} \end{bmatrix},$$
$$\bar{d} \coloneqq \begin{bmatrix} d_0 & d_1 & \dots & d_{N_d} \end{bmatrix}.$$

Using the above definitions, the conditions (2.8) *for a feasible stable LTI FD-filter $\frac{N(q)L(q)}{d(q)}$ can be recast as a linear programming feasibility problem*

$$\begin{cases} \bar{N}\bar{H} = & 0, \\ \frac{\sum \bar{N}\bar{F}}{\sum \bar{d}} = & -1. \end{cases} \tag{2.9}$$

Note, that this programming problem selects a feasible solution of the problem proposed in [21] (Lemma 4.2). The proof is omitted as it is a straight forward adaption from that article.

2-2 Motivating Example

A motivating example can be given to show the generality of the used DAE framework. Consider the following set of non-linear ordinary difference equations:

$$GX(k+1) = AX(k) + B_u u(k) + B_d d(k) + B_f \left(f_a(k) + E_X(B_X X(k), u(k)) f_m(k)\right), \quad (2.10a)$$
$$Y(k) = CX(k) + D_u u(k) + D_d d(k) + D_f \left(f_a(k) + E_Y(B_Y X(k), u(k)) f_m(k)\right), \quad (2.10b)$$

where u is the input signal, d the unknown exogenous disturbance, X the internal state of the system, Y the measurable output, f_a the additive acting set of faults or intrusions and finally f_m the set of faults acting as a multiplication on a non-linear combination of the internal states and input. The matrices G, A, B_d, B_{f_a}, B_{f_m}, B_X, C, D_u, D_d, D_{f_a}, D_{f_m} are constant matrices. Furthermore, we assume that there exist matrices K_X, K_Y such that

$$\begin{aligned} B_X &= K_X C, & B_Y &= K_Y C, & & \\ K_X D_u &= 0, & K_X D_d &= 0, & K_X D_f &= 0, \\ K_Y D_u &= 0, & K_Y D_d &= 0, & K_Y D_f &= 0, \end{aligned}$$

meaning that the internal system states acting non-linearly with the fault are a selection of the entries of the measurable output Y. Finally, the functions E_X, E_Y are non-linear mappings as a function of the known signals. One can inspect that the above set of non-linear difference equations (2.10) can easily be transformed into the non-linear DAE framework (2.1) as

$$x \coloneqq \begin{bmatrix} X \\ d \end{bmatrix}, \qquad z \coloneqq \begin{bmatrix} Y \\ u \end{bmatrix}, \qquad E(z) \coloneqq \begin{bmatrix} E_X(K_X(Y - D_u u), u) \\ E_Y(K_Y(Y - D_u u), u) \end{bmatrix},$$
$$H(q) \coloneqq \begin{bmatrix} -qG + A & B_d \\ C & D_d \end{bmatrix}, \quad L(q) \coloneqq \begin{bmatrix} 0 & B_u \\ -I & D_u \end{bmatrix}, \quad F(q) \coloneqq \begin{bmatrix} B_f \\ D_f \end{bmatrix},$$

and thus, according to the previous subsection, a FDI filter can be designed which can detect present faults in the system.

2-3 Challenges

Recalling the specific DAE framework with a multiplicative and additive faults occurring (2.1), it might be of interest to isolate the impact of one fault. Specifically it might be of interest to isolate the effect of an additive fault from the effect of a multiplicative fault and vice versa. The conditions for isolability follow directly from the condition of detectability (2.5) using the new augmented matrix $\widetilde{H}(q) = \begin{bmatrix} H(q) & F(q) \end{bmatrix}$, where we assume that $\text{Rank}(\tilde{H}(q)) > \text{Rank}(H(q))$. Additionally we assume that the fault has a non-zero relative degree to the measurable output. A sufficient and necessary condition for a linear time-invariant FDI filter. detecting and isolating the additive fault from the multiplicative fault, and vice versa, is stated as:

$$\text{Rank}\left(\begin{bmatrix} \widetilde{H}(q) & F(q) \end{bmatrix}\right) > \text{Rank}(\widetilde{H}(q)).$$

Note that this condition can not be fulfilled, since the matrix $F(q)$ is already contained in the column space of $\widetilde{H}(q)$, meaning that the multiplicative and additive fault are dynamically

inseparable using this methodology. Separation of the two signals requires information of the dynamic difference of the faults over a given past time-span. This research outlines a novel extension of the proposed fault detection mechanism to detect and isolate the linearly dependent additive and multiplicative fault using an augmented moving-horizon least-squares filter.

2-4 Outline of the Proposed Methodology

In a discrete time environment and in the challenging conditions of the previous subsection, the challenge of the research is the decoupling of the addive fault fault f_a and multiplicative fault f_m assuming that their dynamics are linearly dependent. The first proposed theorem in this research can be visualized by the Fault Isolation (FI)-filter in the control diagram in Figure 2-1.

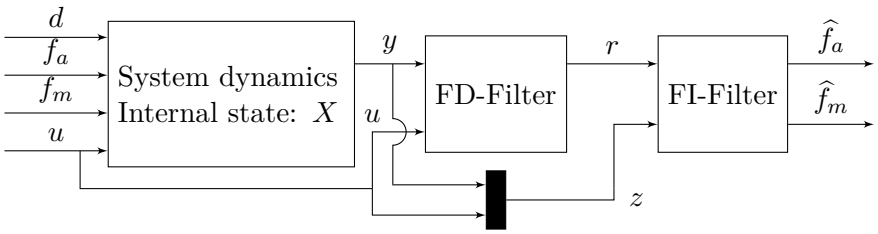

Figure 2-1: A visual representation of the proposed methodology.

where r respresents the residual output of the fault detection filter, i.e., the response of the filter to a non-zero multiplicative and/or additive fault. Note that the detection filter (FD-filter in Figure 2-1) is a feasible filter determined through Lemma 2-1.2. The isolation filter is created using a moving-horizon least-squares filter with a n-steps moving horizon filter. An error analysis containing a guaranteed error upper-bound of the proposed filter is given and subsequently an extension of the isolation filter is given to attack the largest source of error, being the dynamics between the true fault and the residual. Finally a theoretical extension is given to the FD-filter which allows detection of faults to be fully decoupled for an LPV system with measurable parameter variations.

Chapter 3

Theoretical Framework

In this chapter, the main theoretical results of the thesis are provided. First, the main non-linear isolation theorem is presented with a guaranteed upper bound on the estimation error. The error bound is composed of three different sources of possible estimation errors, suggesting potential directions to enhance the performance and applicability of the proposed isolation filter. An extension to the main result is given which deals with the most dominant and hard-to-reduce error term. Finally, the fault-detection algorithm is further extended to account for a LPV system where the parameter variations can be measured. The mathematical proofs for all theorems in this chapter are enclosed in Appendix A.

3-1 Non-linear isolation filter design

Definition 3-1.1 (Regression operator)**.** *For a signal x, assumed to be a scalar-valued function which is constant given a constant sampling interval, a linear operator $\phi_n[x](k) \in \mathbb{R}^{n\times 2}$ can be defined that collects present and past data up to n-steps back of the signal in a matrix as*

$$\phi_n[x](k) \coloneqq \begin{bmatrix} x(k) & x(k-1) & \dots & x(k-n+1) \\ 1 & 1 & \dots & 1 \end{bmatrix}^{\mathsf{T}}, \qquad \forall k \in \mathbb{Z} \tag{3.1}$$

where $n \in \mathbb{Z}^+$. Subsequently, we can define a non-linear operator $\Phi_n[x,y](k) \in \mathbb{R}^2$ which is composed as a non-linear combination of (3.1)*, acting as a linear operator on the present and past measurements of $y \in \mathbb{R}$*

$$\Phi_n[x,y](k) \coloneqq \left(\phi_n^{\mathsf{T}}[x](k)\phi_n[x](k)\right)^{-1}\phi_n^{\mathsf{T}}[x](k)\begin{bmatrix} y(k) \\ y(k-1) \\ \vdots \\ y(k-n+1) \end{bmatrix}. \qquad \forall k \in \mathbb{Z} \tag{3.2}$$

The reduced regression operator, i.e., the regression operator which is only dependent on the pseudo-inverse term as a function of signal x, inside the operator $\Phi_n[x,y](k)$, is defined as:

$$\Phi_n[x](k) \coloneqq \left(\phi_n^\intercal[x](k)\phi_n[x](k)\right)^{-1}\phi_n^\intercal[x](k), \qquad \forall k \in \mathbb{Z}, \tag{3.3}$$

where $\Phi_n[x](k) \in \mathbb{R}^{2\times n}$.

Using the regression operator (3.2) from Definition 3-1.1, the non-linear isolation filter, estimating the unknown faults f_a and f_m, using known measurements $E(z)$ and FD-filter output r, can be written as

$$\begin{bmatrix} \widehat{f}_a \\ \widehat{f}_m \end{bmatrix} = \Phi_n[E(z), r](k), \tag{3.4}$$

where the variables $\widehat{f}_a,\ \widehat{f}_m \in \mathbb{R}$ represent the fault estimates. A filter is designed, which separates the faults f_a and f_m from the measured residual, using a least squares regression by taking in to account the relation between the faults and the residual (2.7).

Definition 3-1.2 (Restricted state and input transfer function)**.** *Given a transfer funcion $W(q)$, with a minimal state space realization (A,B,C,D), the propagation of the input u to the output y over a restricted past finite horizon n at any time k is defined as*

$$\begin{bmatrix} y(k) \\ y(k-1) \\ \vdots \\ y(k-n+2) \\ y(k-n+1) \end{bmatrix} = \underbrace{\begin{bmatrix} CA^{n-1} \\ CA^{n-2} \\ \vdots \\ CA \\ C \end{bmatrix}}_{\mathscr{O}_n} x(k-n+1) + \underbrace{\begin{bmatrix} D & CB & \dots & CA^{n-3}B & CA^{n-2}B \\ & \ddots & \ddots & & \vdots \\ 0 & & D & CB & CAB \\ 0 & \dots & 0 & D & CB \\ 0 & \dots & 0 & 0 & D \end{bmatrix}}_{\mathscr{T}_n} \begin{bmatrix} u(k) \\ u(k-1) \\ \vdots \\ u(k-n+2) \\ u(k-n+1) \end{bmatrix},$$

where the signal $x \in \mathbb{R}^d$ is the internal state and $\mathscr{T}_n \in \mathbb{R}^{n\times n}$ and $\mathscr{O}_n \in \mathbb{R}^{n\times d}$ contain the dynamics of the restricted state and input transfer function.

Under the assumption that $\sigma_n^2\left[E(z)\right](k) \neq 0$ and $V_n\left[E(z)\right](k) \neq 0$, the following theorem provides a guaranteed performance bound for the error behavior of the non-linear isolation filter.

Theorem 3-1.3 (Isolation error bound)**.** *Consider the class of systems* (2.1) *combined with a FD-filter* (2.6) *determined by Lemma 2-1.2. The non-linear isolation filter* (3.4) *has an error behavior between the fault estimate and the mean fault over a window $n \in \mathbb{Z}_+$ which is upper-bounded by*

$$\left\| \begin{bmatrix} \widehat{f}_a - \mu_n\left[f_a\right] \\ \widehat{f}_m - \mu_n\left[f_m\right] \end{bmatrix} \right\|_2 \leq \sqrt{\frac{1+\left|\mu_n\left[E(z)\right]\right|}{nV_n\left[E(z)\right]}} \cdot (e_1+e_2+e_3), \tag{3.5}$$

where the error terms in (3.5) *are defined as*

$$e_1 = \|\mathscr{T}_n(f_m E(z) + f_a) + \mathscr{O}_n x_F(k-n+1)\|_{\mathscr{L}_{n2}}(k), \tag{3.6a}$$

$$e_2 = \sqrt{nV_n\left[f_m\right](k)} \cdot \|E(z)\|_{\mathscr{L}_{n\infty}}(k), \tag{3.6b}$$

$$e_3 = \sqrt{nV_n\left[f_a\right](k)}. \tag{3.6c}$$

Recall that $\|\cdot\|_{\mathscr{L}_{n2}}(k)$, $\|\cdot\|_{\mathscr{L}_{n\infty}}(k)$ *are the restricted norms at time instance* k*. The matrices* $\mathscr{T}_n$ *and* $\mathscr{O}_n$ *are the dynamic matrices of the restricted state and input transfer function (as defined in Definition 3-1.2) of the minimal realization of* $G(q)-I$ *with state* x_F*. The transfer function* $G(q)$ *is defined in* (2.7)*. The operators* $V_n\left[\cdot\right](k)$ *and* $\mu_n\left[\cdot\right](k)$ *represent the variance and mean of a signal at time* k*, as defined in the notational Section 1-4.*

Following the result in Theorem 3-1.3, an intuition is given how system- and filter parameters contribute to the estimation error of the filter (3.5).

Remark 3-1.4. *We note that each component of the error upper-bound* (3.5) *is dependent on the time instance* k*, hence the dependency is deliberately dropped to avoid clutter. The first error term* (3.6a) *is induced by the dynamical behavior between the residual and the true fault. The second term* (3.6b) *is caused by the time-varying behavior of the fault* f_m*, i.e., higher energy of this fault causes higher errors due to the "averaging" property of the least squares filter. The third error term* (3.6c) *follows the same line of reasoning, as it is induced by the energy of the additive fault* f_a *over time-horizon* n*. The mean and variance of the measured signals* $E(z)$ *have a scaling influence on the sum of errors. It is also worth noting that the time-horizon* n *plays a non-trivial role in the estimation error, as it not only acts as a scaling factor on the sum of errors, but it also interacts with the variance and mean of known signals* z *and fault signals* f_a *and* f_m*.*

Following Theorem 3-1.3 and Remark 3-1.4, it should be clear to the reader how the behavior of the estimation error can be influenced. For this research, it is assumed that only the time-horizon n and the mapping of the FD-filter can be influenced. The filtering method is applied in open-loop and hence influencing the properties of signal $E(z)$ lies outside of the scope of this research. The error e_1 can be reduced individually by selecting an FD-filter with fast dynamics acting from the fault to the residual, although depending on the problem setting and requirements for noise sensitivity, the user may be limited in this perspective. The following section provides an extension to the main theorem, allowing a relaxation on the error induced by the FD-filter's dynamics.

3-2 Pre-filter extension

Theorem 3-1.3 concluded with Remark 3-1.4, which elaborated on the main sources of error after the FI-filter. Concluding this remark, it is found that the only controllable error source in an open-loop scenario is the FD-filter dynamics induced error (3.6a). This source could be influenced by the design of the detection filter. Alternatively, we can consider to apply a penalty on the noise sensitivity for pushing down the estimation error. Figure 3-1 proposes a new filter structure that, by augmentation of the pre-filter, allows decoupling of the dynamical effect of the known signal $E(z)$ for constant f_a and f_m.

The filtered signal $\widetilde{E}(z)$ is obtained from the known signal $E(z)$ over n horizon by using the restricted state and input transfer function of filter (2.7)

$$\widetilde{E}_n(z(k)) = \widetilde{\mathscr{O}}_n x_E(k-n+1) + \widetilde{\mathscr{T}}_n E_n(z(k)), \tag{3.7}$$

and the state space propagation matrices $\widetilde{\mathscr{T}}_n$ and $\widetilde{\mathscr{O}}_n$ are the restricted state and input matrices of the minimal realization of the transfer function $G(q)$ (as defined in (2.7)).

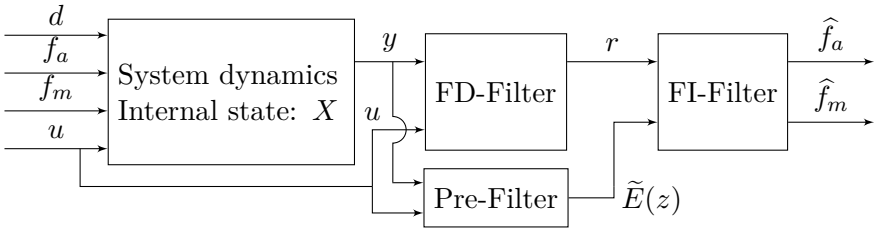

Figure 3-1: Augmentation of the Pre-Filter.

The non-linear regression operator (3.4), estimating unknown fault signals f_a, f_m, can be updated using the FD-filter residual, r, and the filtered known measurement ,$\widetilde{E}(z)$ (3.7), resulting in

$$\begin{bmatrix} \widehat{f}_a \\ \widehat{f}_m \end{bmatrix} = \Phi_n[\widetilde{E}(z), r](k). \tag{3.8}$$

The following theorem provides a guaranteed upper bound for the error behavior of the non-linear isolation filter augmented with the pre-filter.

Theorem 3-2.1 (Pre-filter isolation error bound)**.** *Consider the class of systems* (2.1) *combined with a FD-filter* (2.6) *determined by Lemma 2-1.2. Under the assumption that* $\sigma_n^2\left[\widetilde{E}(z)\right](k) \neq 0$, $V_n\left[\widetilde{E}(z)\right](k) \neq 0$, *the non-linear isolation filter augmented with the pre-filter* (3.8) *has an error behavior between the fault estimate and the mean fault over a window* $n \in \mathbb{Z}_+$, *which is upper-bounded by*

$$\left\| \begin{bmatrix} \widehat{f}_a(k) - \mu_n[f_a] \\ \widehat{f}_m(k) - \mu_n[f_m] \end{bmatrix} \right\|_2 \leq \sqrt{\frac{1 + \left|\mu_n\left[\widetilde{E}(z)\right]\right|}{nV_n\left[\widetilde{E}(z)\right]}} \cdot (\widetilde{e}_1 + \widetilde{e}_2 + e_3), \tag{3.9}$$

where the error terms in (3.9) *are defined as:*

$$\begin{aligned} \widetilde{e}_1(k) =& \|\widetilde{\mathscr{O}}_n x_M(k-n+1) - f^{\square}_{m_n}(k)\widetilde{\mathscr{O}}_n x_E(k-n+1)\|_2 + \|\widetilde{\mathscr{O}}_n x_A(k-n+1) + \widetilde{\mathscr{T}}_n f_{an}(k) - f_{an}(k)\|_2 \\ &+ \|(\widetilde{\mathscr{T}}_n f^{\square}_{m_n}(k) - f^{\square}_{m_n}(k)\widetilde{\mathscr{T}}_n)\|_2 \|E_n(z(k))\|_{\mathscr{L}_{n\infty}}(k) \end{aligned} \tag{3.10a}$$

$$\widetilde{e}_2(k) = \sqrt{nV_n[f_m](k)} \cdot \|\widetilde{E}(z)\|_{\mathscr{L}_{n\infty}}(k). \tag{3.10b}$$

Note, that the third error term e_3 *remains identical to the definition in* (3.6c). *The signals* x_A *and* x_M *represent the internal states of the systems with restricted state and input matrices* $\widetilde{\mathscr{T}}_n$ *and* $\widetilde{\mathscr{O}}_n$ *with inputs* f_a *and* f_m *respectively. The diagonal matrix* $f^{\square}_{m_n}(k)$ *represents the diagonalized vector of the sampled signal vector* $f_{m_n}(k)$ *as defined in the notational Section 1-4. We note that each component of the error upper-bound* (3.9) *is dependent on the time instance* k, *hence the dependency is deliberately dropped to avoid clutter.*

The following Corollary provides an immediate consequence of Theorem 3-2.1, showing the value of this extension.

Corollary 3-2.2 (Perfect dynamical decoupling)**.** *Let the assumptions made in Theorem 3-2.1 hold, and the fault signals f_m and f_a be constant, it can be observed that the variance terms in* (3.10b) *and* (3.6c) *are zero. For the dynamical error upper bound* (3.10a) *it is found that from an arbitrary initial condition $[x_M(0), x_E(0), x_A(0)]$ there exists a finite time $k = T \in \mathbb{Z}_+$ in which we can achieve*

$$\widetilde{e}_1(k+T) = 0, \qquad \forall k$$

which by induction implies that

$$\left\| \begin{bmatrix} \widehat{f}_a(k+T) - f_a \\ \widehat{f}_m(k+T) - f_m \end{bmatrix} \right\|_2 = 0. \qquad \forall k$$

The finite convergence time T is limited by the FI-filter horizon length n and the convergence dynamics of both the stable FD-filter (2.7) *and pre-filter* (3.7) *given a discrete sampling period.*

Given the information from Theorem 3-2.1 and Corollary 3-2.2, it is therefore found that the extension provides means to allow convergence to the true faults in finite time given that these are constant. The pre-filter design allows decoupling of the dynamical effect of the FD-filter from the fault estimates in a constant fault scenario. If the fault signals are time-varying, the same intuitions as in Remark 3-1.4 hold. As a result, an increase of the estimation horizon n will push down the guaranteed performance bound and can, as a result, also push down the estimation error. Although, it will affect the convergence time to the true fault. A decrease in FD-filter dynamics will decrease the dynamical mismatch between the FD-filter residual and the true fault and, as a result, the pre-filter augmented isolation filter will result in a faster convergence of the fault. An addition to these intuitions given in the following remark.

Remark 3-2.3. *Following the results from Theorem 3-2.1 and Remark 3-1.4, an extra remark has to be placed on the dynamical effect of the pre-filter* (3.7) *on the signal $E(z)$. Since the known signal $E(z)$ is now filtered with these dynamics, it is possible that the effect of these dynamics deteriorate the performance bound of the estimation error* (3.9) *through a reduction of $V_n\left[\widetilde{E}(z)\right]$. This phenomenon is caused by the variance or energy of the filtered known signal $V_n\left[\widetilde{E}(z)\right]$, which, dependent on the dynamics chosen for the FD-filter and thus the pre-filter, can reduce the variance of this signal. As a result of a decrease in $V_n\left[\widetilde{E}(z)\right]$, the performance bound increases and thus the estimation error could also increase.*

Concluding the theorems and remarks on the pre-filter, this extension provides means to decouple the dynamical effect of the FD-filter in constant fault scenarios. For time-varying faults, the dynamical mismatch reappears. Note, that the dynamical error induced by a time-varying fault remains identical. The dynamical error induced by a time-varying multiplicative fault can not be guaranteed to be higher or lower for the non-linear isolation filter, as it depends on the trajectory of the multiplicative fault and the dynamics chosen for the FD-filter.

3-3 Time-varying detection extension

In this extension, a tractable FD-filter design approach is proposed that allows fault detection for a class of linear time-varying systems with parameter-varying dynamics. We extend our notion of a LTI DAE model (2.6) to the definition of a linear parameter-varying DAE model

$$H_k(q)[x] + L_k(q)[z] + F_k(q)[f_a] + F_k(q)[E(z)f_m] = 0. \tag{3.11}$$

In this extension, it is assumed that the transfer matrix $H_k(q)$ contains dynamics up to a degree of one. The linear parameter-varying polynomial matrices can be decomposed as an affine representation in the linear parameter as proposed in the following fact.

Fact 3-3.1. *A linear parameter-varying matrix $G_k(q)$ can be written as an affine representation in the linear parameters, as follows:*

$$G_k(q) = G_k^{(0)}(q) + \sum_{i=1}^{m} G_k^{(i)}(q)\rho_{i_k},$$

where $\rho_{i_k} \in \mathbb{R}, \forall i$ represents a set of measurable time-varying parameters.

The detectability conditions for the LTI case (2.4) can be extended to the linear time-varying case

$$\begin{cases} d^{-1}(q)N_k(q)H_k(q) = & 0, \qquad \forall k \\ d^{-1}(q)N_k(q)F_k(q) \neq & 0. \end{cases} \tag{3.12}$$

The above conditions allow us to find a filter to decouple the time-varying behavior of the unknown signal dynamics from the time-varying behavior of the system,

$$\mathcal{M}_k \coloneqq \{z : \mathbb{Z} \to \mathbb{R}^{n_z} |\ \exists x : \mathbb{Z} \to \mathbb{R}^{n_x} :\ H_k(q)[x] + L_k(q)[z] = 0\}, \quad \forall k,$$

such that the following behavior holds:

$$\mathcal{M}_k = \{z : \mathbb{Z} \to \mathbb{R}^{n_z} \mid d^{-1}(q)N_k(q)L_k(q)[z] = 0\}, \quad \forall k. \tag{3.13}$$

A method to transform the conditions (3.12) into non-complex scalar or vector equations is provided in the following lemma. In this lemma, we make the assumption that the maximum degree of matrix $H(q)$ is equal to one, i.e., $d_H = 1$. An extension of this method to higher degrees can be done without loss of generality.

Lemma 3-3.2. *Let $N_k(q)$ be the solution to* (3.12) *for system* (3.11) *where*

$$H_k(q) \coloneqq H_{0_k} + H_1 q, \qquad F_k(q) \coloneqq \sum_{i=0}^{d_F} F_i q^i,$$

$$N_k(q) \coloneqq \sum_{i=0}^{d_N} N_{k_i} q^i.$$

Then the conditions in (3.12) *can be rewritten as*

$$\begin{cases} \bar{N}_k \bar{H}_k = & 0, \qquad \forall k, \\ \|\bar{N}_k \bar{F}_k\|_\infty \neq & 0, \end{cases} \tag{3.14}$$

where

$$\bar{N}_k \coloneqq \begin{bmatrix} N_{0_k} & N_{1_k} & \dots & N_{d_{N_k}} \end{bmatrix},$$

$$\bar{H}_k \coloneqq \begin{bmatrix} H_{0_{k-1}} & H_1 & 0 & \dots & 0 \\ 0 & H_{0_{k-2}} & H_1 & 0 & \vdots \\ \vdots & & \ddots & \ddots & 0 \\ 0 & \dots & 0 & H_{0_{k-d_N-1}} & H_1 \end{bmatrix},$$

$$\bar{F} \coloneqq \begin{bmatrix} F_{0_{k-1}} & F_{1_{k-1}} & \dots & F_{d_{F_{k-1}}} & 0 & \dots & 0 \\ 0 & F_{0_{k-2}} & F_{1_{k-2}} & \dots & F_{d_{F_{k-2}}} & 0 & \vdots \\ \vdots & & \ddots & \ddots & & \ddots & 0 \\ 0 & \dots & 0 & F_{0_{k-d_N-1}} & F_{1_{k-d_N-1}} & \dots & F_{d_{F_{k-d_N-1}}} \end{bmatrix},$$

$$\bar{d} \coloneqq \begin{bmatrix} d_0 & d_1 & \dots & d_{d_d} \end{bmatrix},$$

where d_N, d_F, d_d represent the maximum degree of matrices $N(q)$, $F(q)$ and $d(q)$ respectively.

Proof. It is easy to observe that the causal input-output relation (3.13) can be rewritten as

$$\begin{aligned} \sum_{i=0}^{d_d} d_i q^{-i} r_x &= \sum_{i=1}^{d_N+1} N_{i_k} q^{-i} [H_{0_k} + H_1 q[x]], \\ &= \sum_{i=1}^{d_N+1} N_{i_k} (H_{0_{k-i}} q^{-i}[x] + H_1 q^{-i+1}[x]), \end{aligned}$$

and the Right-hand side (RHS) is equivalent to

$$\bar{N}_k \bar{H}_k \Big(\begin{bmatrix} I & q^{-1}I & \dots & q^{-k}I \end{bmatrix} [x] \Big).$$

The same line of reasoning applies for the polynomial matrix $\bar{F}_k$. □

The following fact provides a sufficient condition for the existence of a LPV FD-filter (3.13).

Fact 3-3.3. *There exists a solution $N_k(q)$ to the conditions in* (3.12) *iff for all trajectories of the measurable parameter variation the following condition is fulfilled*

$$Rank\Big(\begin{bmatrix} \bar{H}_k & \bar{F}_k \end{bmatrix} \Big) > Rank\Big(\bar{H}_k \Big). \qquad \forall k \tag{3.15}$$

Fact 3-3.3 provides a necessary and sufficient solvability condition for the problem in (3.12). The proof is omitted as it is a straightforward adaption from [21] (Fact 4.4). Using the results from Lemma 3-3.2, the main theorem for the LPV fault detection filter can be proposed.

Theorem 3-3.4 (Linear parameter-varying fault detection)**.** *Let the matrices $\bar{H}_k$, $\bar{L}_k$ and $\bar{F}_k$ be given for all past and present time instances $k \in \mathbb{Z}$ and let condition* (3.15) *hold. A LPV fault detection filter of the form* (3.13) *can be found at every time instance k, satisfying the*

conditions (3.12)*, by solving the following convex Quadratic Programming (QP) optimization problem:*

$$\begin{cases} \max_{\bar{N}_k} & \bar{N}_k \bar{F}_{k_j}, \\ s.t. & \|\bar{H}_k^\intercal \bar{N}_k^\intercal\|_2^2 = 0, \\ & \|\bar{N}_k^\intercal\|_2^2 \leq 1, \end{cases} \tag{3.16}$$

in which the subscript j selects the j_{th} column from the matrix $\bar{F}$. An approximate analytical solution exists for (3.16) *and is given as*

$$\bar{N}_k^*(\gamma) = \frac{1}{2}\bar{F}_{k_j}^\intercal (I + \gamma \bar{H}_k \bar{H}_k^\intercal)^{-1} \tag{3.17}$$

where (3.17) *approaches the true optimum of* (3.16) *for* $\lim_{\gamma\to\infty} \bar{N}_k^*(\gamma)$.

The near-optimal time-varying filter $\bar{N}_k^*(\gamma)$ is the solution to the strongly convex dual problem for which weak duality holds. The size of the duality gap is governed by the magnitude of the Lagrange multiplier γ.

Corollary 3-3.5. *Practical limitations of the minimal state-space realization for LPV filters as proposed in [30] require us to apply the filter in a LPV-IO representation such that the LPV mapping from $z \mapsto r$ as proposed in* (3.13) *can be practically implemented as*

$$r(k) = \bar{N}_k \bar{L}_k \begin{bmatrix} z(k-1) & z(k-2) & \dots & z(k-d_N) \end{bmatrix}^\intercal - \sum_{i=0}^{d_d} d_i r(k-i)$$

where the matrix $\bar{L}_k$ is defined as

$$\bar{L} := \begin{bmatrix} L_{0_{k-1}} & L_{1_{k-1}} & \dots & L_{d_{F_{k-1}}} & 0 & \dots & 0 \\ 0 & L_{0_{k-2}} & L_{1_{k-2}} & \dots & L_{d_{L_{k-2}}} & 0 & \vdots \\ \vdots & & \ddots & \ddots & & \ddots & 0 \\ 0 & \dots & 0 & L_{0_{k-d_N-1}} & L_{1_{k-d_N-1}} & \dots & L_{d_{L_{k-d_N-1}}} \end{bmatrix}$$

3-4 Discussion on the theoretical framework

In this chapter, the main foundation of the novel contributions of this thesis research has been provided. The combination of the developed methods provides means for a fault detection and isolation filter which can estimate the additive fault and multiplicative fault for a class of LTI and LPV models.

In the first theoretical contribution, the non-linear isolation filter has been proposed with a guaranteed performance bound. This filter is able to, combined with the nullspace computation based FD-filter (proposed in [21]), estimate the additive and multiplicative faults using least-squares regression. The guaranteed performance bound shows the main strengths and weaknesses of the filter and, above all, methods to increase or reduce the estimation error by adjusting the performance bound.

In the second theoretical contribution, an extension was made for the non-linear isolation filter. In the first contribution it was given that the dynamics of the FD-filter could deteriorate the FI-filter results if the dynamical content was too high. By a novel extension, called the pre-filter, this dynamical content was taken into account in the least-squares regression problem. As a result, the estimation error is guaranteed to converge in finite-time given that the fault signals acting on the system are of a constant nature.

In the third theoretical contribution, the used FD-filter method was extended to support LPV systems instead of only LTI systems. A QP optimization problem was proposed to allow decoupling of the unknown disturbances from the fault. This optimization problem was shown to be analytically solvable by the use of duality theorem. As a result, a filter is developed which allows decoupling of the LPV nature of a system from the fault-sensitive residual without the necessity of a LP or QP solver.

Chapter 4

An Application to the Lateral Control of Autonomous Vehicles

In this chapter, the lateral model of the autonomous vehicle in lateral motion is derived. The lateral dynamics of this vehicle, modeled as a two degree of freedom single track model with linearized lane error dynamics [31], will be inserted in the main framework of the theorems discussed in Chapter 3. In the following section, following a set of boundary conditions and simulation parameters, the theorems from the main results will be used on the linearized vehicle model to show that our objective has been fulfilled. After analyzing these linear results, a sensitivity analysis is applied for the FD-filter to investigate the robustness of the method in a linearized scenario.

4-1 Boundary conditions and simulation parameters

Before modeling the lateral motion of the vehicle, a few preliminary boundary conditions have to be set that allow the use of the single-track model and the theorems developed in Chapter 3. The case study involves an autonomous vehicle controlled by lane-keeping or path-following controller in highway scenarios. It is assumed that the vehicle is always driving at an approximately constant longitudinal velocity, the velocities considered for the longitudinal velocity V_x satisfy

$$70\text{km} \cdot \text{h}^{-1} \leq V_x \leq 120\text{km} \cdot \text{h}^{-1}. \tag{4.1}$$

Due to the approximately constant longitudinal velocity, the longitudinal acceleration can also be assumed approximately zero. Additionally the lateral acceleration is bounded by the sufficiently large road radii and bank angles of the public highways in the Netherlands [32], such that for the longitudinal and lateral accelerations a_x and a_y we can reasonably assume that

$$a_x \approx 0$$

$$a_y \leq 3\mathrm{m} \cdot \mathrm{s}^{-2}$$

Given these boundary conditions, the use of a single-track model is allowed (given the assumptions from the linear model in Appendix B [33]). The model parameters for the vehicle used in this chapter and Chapter 5 are based on a 2010 model Toyota Prius and are shown in Table 4-1. The model parameters relate to the model as described in Appendix B. The parameters in this table are identified by TNO, no additional identification cycle for the parameters is applied in this thesis.

Parameter	Value	Unit
l_f	1.108	[m]
l_r	1.5920	[m]
m	1625	[kg]
I_z	2865.61	$[\mathrm{kg} \cdot \mathrm{m}^2]$
C_f	$-1.17 \cdot 10^5$	$[\mathrm{N} \cdot \mathrm{rad}^{-1}]$
C_r	$-1.43 \cdot 10^5$	$[\mathrm{N} \cdot \mathrm{rad}^{-1}]$
g	9.81	$[\mathrm{m} \cdot \mathrm{s}^{-2}]$
h	0.01	[s]

Table 4-1: Model parameters used for the simulations.

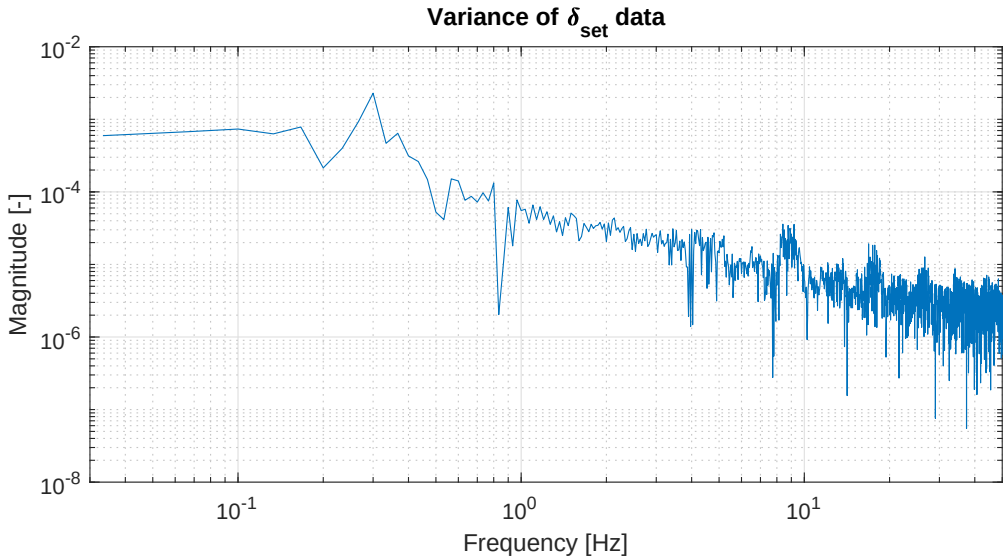

Figure 4-1: Fast Fourier transform of the controller input signal δ_{set} at $70\mathrm{km} \cdot \mathrm{h}^{-1}$, magnitude is given in radians.

Note that the symbol h represents the discrete sampling interval which is based on the maximal sampling frequency for which measurements will be available on the experimental platform. For the non-linear isolation filter and pre-filter extensions the fault estimates rely on

a sufficient variance of the input signal δ_{set} (comparable to the notion of persistence of excitation [34]). A low or even zero variance of the signal δ_{set} will result in an unbounded estimation bound and error as can be seen in Theorem 3-1.3 and Theorem 3-2.1. To support this relation, an assumption will be made on a "natural" variance of the input signal from the controller, i.e., we assume that the vehicle is not always perfectly tracking the lane. This variance is primarily caused by exogenous disturbances, camera inaccuracies and system delays. The variance is selected, based on a set of data collected by TNO, at the minimal velocity of $70\text{km} \cdot \text{h}^{-1}$. A fast Fourier transfom of a subset of this data is shown in Figure 4-1. The data shows a dominating frequency of 0.3Hz with a magnitude of approximately $2.3 \cdot 10^{-3}$rad. Based on these observations, the lane-keeping input signal is simulated as

$$\delta_{set} = 2.3 \cdot 10^{-3} \sin(0.3 \cdot 2\pi \cdot t) \tag{4.2}$$

This signal will be used as an input signal to the linear system in the simulation cases.

4-2 The linear vehicle model

A lateral single-track vehicle model captures the most dominant lateral dynamics of a vehicle in lateral motion under a set of assumptions [33](a part of these assumptions is thoroughly covered in Appendix B, the other part is covered by the proposed boundary conditions). A schematic representation of the model can be found in Figure 4-2.

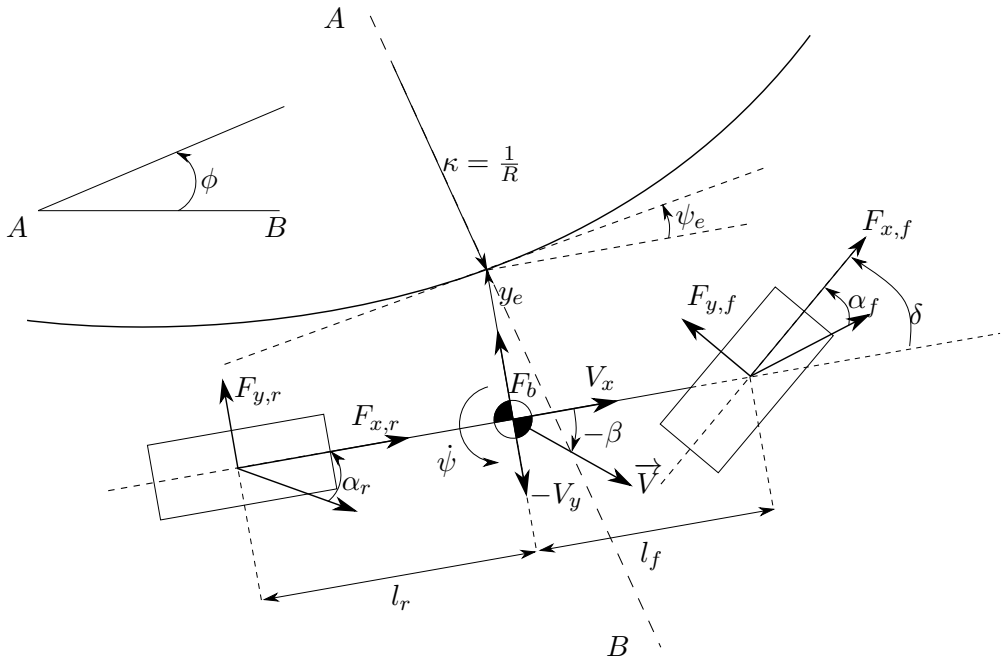

Figure 4-2: Schematic diagram of the 2-DOF bicycle model with lane error dynamics.

The lateral dynamics of a vehicle can be modeled using a two degree of freedom single-track bicycle model where the measurement of the yaw-rate is available from the vehicle's sensors.

Subsequently, for the purpose of autonomous lane-keeping, the model can be augmented with the lateral distance error and heading error states which are measured by the on-board camera [8]. The curvature of the road is imposed as an uncontrollable input and is thus handled as an exogenous disturbance. Another exogenous disturbance is the bank angle of the road, which is the angle of the road over cross-section $A - B$ as shown in Figure 4-2. Finally, the fault model is introduced in the main model showing that the transfer function from both faults to the output is identical, thus leading to the conclusion of undetectability or unobservability as was introduced in the problem statement in Chapter 2. Following the derivations in Appendix B, the state-space model of the linear single-track model with augmented faults and disturbances can be written as

$$\underbrace{\begin{bmatrix} \dot{V}_y \\ \ddot{\psi} \\ \dot{y}_e \\ \dot{\psi}_e \end{bmatrix}}_{\dot{X}} = \underbrace{\begin{bmatrix} \frac{C_f+C_r}{mV_x} & \frac{C_f l_f - C_r l_r}{mV_x} - V_x & 0 & 0 \\ \frac{l_f C_f - l_r C_r}{V_x I_z} & \frac{l_f^2 C_f + l_r^2 C_r}{V_x I_z} & 0 & 0 \\ -1 & 0 & 0 & V_x \\ 0 & -1 & 0 & 0 \end{bmatrix}}_{A} \underbrace{\begin{bmatrix} V_y \\ \dot{\psi} \\ y_e \\ \psi_e \end{bmatrix}}_{X} + \underbrace{\begin{bmatrix} \frac{-C_f}{m} \\ \frac{-l_f C_f}{I_z} \\ 0 \\ 0 \end{bmatrix}}_{B} (f_m \delta_{set} + f_a) + \underbrace{\begin{bmatrix} 0 & g \\ 0 & 0 \\ 0 & 0 \\ V_x & 0 \end{bmatrix}}_{B_d} \underbrace{\begin{bmatrix} \kappa \\ \sin(\phi) \end{bmatrix}}_{d}, \tag{4.3a}$$

$$y = \underbrace{\begin{bmatrix} 0 & 1 & 0 & 0 \\ 0 & 0 & 1 & 0 \\ 0 & 0 & 0 & 1 \end{bmatrix}}_{C} \underbrace{\begin{bmatrix} V_y \\ \dot{\psi} \\ y_e \\ \psi_e \end{bmatrix}}_{X}. \tag{4.3b}$$

This vehicle model is an LTI state-space model for a constant longitudinal velocity V_x. As proposed in [33], given that the longitudinal velocity is slowly time-varying, it can also be used as a LPV state-space model.

4-3 Implementation of the developed methods

This section shows the systematic approach of implementing the main results of this research on the case study. First, the LTI FD-filter is designed. Subsequently, the non-linear isolation algorithm is applied and simulation results are presented together with a discussion. Following these results, the pre-filter extension is added to show the striking effect it has on the isolation performance. Finally, the FD-filter is extended to a linear parameter-varying scenario and simulations results are provided to show the performance of the LPV filter and the isolation techniques combined.

4-3-1 Application of the fault detection filter

First, the system (4.3) is adjusted to rewrite it as a DAE set of equations (2.1). As a result, the state-space equations from (4.3) are rewritten as

$$\underbrace{\begin{bmatrix}\dot{V}_y\\ \ddot{\psi}\\ \dot{y}_e\\ \dot{\psi}_e\end{bmatrix}}_{\dot{X}} = \underbrace{\begin{bmatrix}\frac{C_f+C_r}{mV_x} & \frac{C_f l_f - C_r l_r}{mV_x} - V_x & 0 & 0\\ \frac{l_f C_f - l_r C_r}{V_x I_z} & \frac{l_f^2 C_f + l_r^2 C_r}{V_x I_z} & 0 & 0\\ -1 & 0 & 0 & V_x\\ 0 & -1 & 0 & 0\end{bmatrix}}_{A}\underbrace{\begin{bmatrix}V_y\\ \dot{\psi}\\ y_e\\ \psi_e\end{bmatrix}}_{X} + \underbrace{\begin{bmatrix}\frac{-C_f}{m}\\ \frac{-l_f C_f}{I_z}\\ 0\\ 0\end{bmatrix}}_{B}\delta_{set},$$
$$+ \underbrace{\begin{bmatrix}\frac{-C_f}{m}\\ \frac{-l_f C_f}{I_z}\\ 0\\ 0\end{bmatrix}}_{B_f}\underbrace{((f_m-1)\delta_{set}+f_a)}_{f} + \underbrace{\begin{bmatrix}0 & g\\ 0 & 0\\ 0 & 0\\ V_x & 0\end{bmatrix}}_{B_d}\underbrace{\begin{bmatrix}\kappa\\ \sin(\phi)\end{bmatrix}}_{d}, \tag{4.4a}$$

$$y = \underbrace{\begin{bmatrix}0 & 1 & 0 & 0\\ 0 & 0 & 1 & 0\\ 0 & 0 & 0 & 1\end{bmatrix}}_{C}\underbrace{\begin{bmatrix}V_y\\ \dot{\psi}\\ y_e\\ \psi_e\end{bmatrix}}_{X}. \tag{4.4b}$$

Notice that the above state-space description is different from (4.3) as the total effect of the faults is now written as an additive fault. Furthermore, it is worth noting that the system is described in continuous-time, whereas the main results are fitted to work with discrete-time systems. It is therefore assumed that the system related signals X, δ_{set}, f and d are piecewise constant signals, i.e., constant within the discrete sampling interval h. Using the exact solution for a continuous time LTI system, the model can be transformed to discrete time

$$X(k+1) = \underbrace{e^{Ah}}_{\mathcal{A}}X(k) + \underbrace{\int_0^h e^{As}B ds}_{\mathcal{B}}\delta_{set}(k) + \underbrace{\int_0^h e^{As}B_f ds}_{\mathcal{B}_f} f(k) + \underbrace{\int_0^h e^{As}B_d ds}_{\mathcal{B}_d} d(k), \tag{4.5a}$$

$$y(k) = Cx(k). \tag{4.5b}$$

Substitution of the discrete system matrices (4.5) in (2.1) yields the following DAE

$$\underbrace{\begin{bmatrix}-qI+\mathcal{A} & \mathcal{B}_d\\ C & 0\end{bmatrix}}_{H(q)}\begin{bmatrix}X\\ \kappa\\ \sin(\phi)\end{bmatrix} + \underbrace{\begin{bmatrix}0 & \mathcal{B}\\ -I & 0\end{bmatrix}}_{L}\begin{bmatrix}\dot{\psi}\\ y_e\\ \psi_e\\ \delta_{set}\end{bmatrix} + \underbrace{\begin{bmatrix}\mathcal{B}_f\\ 0\end{bmatrix}}_{F}[f_a] + \underbrace{\begin{bmatrix}\mathcal{B}_f\\ 0\end{bmatrix}}_{F}[(f_m-1)\delta_{set}] = 0. \tag{4.6}$$

Following (4.6) and the condition posed in (2.5), an FD-filter can be found which rejects the presence of the unmeasurable states in x and the disturbances in d and detects the faults f_m and f_a if and only if

$$\text{Rank}\left(\begin{bmatrix} -qI+\mathcal{A} & \mathcal{B}_d & \mathcal{B}_f \\ C & 0 & 0 \end{bmatrix}\right) > \text{Rank}\left(\begin{bmatrix} -qI+\mathcal{A} & \mathcal{B}_d \\ C & 0 \end{bmatrix}\right). \tag{4.7}$$

A sampling interval of $h = 0.01$s was already chosen earlier as it is the same sampling time of the required measurements in the experimental vehicle in Chapter 5. By numerically checking the above condition (4.7) for a subset of velocities $70\text{km}\cdot\text{h}^{-1} \leq V_x \leq 120\text{km}\cdot\text{h}^{-1}$, it can be verified that the condition holds. After checking the conditions with intervals of $0.01\text{km}\cdot\text{h}^{-1}$ from the minimum velocity up to the maximum velocity, it is assumed that the detectibility condition holds for all velocities within the boundary condition. Therefore, a solution $N(q)$ for a fault detection filter $d^{-1}(q)N(q)L(q)$ (2.6) can be found such that the conditions in (2.4) are fulfilled. In Chapter 3, an additonional condition has been imposed for synthesis of the fault detection filter. In Lemma 2-1.2, a methodology is described which proposes a linear program to find an optmal solution satisfying (2.4), while the DC-gain of the fault transfer function (2.7) is equal to one. A solution to this problem is found by solving the following Linear Programming (LP) feasibility problem:

$$\begin{cases} \bar{N}\bar{H} = & 0, \\ \frac{\sum \bar{N}\bar{F}}{\sum \bar{d}} = & 1, \end{cases} \tag{4.8}$$

where the matrices are polynomial matrices composed as

$$\bar{N} \coloneqq \begin{bmatrix} N_0 & N_1 & \dots & N_{d_N} \end{bmatrix},$$

$$\bar{H} \coloneqq \begin{bmatrix} H_0 & H_1 & \dots & H_{d_H} & 0 & \dots & 0 \\ 0 & H_0 & H_1 & \dots & H_{d_H} & 0 & \vdots \\ \vdots & & \ddots & \ddots & & \ddots & 0 \\ 0 & \dots & 0 & H_0 & H_1 & \dots & H_{d_H} \end{bmatrix},$$

$$\bar{F} \coloneqq \begin{bmatrix} F_0 & F_1 & \dots & F_{d_F} & 0 & \dots & 0 \\ 0 & F_0 & F_1 & \dots & F_{d_F} & 0 & \vdots \\ \vdots & & \ddots & \ddots & & \ddots & 0 \\ 0 & \dots & 0 & F_0 & F_1 & \dots & F_{d_F} \end{bmatrix},$$

where d_N, d_H and d_F are the degrees of the polynomial matrices $N(q)$, $H(q)$ and $F(q)$ respectively. For the case study it holds that $d_H = 1$, $d_F = 0$. This feasibility problem (4.8) can be solved numerically in an efficient manner using the GUROBI solver [35]. The input-output relation of the filter is thus

$$d^{-1}(q)N(q)L(q)\begin{bmatrix} \dot{\psi} & y_e & \psi_e & \delta_{set} \end{bmatrix}^\intercal = r, \tag{4.9}$$

$$= -\, d^{-1}(q)N(q)F(q)[(f_m - 1)\delta_{set} + f_a], \tag{4.10}$$

showing that a relation is found from the known inputs to the unknown and desired output (the residual r). Two variables remain to be chosen: the order of the filter $N(q)$ and the

stable polynomial $d(q)$. It is decided to find a total FD-filter which is stable and strictly proper, hence deg($d(q)$)>deg($N(q)L$). Since the highest relative degree of the output to a disturbance or fault (in this case the bank angle) is two we need at least a filter with $d_N = 2$ and thus a third-order stable transfer function $d(q)$ is sufficient.

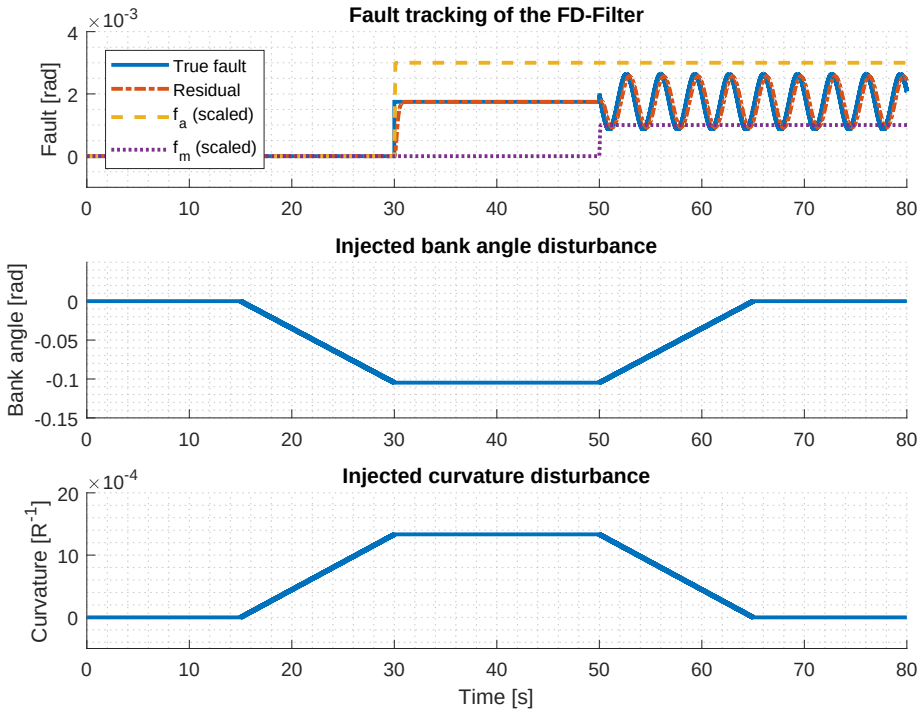

Figure 4-3: The disturbance rejecting and fault detecting performance of the FD-filter with poles at $q = 0.9048$.

For the first simulations, showing the detection peformance, the poles of the third-order transfer function $d(q)$ are placed at $q = 0.9048$ (a relatively slow pole to emphasize the dynamical content of the FD-filter). It is debatable whether or not placing three poles on the same location is beneficial for this application or not, due to the algebraic multiplicity. It was however outside the scope of this thesis to research the optimal pole placement for this specific application. Should there be a specifically desired convergence behavior in terms of damping ratio and settling time, one could approach a second-order transfer function and place the remainder of the poles further towards the origin.

The filter is implemented by converting the optimized FD-filter into a minimal state-space realization and by initializing it at $x(0) = 0$. In practice. zero initial conditions might not always correspond to the true state of the system. Thus, when initializing the filter, there might be a false positive or false negative fault as long as the initial condition has not diminished. Rejection of the effect of false initial conditions has not been taken into account in this thesis work. The effect of these initial conditions are only found at initialisation of the filter, as their effects diminish due to the asymptotic convergence rate of the stable FD-filter. Figure 4-3 shows the first result for a third-order fault detection filter to approach this second

order convergence behavior. At $t = 15$s two disturbances are injected, after which an additive fault $f_a = 0.1$deg is injected at $t = 30$s, subsequently at $t = 50$s a multiplicative fault $f_m = 0.9$ is injected which oscillates due to a sinusoidal input signal δ_{set} (4.2). Following these results, the conclusion can be drawn that the effect of the disturbances is rejected. Furthermore, the combined fault f is detected and tracked by the residual r, which presents itself as a filtered version of f. Now that a clear methodology for FD-filter synthesis has been introduced, the developed methods can be applied on the case study and subsequently analyzed.

4-3-2 Application of the non-linear isolation filter

In Section 3-1, the non-linear isolation filter is introduced, with the purpose to separate the unknown faults f_m and f_a from the known residual r. The residual is an output from (4.9) and is related to the fault as in (4.10). This subsection shows how to implement the developed methods on our case study. The results also show the theoretical shortcomings that are resolved in the following subsection. Using the regression operator from Definiton 3-1.1, in combination with the known input δ_{set} and the residual from FD-filter (4.9), the non-linear isolation filter, estimating the fault signals f_m and f_a, can be defined as

$$\begin{bmatrix} \widehat{f}_a \\ \widehat{f}_m \end{bmatrix} = \Phi_n[\delta_{set}, r](k), \tag{4.11}$$

as defined by the regression operator from Definition 3-1.1. Following the results from Theorem 3-1.3, the estimation error of (4.11) is guaranteed to be upper-bounded by

$$\underbrace{\left\| \begin{bmatrix} \widehat{f}_a - \mu_n[f_a] \\ \widehat{f}_m - \mu_n[f_m] \end{bmatrix} \right\|_2}_{\theta_e} \leq \underbrace{\sqrt{\frac{1 + |\mu_n[\delta_{set}]|}{nV_n[\delta_{set}]}} \cdot (e_1 + e_2 + e_3)}_{\Theta_e}, \tag{4.12a}$$

$$\begin{aligned} e_1 &= \| \mathscr{T}_n(f_m \delta_{set} + f_a) + \mathscr{O}_n x_F(k - n + 1) \|_{\mathscr{L}_{n2}}(k), \\ e_2 &= \sqrt{nV_n[f_m](k)} \cdot \|\delta_{set}\|_{\mathscr{L}_{n\infty}}(k), \\ e_3 &= \sqrt{nV_n[f_a](k)}, \end{aligned}$$

where $\mathscr{T}_n$ and $\mathscr{O}_n$ are a result of the restricted state and input transfer function from Definition 3-1.2 for which the state space matrices are provided by the minimal realization of the filter (4.9). As a result, the FD-filter and FI-filter combination is found, see Figure 4-4.

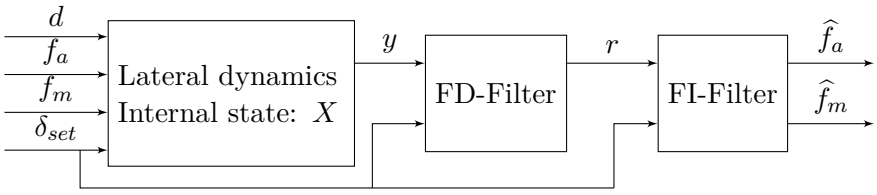

Figure 4-4: A visual representation of the FD-filter and FI-filter in the case study.

As proposed in Section 3-1 in Remark 3-1.4, the estimation error can be pushed down by several sources of influence (for example an increased variance of the known signals), in the following simulations these sources of influence are exploited. It is shown how these variations affect the estimation error θ_e and its bound Θ_e as defined in (4.12a).

Case 1: The horizon of the FI-filter

The estimation horizon n of the non-linear isolation filter plays a dominant role in the upper-bound of the estimation error as shown in (4.12). Not only does it affect the magnitude of the upper bound as a constant, it also affects the variance and mean terms because it defines the window over which the mean or variance is calculated. To find the effect of the horizon on the estimation error and its upper bound, simulations have been applied with constant faults $f_m = 0.5$ and $f_a = 0.1$deg. The input signal δ_{set} is excited by the signal described in (4.2) at a velocity of $V_x = 70\text{km} \cdot \text{h}^{-1}$. The disturbances are applied identically to Figure 4-3, but will not be seen in the estimation error as they are already decoupled after the FD-filter. For an estimation horizon of $n = 10$, $n = 100$ and $n = 500$ the simulation results are shown in Figure 4-5.

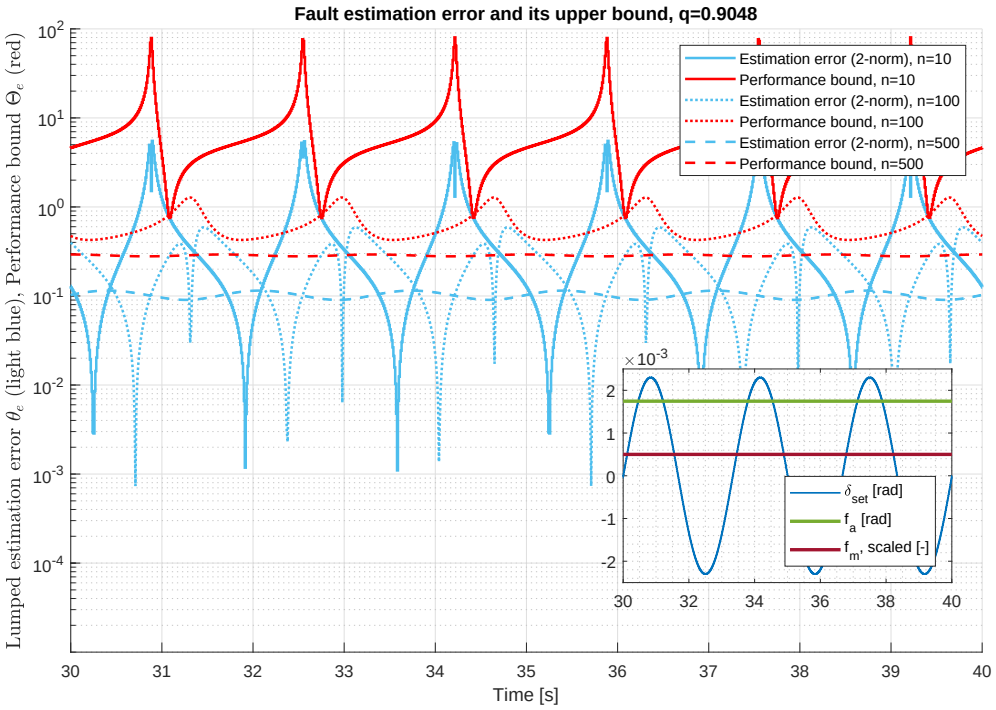

Figure 4-5: The estimation error θ_e and the performance bound Θ_e (as given in (4.12a)) of the FI-filter for $n = 10$, $n = 100$ and $n = 500$ for a fixed pole location of $q = 0.9048$.

Not only in these simulations, but also in the other simulations in this subsection, the effect of the initial condition of the isolation filter is not shown. For $n = 10$ it can be seen that the determined upper bound touches the 2-norm of the estimation error at some points in the simulation. As a result, pushing down the upper-bound should also push down those specific points of the estimation error. The oscillatory behavior of the estimation error and its upper-bound is clearly caused by the sinusoidal input δ_{set} combined with the fact that we assume in the first theorem (Theorem 3-1.3) that there are no dynamics acting between the true fault and the residual. For $n = 100$ (also shown in Figure 4-5), the effect of an increasing horizon becomes quite clear: the upper-bound is pushed down further and hence

the estimation error and its mean are pushed down further. The bound shows that there is still room for improving the estimation error, hence the horizon n is further increased to $n = 500$.

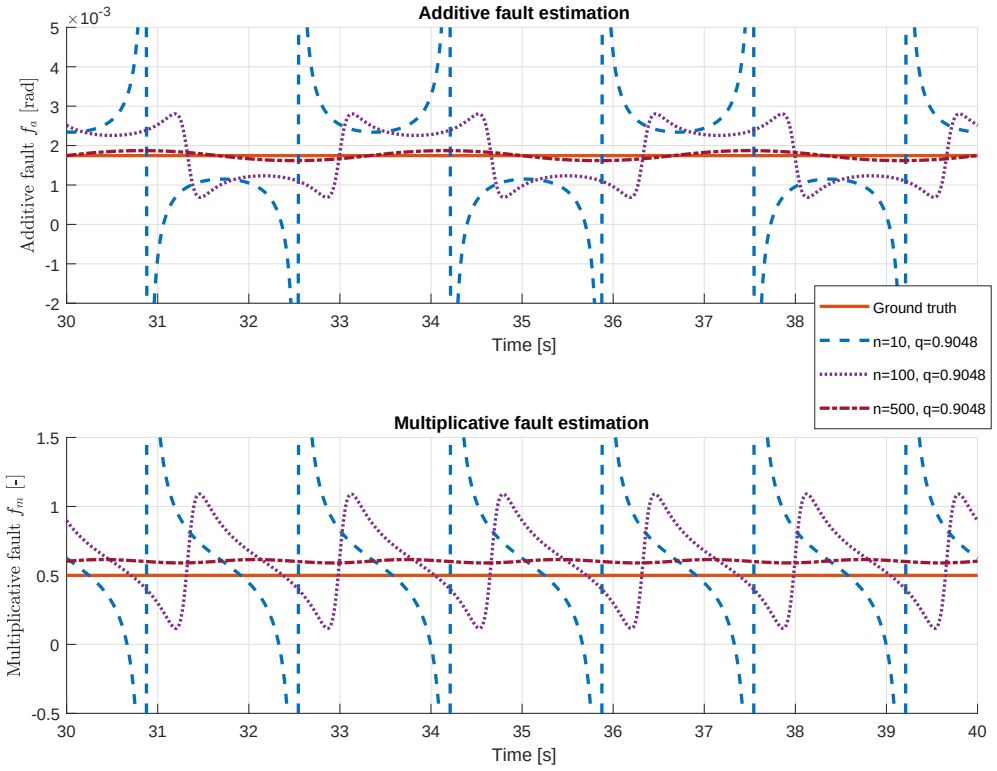

Figure 4-6: Separate fault estimation errors of the FI-filter for $n = 10$, $n = 100$ and $n = 500$ for a fixed pole location of $q = 0.9048$.

In this final simulation it is depicted (in Figure 4-5) that the upper-bound is no longer close to the estimation error. The variance of the estimation error and its upper bound has diminished and a near steady-state estimation error seems to have been reached, the minima of the estimation error have significantly increased as a result of the averaging effect of the filter. Pushing the horizon even further will decrease the estimation error further but will also degradate the dynamical performance of the filter as the convergence time grows proportionally with the estimation horizon n.

The separate estimation results are shown in Figure 4-6. In these results it is found that for a low estimation horizon, the estimations of the faults show an asymptotic behavior due to the dynamics of the FD-filter. Furthermore, it shows that this asymptotic behavior of the estimation error is reduced with an increasing estimation horizon. For $n = 500$, the estimation error of the additive fault converges to the true additive fault. However, for the same horizon $n = 500$, the multiplicative fault has an offset with respect to the true f_m. For larger n, this will reduce to the true multiplicative fault, although it will drastically affect transient

behavior of the filter. It can be concluded from these results that the performance of the filter is not satisfactory, it requires high estimation horizons to find a steady-state fault as a result. This conclusion is drawn, without even having had a look at the behavior of the filter for time-varying faults. The following subsection provides simulation results of the filter by adjusting the poles of the FD-filter and the transfer function from fault to residual (equivalent to (2.7)).

Case 2: The dynamics of the FD-filter

As mentioned in Remark 3-1.4, the dynamical content of the transfer function describing the mapping $f \mapsto r$ has a large influence on the estimation error. This is caused by the assumption that the relation between the residual and the fault is static while in reality this is a dynamical relationship. By placing the poles of transfer function $d(q)$ further towards the origin, the significance of this dynamical mismatch can be reduced. The format of the transfer function $d(q)$ is simply a third-order transfer functions with three poles at the same location. As a benchmark, the simulations are started in the same scenario as in Figure 4-5, and the results are shown in Figure 4-7.

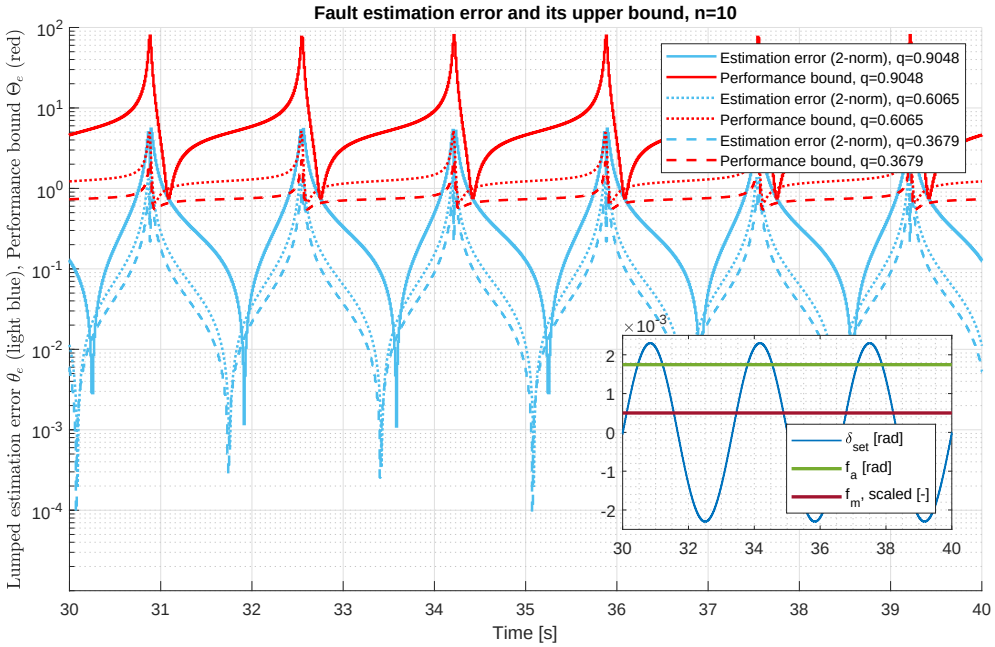

Figure 4-7: The estimation error θ_e and the performance bound Θ_e (as given in (4.12a)) of the FI-filter for $q = 0.9048$, $q = 0.6065$ and $q = 0.3679$ and a fixed horizon of $n = 10$.

The first step towards the origin is made with a triple pole location at $q = 0.6065$. The variance and mean of the upper-bound exponentially decrease with respect to $q = 9.9048$. The second and final step towards the unit circle is made with $q = 0.3679$ where the effect of a smaller pole diminishes. The estimation error marginally decreases, which can again be explained by the logarithmic decrease in upper-bound and estimation error. Reducing the polepairs further towards the origin will eventually diminish the estimation error and its

upper-bound, although it will impose a sensitivity trade-off as the filter will become more sensitive to sensor noise and uncertainties in the model and parameters.

The separate estimation results are shown in Figure 4-8. In these results it is found that, by placing the poles further towards the origin, it results in a scaled down estimation error. The asymptotic behavior of the estimation error remains, though the peak to peak amplitude is pushed down. By placing the poles on the origin, the estimation error can be minimized for this degree of freedom (essentially making a deadbeat filter). A practical use of this setting is however absent, as all noise and disturbances in the system will be amplified. Resulting in large sensitivity problems. As mentioned in Chapter 3, the augmentation of the pre-filter is designed to partially overcome this problem. This result is discussed in the next section.

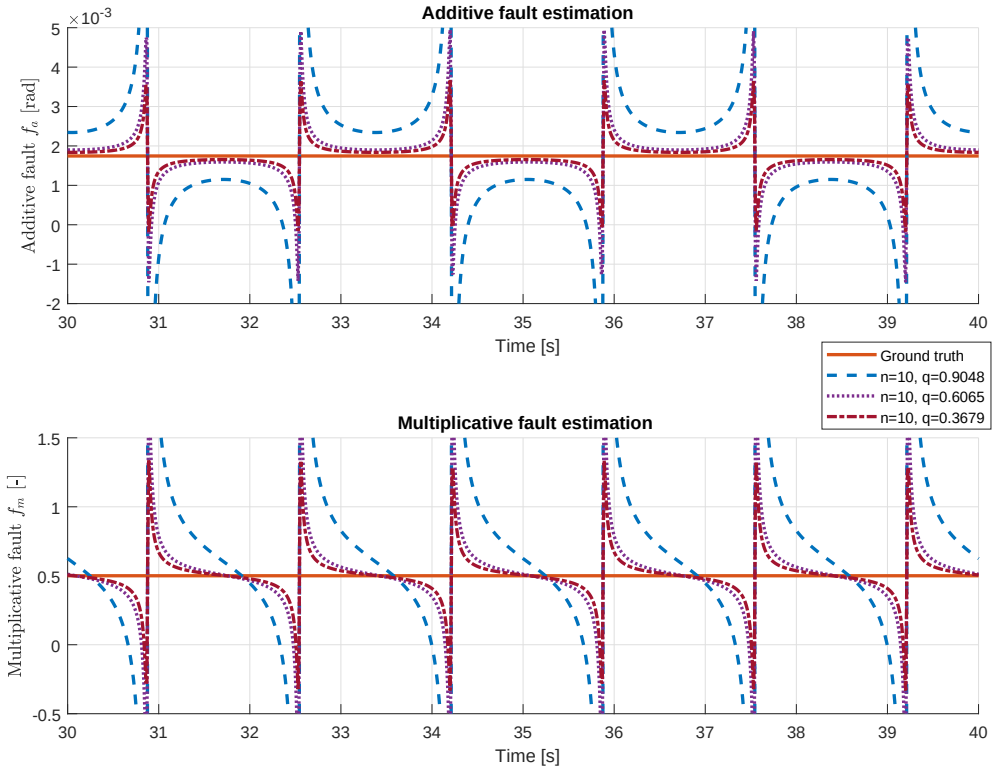

Figure 4-8: Separate fault estimation errors of the FI-filter for $q = 0.9048$, $q = 0.6065$ and $q = 0.3679$ and a fixed horizon of $n = 10$.

4-3-3 Application of the pre-filter extension

In Section 3-2, an extension to the non-linear isolation filter is introduced which deals with one of the big sources of error: the dynamical content of the mapping $f \mapsto r$. By exploiting the known relationship between the true fault and the residual, the input is pre-filtered to adjust itself to the dynamical behavior of the residual. As a result, the estimation error is only non-zero when the fault is time-varying. Seeing that we have made the assumption that

the faults appear in the real system as slowly time-varying signals, this method should show a definite improvement on the estimation error of the faults. The known input signal is filtered with the pre-filter (2.7) such that

$$\widetilde{\delta}_{set} = -\frac{N(q)F}{d(q)}[\delta_{set}],$$

where $\widetilde{\delta}_{set}$ is the case study equivalent of $\widetilde{E}(z)$ from (3.7). The pre-filtered signal is subsequently substituted in the regression operator (3.8) such that we find the non-linear isolation filter with augmented pre-filter, resulting in a new estimation result of the fault parameters

$$\begin{bmatrix} \widehat{f}_a \\ \widehat{f}_m \end{bmatrix} = \Phi_n[\widetilde{\delta}_{set}, r](k). \tag{4.13}$$

As for the non-linear isolation filter, the pre-filter augmented non-linear isolation filter has the following guaranteed upper-bound (3.9):

$$\underbrace{\left\| \begin{bmatrix} \widehat{f}_a(k) - \mu_n[f_a] \\ \widehat{f}_m(k) - \mu_n[f_m] \end{bmatrix} \right\|_2}_{\widetilde{\theta}_e} \leq \underbrace{\sqrt{\frac{1 + \left|\mu_n\left[\widetilde{\delta}_{set}\right]\right|}{nV_n\left[\widetilde{\delta}_{set}\right]}} \cdot (\widetilde{e}_1 + \widetilde{e}_2 + e_3)}_{\widetilde{\Theta}_e}, \tag{4.14}$$

$$\begin{aligned}
\widetilde{e}_1(k) =& \|\mathscr{O}_n X_M(k-n+1) - f^{\square}_{m_n}(k)\mathscr{O}_n X_E(k-n+1)\|_2 && (4.15)\\
&+ \|\mathscr{O}_n X_A(k-n+1) + \mathscr{T}_n f_{an}(k) - f_{an}(k)\|_2 && (4.16)\\
&+ \|(\mathscr{T}_n f^{\square}_{m_n}(k) - f^{\square}_{m_n}(k)\mathscr{T}_n)\|_2 \|\widetilde{\delta}_{set}\|_{\mathscr{L}_{n\infty}}(k),\\
\widetilde{e}_2(k) =& \sqrt{nV_n[f_m](k)} \cdot \|\widetilde{\delta}_{set}\|_{\mathscr{L}_{n\infty}}(k),\\
e_3(k) =& \sqrt{nV_n[f_a](k)}.
\end{aligned}$$

Following the observations in Corollary 3-2.2, we have thus created a filter which perfectly decouples the additive and multiplicative faults from the dynamical effect of the FD-filter. The resulting filter structure is shown in Figure 4-9. As for the non-linear isolation filter, simulations are performed to find ways of improving the performance for the pre-filter augmented non-linear isolation filter. A variation of the estimation horizon and pole location will show the tuning variables and their effect on the total estimation error.

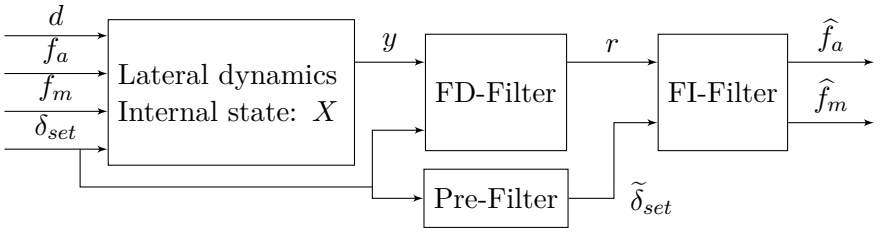

Figure 4-9: A visual representation of the FD-filter and FI-filter with augmented Pre-Filter in the case study.

Case 1: The horizon of the FI-filter

As for the non-linear isolation filter, the behavior of the pre-filter augmented isolation filter is simulated for different estimation horizons n. As a result, it is expected that there is only an estimation error when a change in fault is initiated. The time for which this estimation error is present is dependent on the estimation horizon n and the pole location of filter $d(q)$. This effect has been elaborated upon in Corollary 3-2.2. Figure 4-10 shows the simulation results for estimation horizons $n \in \{10,\ 100,\ 500\}$. The faults are initialized at the same condition as in the previous subsections $f_m = 0.5$ and $f_a = 0.1$deg, but are increased to $f_m = 0.6$ at $t = 40$s and $f_a = 0.12$deg at $t = 50$s during the simulation, to demonstrate the effect of a time-varying fault on the estimation error.

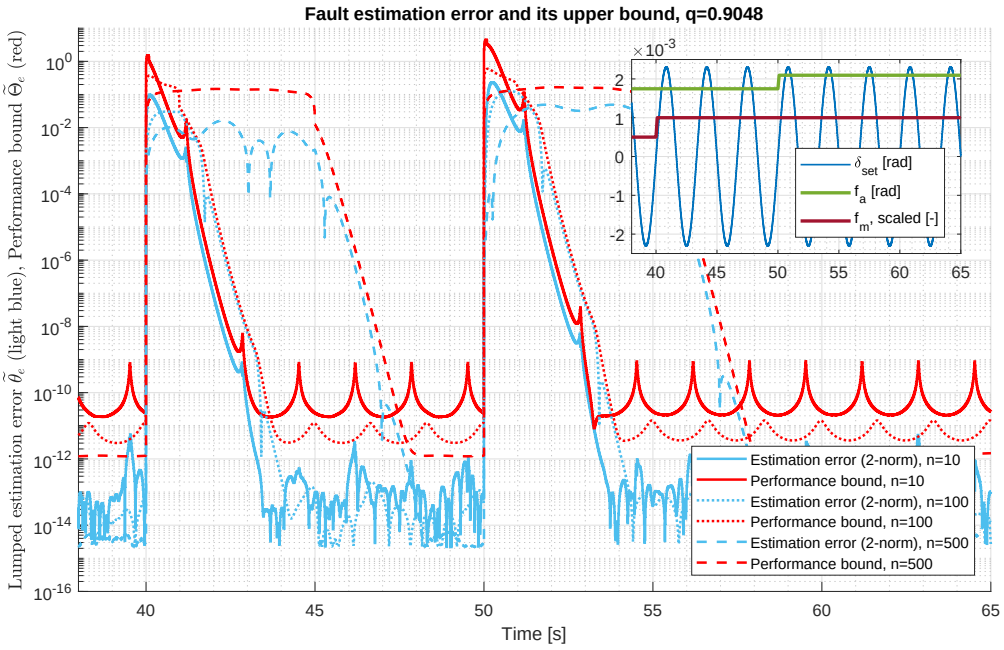

Figure 4-10: The estimation error $\widetilde{\theta}_e$ and the performance bound $\widetilde{\Theta}_e$ (as given in (4.14)) of the FI-filter with augmented pre-filter for $n = 10$, $n = 100$ and $n = 500$ for a fixed pole location of $q = 0.9048$.

For all estimation horizons, it becomes clear that for a constant fault the error diminished close to zero apart from a small numerical error. For all investigated estimation horizons, the upper-bound again provides a tight fit on the estimation error, hence it can be seen that from $n = 10$ to $n = 100$ and $n = 500$ the maximum estimation error keeps decreasing. However, in contrast to previous simulations (where the time-varying faults were not investigated), the estimation horizon directly affects the convergence time of the fault estimation as well. This effect can be observed in Figure 4-10. For an estimation horizon of $n = 500$ it takes the fault estimation much longer to converge (up to $6 - 7$s) in comparison to an estimation horizon of $n = 10$ which converges in roughly 2s and for which the convergence time is primarily governed by the pre-filter and residual dynamics.

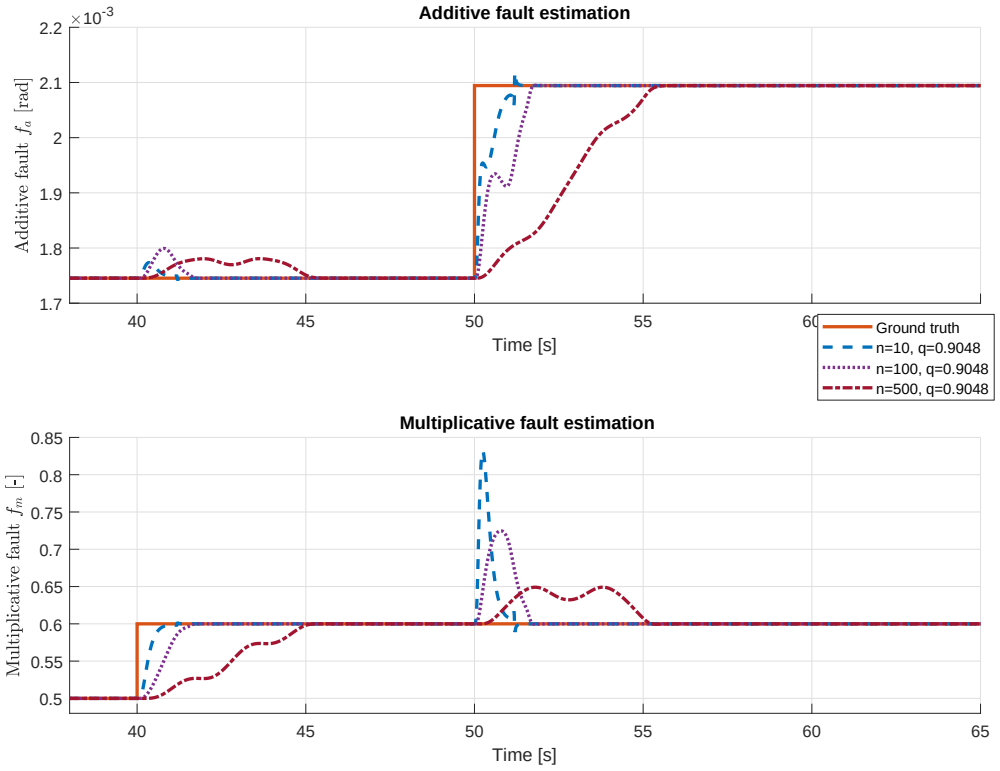

Figure 4-11: Separate fault estimation errors of the FI-filter with augmented pre-filter for $n = 10$, $n = 100$ and $n = 500$ for a fixed pole location of $q = 0.9048$.

The separate estimation results are shown in Figure 4-11. In these results it is found that the pre-filter has a striking effect with respect to the previous results. For $n = 10$ the faults converge within 1 to 2s after which the fault estimate remains settled. For $n = 500$ the estimation converges only after 5s. It becomes clear from these results a coupling is acting between the additive and multiplicative fault. The coupling effect results in so-called "false positives" for the detection of either the additive or multiplicative fault, whenever one or the other change over time. The effect of this coupling can be reduced by increasing the estimation horizon. Although, this will affect the convergence rate for time-varying faults and thus it will also increase the time for which the coupling will occur. The next subsection shows the effect of adjusting the polepairs of the FD-fiter and hence also of the pre-filter.

Case 2: The dynamics of the FD-filter

In Case 1, we came to the conclusion that for $q = 0.9048$ the convergence time to the true fault is around 2s due to the dynamics of the filter. In the following case the poles are placed further towards the origin to observe the effect on the convergence time and magnitude of the estimation error. The simulation results can be found in Figure 4-12 where the simulation case is the same as for the previous case in terms of time-varying faults.

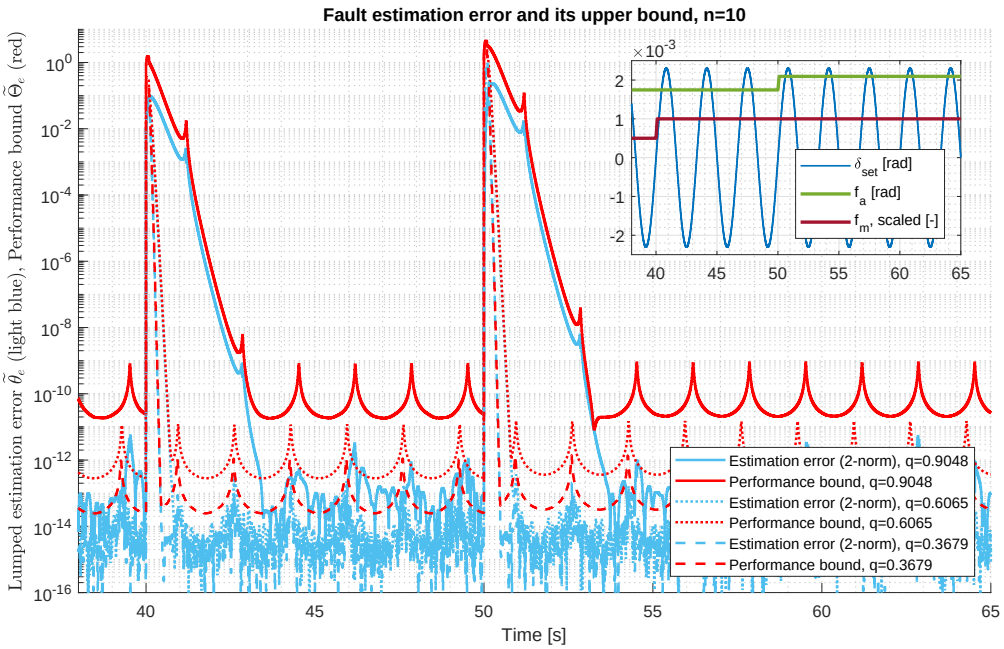

Figure 4-12: The estimation error $\widetilde{\theta}_e$ and the performance bound $\widetilde{\Theta}_e$ (as given in (4.14)) of the FI-filter with augmented pre-filter for $q = 0.9048$, $q = 0.6065$ and $q = 0.3679$ and a fixed horizon of $n = 10$.

For $q = 0.6065$ the estimation time decreases from 3s to 0.8s and the estimation error and its bound decrease with it. After shifting the poles to $q = 0.3679$, it can again be seen that the effect of placing the poles towards the origin shows an asymptotic behavior. The effect on the convergence time and magnitude exponentially diminishes. Placing the poles further towards the origin will again impose a sensitivity problem for which the filter will become less robust to noise and potentially unmodeled disturbances. Following the performance of the pre-filter with respect to the non-linear isolation filter the conclusion can be drawn that an estimation method has been developed which can reject unknown disturbances while perfectly estimating the fault parameters f_m and f_a. Furthermore, the guaranteed upper-bound provides a tool to find ways to push down the estimation error. Additionally, it can provide a tool for active fault isolation and fault tolerant control will be discussed in Chapter 6.

The separate estimation results are shown in Figure 4-13. In this final set of results, it is found that a reduction of the polepairs towards zero results, as expected, in faster convergence times. First, it can be seen that the convergence time exponentially decreases. The effects are large from $q = 0.9048$ to $q = 0.6065$, reducing the convergence time from 0.75s to 0.25s. Placing the poles to $q = 0.3679$ from $q = 0.6065$ has a reduced effect. Additonally, the trade-off that has previously been proposed still holds, a reduction towards the origin will result in high sensitivity problems. However, in these results an additional effect of the reduction of the polepairs becomes apparent. As the polepairs decrease towards the origin, the coupling effect during a change in multiplicative fault decreases. However, the coupling effect of a time-varying additive fault increases on the multiplicative fault. This could be explained

by the fact that the faults are implemented at the point where δ_{set} is highly time-varying. As a result of this phenomenon a high time-variation of the fault has a larger chance of being captured in the multiplicative fault (i.e., the cross-correlation between the input δ_{set} and the change in fault of f_a is high).

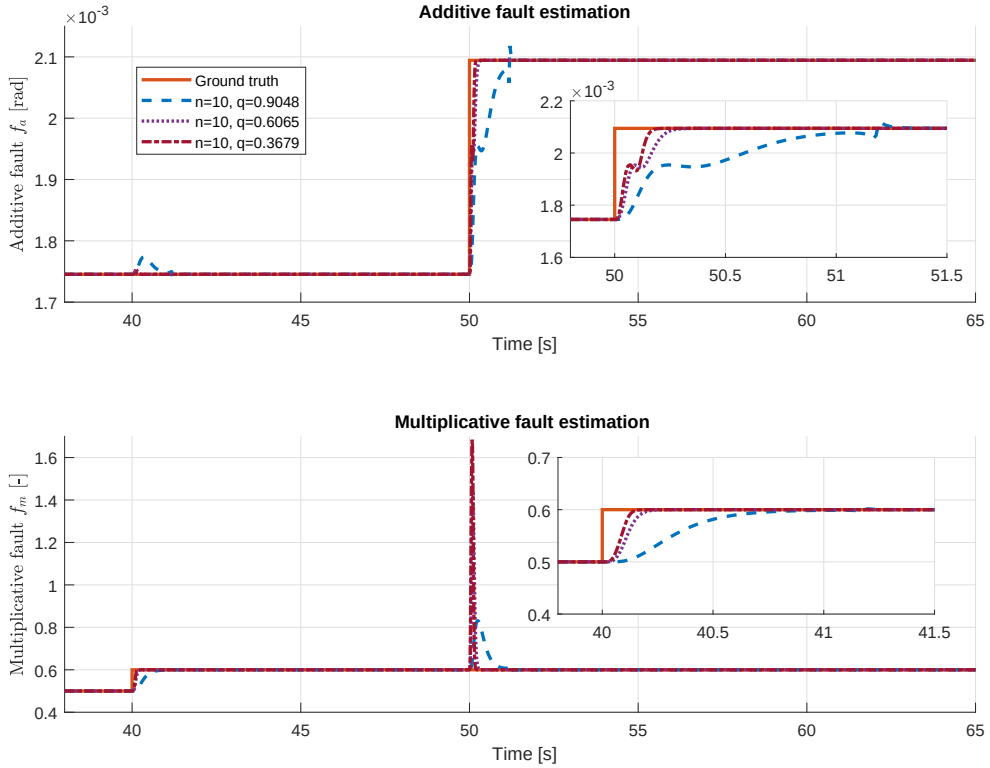

Figure 4-13: Separate fault estimation errors of the FI-filter with augmented pre-filter for $q = 0.9048$, $q = 0.6065$ and $q = 0.3679$ and a fixed horizon of $n = 10$.

4-3-4 Conversion to a linear parameter-varying filter

During highway lane-keeping it can never be guaranteed that the vehicle is driving at the same constant velocity, even though our developed filter only guarantees performance on the velocity at which it is synthesized. For this reason, the LPV FD-filter is developed in the main theorems. In Section 3-3 a LPV FD-filter synthesis method is given. Throughout this section, the methodology of actually applying such a filter on a real system and how the conditions of existence can be checked is provided. The section will end with simulations showing the performance with respect to the LTI FD-filter. The LTI system (4.4) is recast to a LPV system given that the longitudinal velocity is time-varying. When keeping the longitudinal velocity V_x as a linear acting variable, the system can be discretized as a function of V_x using

the notion of complete discretization analogous to the approach in [36]:

$$X(k+1) = \underbrace{e^{A(V_x)h}}_{\mathcal{A}_k} X(k) + \underbrace{\int_0^h e^{A(V_x)s} B ds}_{\mathcal{B}_k} \delta_{set}(k) + \underbrace{\int_0^h e^{A(V_x)s} B_f ds}_{\mathcal{B}_{f_k}} f(k) + \underbrace{\int_0^h e^{A(V_x)s} B_d(V_x) ds}_{\mathcal{B}_{d_k}} d(k),$$

$$y(k) = Cx(k).$$

As in (4.6) the discrete time-varying state-space representation $(\mathcal{A}_k, [\mathcal{B}_k \ \mathcal{B}_{d_k}], \mathcal{C}, \mathcal{D})$ can be used in the LPV DAE equation format (3.11)

$$\underbrace{\begin{bmatrix} -qI + \mathcal{A}_k & \mathcal{B}_{d_k} \\ C & 0 \end{bmatrix}}_{H_k(q)} \begin{bmatrix} x \\ \kappa \\ \sin(\phi) \end{bmatrix} + \underbrace{\begin{bmatrix} 0 & \mathcal{B}_k \\ -I & 0 \end{bmatrix}}_{L_k} \begin{bmatrix} \dot{\psi} \\ y_e \\ \psi_e \\ \delta_{set} \end{bmatrix} + \underbrace{\begin{bmatrix} \mathcal{B}_{f_k} \\ 0 \end{bmatrix}}_{F_k} [f_a] + \underbrace{\begin{bmatrix} \mathcal{B}_{f_k} \\ 0 \end{bmatrix}}_{F_k} [(f_m - 1)\delta_{set}] = 0. \tag{4.17}$$

Following the condition (3.15), a LPV filter can be found for the system if and only if

$$\text{Rank}\left(\begin{bmatrix} \bar{H}_k & \bar{F}_k \end{bmatrix}\right) > \text{Rank}\left(\bar{H}_k\right), \qquad \forall k.$$

This condition implies that for all possible feasible trajectories of the longitudinal velocity this condition should be checked. A question not solved in the theorems, is the tractibility of finding such a solution for the system in the case study. Using a symbolic solver, the state-space matrices can be discretized while keeping the longitudinal velocity as a variable. By defining for a third-order filter three variables ρ_i, $i \in \{1, 2, 3\}$, each representing a longitudinal velocity V_x at a different time instance (i.e., $\rho_1 = V_x(k-1)$, $\rho_2 = V_x(k-2)$, $\rho_3 = V_x(k-3)$), the rank condition can be rewritten as

$$\begin{aligned} &\text{Rank}\left(\begin{bmatrix} H_0(\rho_1) & H_1 & 0 & 0 & F_0(\rho_1) & 0 & 0 \\ 0 & H_0(\rho_2) & H_1 & 0 & 0 & F_0(\rho_2) & 0 \\ 0 & 0 & H_0(\rho_3) & H_1 & 0 & 0 & F_0(\rho_3) \end{bmatrix}\right) \\ &> \text{Rank}\left(\begin{bmatrix} H_0(\rho_1) & H_1 & 0 & 0 \\ 0 & H_0(\rho_2) & H_1 & 0 \\ 0 & 0 & H_0(\rho_3) & H_1 \end{bmatrix}\right), \qquad \forall \rho_1,\ \rho_2,\ \rho_3. \end{aligned}$$

Using this condition, it is symbolically validated that for any non-zero combination $\rho_1, \rho_2, \rho_3 \neq 0$, a solution to the LPV FD-filter exists for any positive real longitudinal velocity trajectory of the single-track model. As a result, the optimal filter can be found by the equation (3.17) and is written as

$$\bar{N}_k^*(\gamma) = \frac{1}{2} \bar{F}_{k_j}^\intercal (I + \gamma \bar{H}_k \bar{H}_k^\intercal)^{-1}.$$

The scheduling parameter γ represents the Lagrange multiplier and governs the duality gap of the filter with respect to the true optimal disturbance decoupling filter as has been discussed in Theorem 3-3.4. The variable j selects a row from the fault polynomial matrix. In a discrete-time scenario, it does not matter which row is chosen as long as it affects a part of the polynomial present in the final representation $N_k(q)F_k$. Given that the relative degree of

the output to the fault is equal to 1 and the $\deg(N_k(q)L_k) = 2$, this implies that only the first two rows of F_k play a role in the final transfer function $N_k(q)F_k$. Therefore, it can be guaranteed, that this will result in a first-order transfer function. The last step remaining for a fully functioning LPV filter for the case study, is multiplication by the inverse of the DC-gain of the fault transfer function as this will guarantee that the residual always converges to the magnitude of the true fault. As a result, the total implementation of the LPV filter from input to output can be written as

$$\frac{N_k(q)L_k(q)}{d(q)} \frac{-d(1)}{N_k(1)F_k(1)} \begin{bmatrix} y & \delta_{set} \end{bmatrix}^\intercal = r, \tag{4.18}$$

$$= \frac{N_k(q)F_k(q)}{d(q)} \frac{d(1)}{N_k(1)F_k(1)} [(f_m - 1)\delta_{set} + f_a]. \tag{4.19}$$

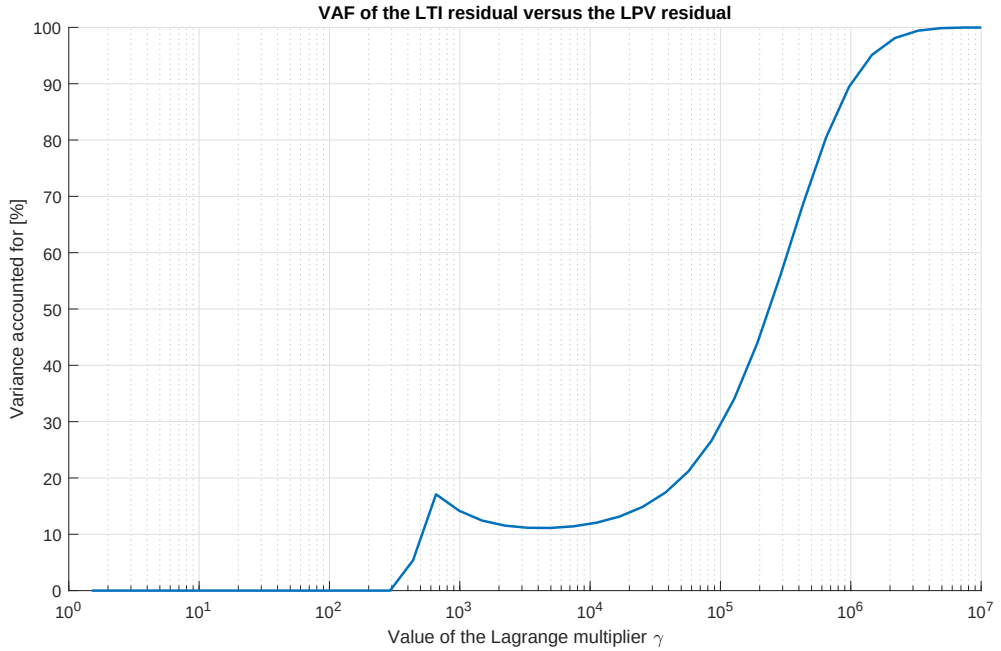

Figure 4-14: Effect on the variance accounted for of the LPV filter compared to an LTI filter for varying Lagrange multipliers γ.

To provide an intuition behind the effect of the magnitude of the Lagrange multiplier on the quality of the FD-filter, simulations have been performed over a range of numerically feasibile Lagrange multipliers for which the results are shown in Figure 4-14. As a performance measure, the Variance Accounted For (VAF) [37] is chosen in simulation conditions identical to Subsection 4-3-1. It can be seen that for $\gamma > 8 \cdot 10^6$ the LPV filter approaches the LTI result. At $\gamma = 10^7$ it is found that VAF = 99.98%. Hence, throughout the remainder of the simulations, this value for γ is chosen. Choosing a higher value will further increase the VAF (up to 100% for the multiplier going to infinity) but may also face numerical limitations. Now, a similar simulation study can be done as in Figure 4-3 but with a slowly time-varying longitudinal velocity V_x. Identical simulation conditions are chosen for faults and disturbances as in Subsection 4-3-3 but the longitudinal velocity is given a slowly varying sinusoidal

behavior. Figure 4-15 provides the results for this simulation; note that the disturbances are identical to Figure 4-3 and are hence omitted to avoid cluttered results.

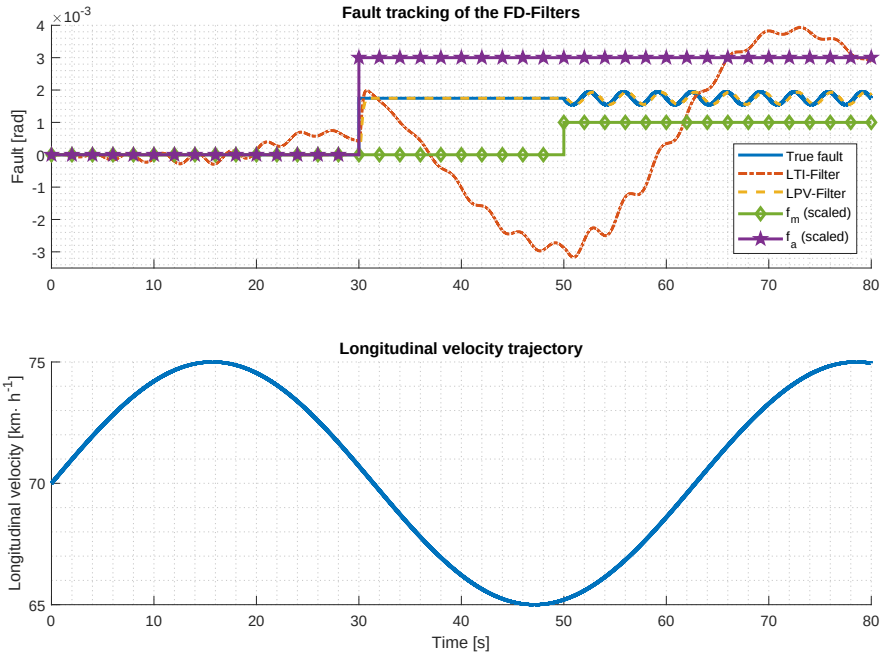

Figure 4-15: Simulation results of the detection of faults for a LTI FD-filter versus a LPV FD-filter for a time-varying longitudinal velocity.

In the simulation results, it is found that the LPV filter is decoupling the change in longitudinal velocity and is tracking the true fault similar to the LTI filter in Figure 4-3. The LTI filter has poor tracking behavior since it is synthesized at a velocity of $70\text{km} \cdot \text{h}^{-1}$ and is thus continuously stepping out of its linearized range. A very important note to the functioning of the LPV filter in this case study is related to the validity of the model under time-varying conditions. Longitudinal accelerations and deccelerations are caused by a longitudinal force acting on the tyres. However, the assumption has been made that this force is negligible and thus does not affect the yaw dynamics and tyre limits in a significant way. We therefore relax our assumption of constant longitudinal velocity to having a slowly time-varying longitudinal velocity for which the assumption on yaw dynamics still hold.

4-3-5 Fault isolation and parameter-varying detection, a unifying approach

A final step towards full implementation of the developed methods in an experimental setting lies in combining the best of both worlds. The non-linear FI-filter with the pre-filter can be used in combination with the LPV FD-filter to enable fault detection and isolation of a vehicle travelling at a non-constant longitudinal velocity. The approach is simple: as the non-linear FI-filter receives a fault residual, which is decoupled from the parameter-varying system behavior, this residual should be identical to the residual received from an LTI filter at constant velocity. The only aspect changing in the LPV scenario is the format of the

pre-filter, as this will also become an LPV filter with the I/O transfer function

$$\widetilde{\delta}_{set} = \frac{N_k(q)F_k(q)}{d(q)} \frac{d(1)}{N_k(1)F_k(1)} [\delta_{set}]. \tag{4.20}$$

As a result, a filter is created with a schematical representation as in Figure 4-16.

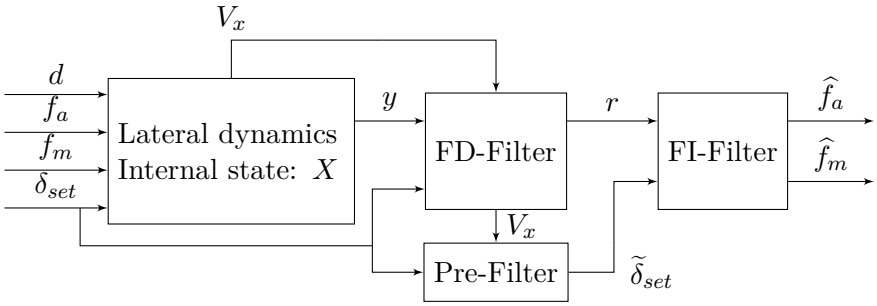

Figure 4-16: A visual representation of the LPV FD-filter and FI-filter with augmented LPV Pre-Filter in the case study.

No new guaranteed upper-bound is proposed for the combination of the two theorems combined. Regardless of the lack of a new upper-bound, the intuitions gained in the previous chapters for pushing down the estimation error still hold (as only $\tilde{e}_1$ (3.10a) is affected by the change of FD-filter). For this reason, the same simulations as in Subsection 4-3-3 are applied with the time-varying velocity as in Figure 4-15 and the results are briefly discussed. Instead now, since the awareness of adjustment of pole locations and estimation horizons is already present, we look at the effect of the value of the Lagrange multiplier on the degree of decoupling of the LPV filter. The results for this simulation can be found in Figure 4-17.

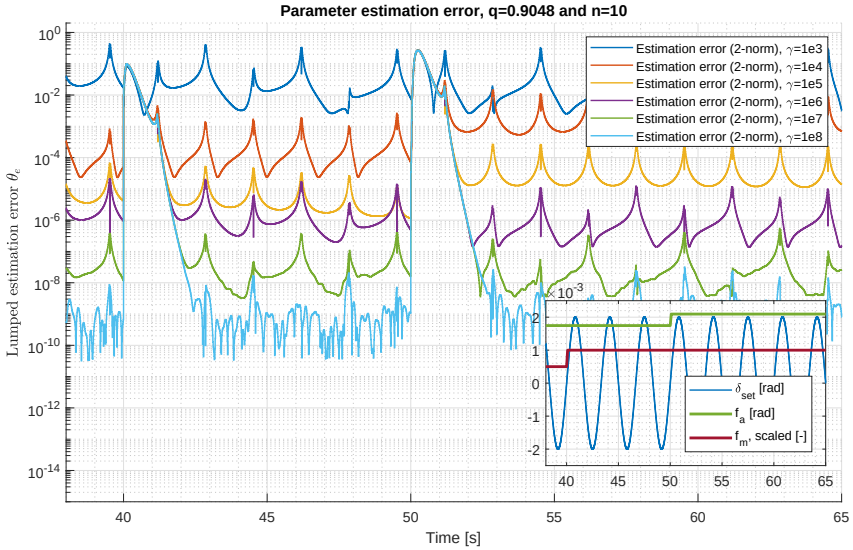

Figure 4-17: Performance of the LPV filter together with the pre-filter augmented non-linear isolation filter for varying Lagrange multipliers γ.

These results give an intuition behind our findings in Figure 4-14: low value Lagrange multipliers provide poor detection results and as a result poor isolation performance. For the previously chosen value $\gamma = 10^7$ it can be seen that the parameter-varying effect is not fully decoupled as are not as close to numerical precision as in the previous results, this performance could be improved by further increasing the multiplier towards infinity, though this will be limited by the numerical precision of the processor used. Nonetheless, this result shows that our hypothesis on the plug and play behavior of replacing the LTI FD-filter with a LPV FD-filter holds, fault isolation is achieved up to a high numerical accuracy.

4-4 Sensitivity analysis

A theoretical shortcoming of many model-based methods is that these rely on having accurate knowledge on the description of the model. For controllers, inaccuracies of this information could result in an unstable system, for observers it could result in poor estimates of the desired signals. In our specific scenario, an unaccurate model description could result in false positives or false negatives, i.e., detecting a fault occurence in the absence of one and vice versa. Considering the LTI scenario without loss of generality, the uncertainty in the model can be viewed in the DAE equation as

$$(H(q) + \Delta H(q))[x] + (L(q) + \Delta L(q))[z] + (F(q) + \Delta F(q))[f] = 0,$$

where $\Delta H(q)$, $\Delta L(q)$ and $\Delta F(q)$ are polynomial matrices caused by parameter or model mismatch between the true system and the modeled system. Hence, by finding an FD-filter satisfying conditions (2.4), the behavior of the system (2.3) is recast as

$$\mathcal{M} = \{z \in \mathcal{W}^{n_z} | N(q)L(q)[z] = -N(q)\Delta L(q)[z] - N(q)\Delta H(q)[x]\}, \tag{4.21}$$

and in the presence of a fault, the following description holds without and with uncertainty respectively

$$\begin{aligned} N(q)L(q)[z] &= -N(q)F(q)[f], \\ N(q)L(q)[z] &= \underbrace{-N(q)\Delta L(q)[z] - N(q)\Delta H(q)[x] - N(q)\Delta F(q))[f]}_{\Delta_f} - N(q)F(q)[f], \end{aligned}$$

such that Δ_f represents the total fault bias due to parameter uncertainty. From here it can be seen that not only is the uncertainty a function of the dynamics of the vehicle, it is also a function of the trajectories of x, z and f. Chapter 6 discusses some future propositions for this problem, though within the scope of this thesis it is only evaluated what the sensitivity for certain parameter changes is on the detected fault. The results of this sensitivity analysis can be used for tuning of the filter for the experimental work in the next chapter as well as showing a degree of robustness against parameter uncertainty. In Chapter 5, it is argued that the already occuring steering angle offset on the vehicle is 0.5deg, giving an idea how the false induced faults in this chapter compare with a realistic fault in the system. The sensitivity analysis is done by letting the single-track model drive in a steady-state cornering scenario at a constant longitudinal velocity, subsequently a constant fault of $f_a = 0.1$deg is injected and the ∞-norm between the true fault and the residual is evaluated to find a worst case "false fault". This false fault is only evaluated at the residual from the FD-filter. The corner radius

and banking angle are governed by the national legislation of highway construction [32] and are shown for the velocities of our interest in Table 4-2.

Bank angle [deg]	$120\text{km} \cdot \text{h}^{-1}$	$90\text{km} \cdot \text{h}^{-1}$	$70\text{km} \cdot \text{h}^{-1}$
1.43	1500m	700m	350m
1.72	1350m	630m	315m
2.00	1200m	560m	280m
2.29	1050m	490m	250m
2.58	900m	420m	215m
2.86	750m	350m	180m
3.15		340m	175m
3.43		330m	170m
3.72			165m
4.00			160m

Table 4-2: Highway legislation [32] for cornering radii and bank angles at a constant velocity V_x.

The lateral acceleration of the vehicle with respect to the road, caused by the centripetal force of the vehicle driving along a corner, can be denoted as

$$a_y = V_x^2 \kappa.$$

As a result, it can be found that the highest lateral accelerations during lane-keeping on a highway occur at $70\text{km} \cdot \text{h}^{-1}$, hence the set of cornering radii and bank angles for this velocity is used for simulation and extrapolated at the maximum bank angle of 4 degrees to allow a lateral acceleration up to $3\text{m} \cdot \text{s}^{-2}$. For the sensitivity analysis the effects of separately changing parameters is considered, hence the coupling of changing a specific parameter and its effect on another parameter is omitted as this will give better insight of the sensitivities of the single-track model in general.

First, the effect of a changing front and rear cornering stiffness is investigated. A loss or increase in tyre cornering stiffness can be induced by a loss of tyre-road friction, a change in tyre pressure or an increased or decreased vertical load (hence changing the friction coefficient following the effect tyre load sensitivity [31]).

The false fault is defined as the infinity norm of the residual over the simulation time. As a result, the false fault is not directional. The cornering stiffnesses have been increased and decreased up to 10% , the results of this set of simulations can be found in Figure 4-18. Note that for this simulation, only the front cornering stiffness C_f has been given an uncertainty. It has been found that the sensitivity for a change in rear cornering stiffness C_r is approximately the same and thus the result is omitted.

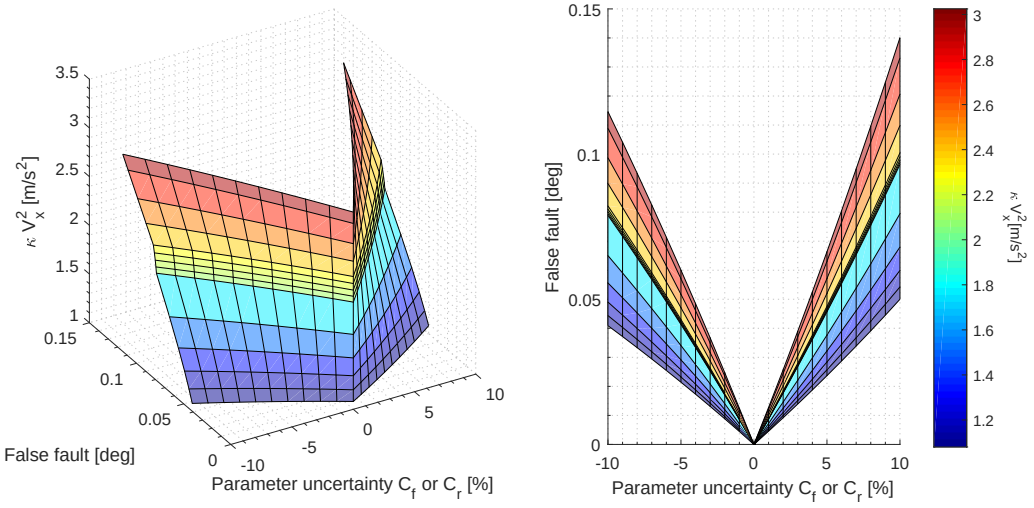

Figure 4-18: Sensitivity plot of the induced faulse fault by introducing an uncertainty in the cornering stiffness.

From Figure 4-18 it can be observed that for higher lateral accelerations the false fault has an increasingly larger sensitivity for parameter uncertainty. A maximum false fault of 0.14deg is introduced at a lateral acceleration of $3\text{m} \cdot \text{s}^{-2}$ for a 10% increase in cornering stiffness. A lower faulse fault is introduced for a percentualy decreasing cornering stiffness, this phenomenon can be explained using the definition of the understeer gradient

$$K_u = \frac{m_r}{C_r} - \frac{m_f}{C_f}, \tag{4.22}$$

where in (4.22) m_r represents the mass on the rear axle of the vehicle and m_f represents the mass on the front axle of the vehicle. An understeered vehicle ($K_u > 0$) provides in theory and practice a stable system and an oversteered vehicle ($K_u < 0$) results in an unstable vehicle above a critical longitudinal velocity defined by [31]

$$V_{\text{crit}} = \sqrt{\frac{g(l_f + l_r)}{K_u}}.$$

The vehicle is initially understeered and thus stable, hence if the magnitude of the front cornering stiffness becomes larger it results in a decreased understeer gradient. As a result, the vehicle becomes more unstable and thus results in more oscillatory state responses and thus higher false fault extrema, explaining the difference in an increase or decrease of the cornering stiffness. In the next simulation the yaw-inertia is increased and decreased with 10% while keeping the center of gravity at the same location, the results are shown in Figure 4-19. In Figure 4-19, it can be observed that the result of an increasing or decreasing yaw-inertia on the center of gravity location has a minor impact on the introduced faulse fault. This can be explained from the perspective that a higher yaw inertia results in a slower lateral response of the vehicle and as a result lower state extrema and lower faulse fault extrema, from a different perspective a change in yaw inertia results in the scaling of a row in the continuous time A matrix, hence it could result in a small or negligible effect on the null-space of the discrete time $H(q)$ polynomial matrix.

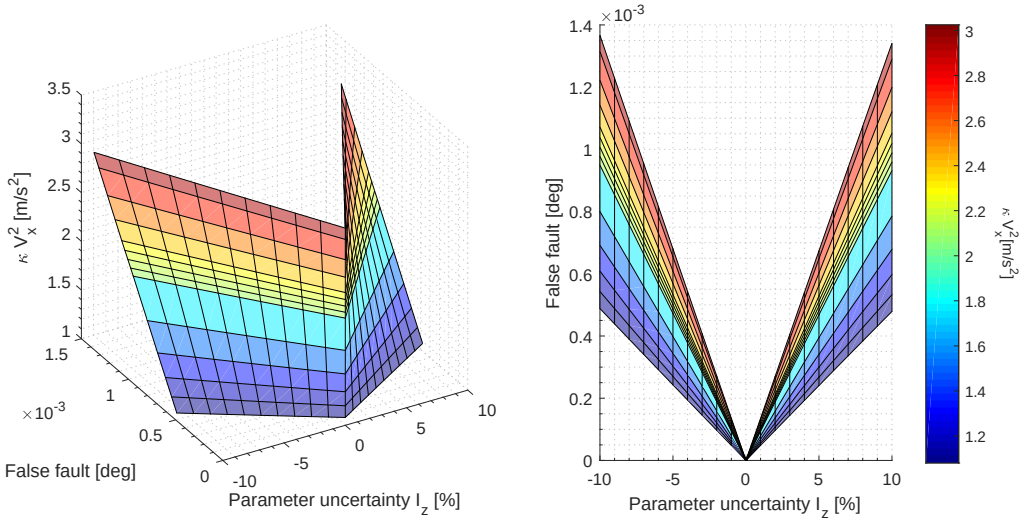

Figure 4-19: Sensitivity plot of the induced faulse fault by introducing an uncertainty in the yaw inertia.

Sensitivities for increasing or decreasing the mass of the vehicle at the center of gravity have been evaluated, but have been found to result in differences of 10^{-11}deg at a maximum of 10% uncertainty and is hence omitted from the results. A more realistic scenario is an addition of a point-mass on a different point than the center of gravity. For the following and final sensitivity simulation a point mass of 200kg, representing the addition of persons or luggage in the vehicle, is added from an increasing distance from the center of gravity towards the rear of the vehicle. The results for this analysis are shown in Figure 4-20.

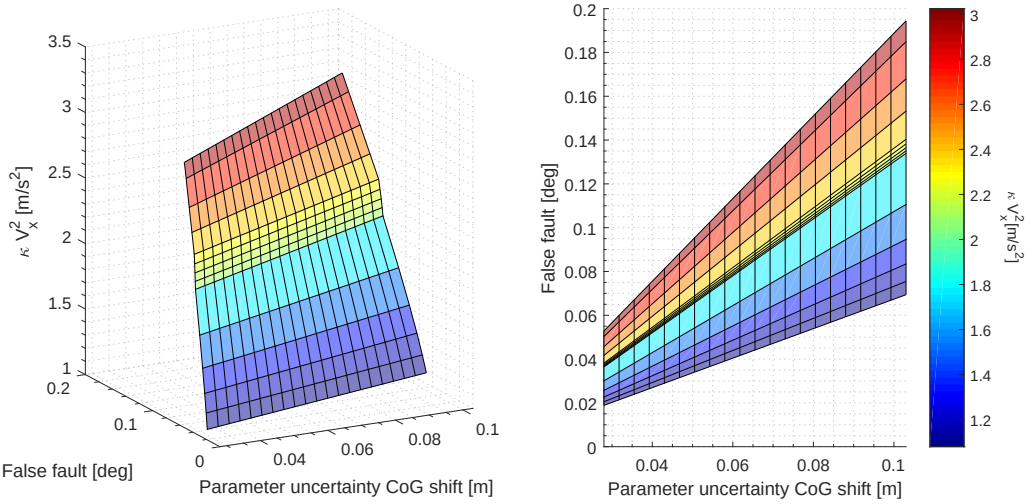

Figure 4-20: Sensitivity plot of the induced faulse fault by introducing an uncertainty in the center of gravity location.

The vehicle grows further to instabillity as it's understeer gradient (4.22) decreases for a

higher mass towards the rear axle, furthermore looking at the appearance of the center of gravity location in the lateral dynamics (4.4) it can be argumented that a shift of center of gravity location results in a non-trivial change in the nullspace of $H(q)$, resulting in a relatively high sensitivity for this parameter. The results from this sensitivity analysis show that for high parameter deviations the false induced fault can grow up to $0.1 - 0.2$deg. Comparing this to a realistic offset of 0.5deg from Chapter 5 makes it an acceptable error dependent on the purpose of the estimated faults, using it in a form of feedback control could result in steady-state errors, while for pure detection purposes it could be rejected as being a true fault due to its potentially highly time-varying behavior as a result of the sensitivity for the state, disturbance, output, input and fault signals. All of these arguments are extended in Chapter 6 as a proposition for future works towards useful applications of the developed methods in this thesis.

4-5 Discussion on the case study

In this chapter, the developed theoretical framework from Chapter 3 has been applied on the case study as proposed in the introduction in Chapter 1 (fault detection and isolation in the lateral control of an autonomous vehicle).

First, the boundary conditions and system parameters have been defined for the autonomous vehicle. The boundary conditions and parameters provided a set of admissible inputs for the simulations in the remainder of the chapter. Subsequently, the system model was introduced which was shown to be easily adaptable to the developed framework in Chapter 3.

In the following section, a baseline FD-filter was created with the provided system model. The developed FD-filter was to fullfil the criteria set for an appropriate FD-filter in Chapter 3 (i.e., the rejection of unkown states and disturbances while remaining sensitive to the fault).

Following the applied design methodology of the FD-filter, the FI filter has been demonstrated. By applying the theorems of the non-linear isolation filter to the case study system, combined with the valid FD-filter design, a full combined filter could be demonstrated. The performance bound was shown to be valid and was shown to be a useful tool in tuning of the filter for different purposes. Application of the filter combination showed a high sensitivity for the pole-placement of the FD-filter, as was expected from the performance bound shown in Section 3-1. This problem was shown to be solved in the subsequent section.

In the next section, the pre-filter was designed for the case study. Simulation of the isolation flter with augmented pre-filter showed that for a constant fault scenario the estimate converges to the true fault in finite time (approximately as fast as the estimation horizon is long, dependent on the pole location). An increasing horizon decreased the convergence rate while also decreasing the maximum amplitude of the error. The simulation results further showed that a coupling occurs between the additive and multiplicative fault if either of them are time-varying. The effect of this coupling can be manipulated by changing the estimation horizon or pole location.

In the following section, the LPV FD-filter was created for the case study system, where the

parameter variation is caused by a time-varying longitudinal velocity. Simulations showed that the parameter-varying effect is fully decoupled for the LPV filter whereas the quality of the residual of the LTI filter was dramatically reduced. Following up this result, the LPV filter was combined with the non-linear isolation filter with augmented pre-filter. No new upper-bound was generated for this case. These simulations for this case yielded positive results, for a parameter-varying system the additive and multiplicative fault were correctly detected and isolated. The aforementioned results lead to the conclusion that a method has been developed wiich satisfies the problem statement.

Finally, a sensitivity nalysis has been applied on the FD filter to find the primary sensitivities for model deviations in the filter design. The sensitivities have been determined by using a physically intuitive test-case, showing that the main sensitivities were governed by balance of the vehicle (i.e., the longitudinal center of gravity location and the front and rear lumped cornering stiffnesses).

Chapter 5

Experimental Results

In the previous chapters, theorems have been created that solve the main problem statement of the thesis research. Subsequently, these theorems have been applied in the the case study in lateral control for autonomous vehicles. Additionally, an elaboration has been given on the case study under investigation and how the proven theorems can be applied in this case study. Using simulations for the case study, promising results were shown for the fault detection and isolation for lateral control of autonomous vehicles. To strengthen the conclusions from these simulations, the developed methods were experimentally validated on a Toyota Prius (model 2010). This chapter will start with overview of the experimental setup in Section 5-1. Subsequently, in Section 5-2, a set of methods is given to incorporate the sensor and actuator delays delays and measurement inaccuracies in the filter. Finally, in Section 5-3 the experimental results of the tests are shown and discussed.

5-1 Experimental setup

A modified front-wheel driven Toyota Prius from 2010 has been used to perform the experimental tests. The vehicle is a modified version from the original, as it is equipped with Rapid Control Prototyping (RCP) hardware to enable on the fly testing of controllers and observers. All the measurements mentioned in (4.4) are available over the vehicle Controller Area Network (CAN) bus and can thus be used for the testing of our filters. First, the equipment of the vehicle and the vehicle itself are elaborated upon and subsequently the test area and the experiments are elaborated.

5-1-1 Vehicle and sensors

The FDI-filter is implemented on a Speedgoat Real-Time Target Machine (Figure 5-2). Use of this platform allows building a Simulink model and Matlab code directly on the vehicle using code generation. All the required actuation for the Toyota Prius, i.e., the driveline and the Electrical Power Steering (EPS) steering actuator, are originally manufactured by Toyota

and are identical to the standard actuation in commercially available vehicles. The lateral controller is toggled through the Human Machine Interface (HMI) (Figure 5-1) and the faults are injected through the external mode Simulink interface.

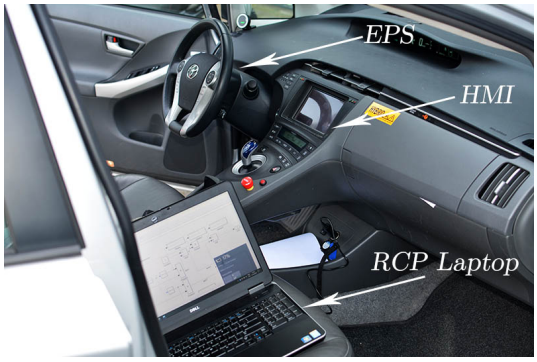

Figure 5-1: Interior of the vehicle.

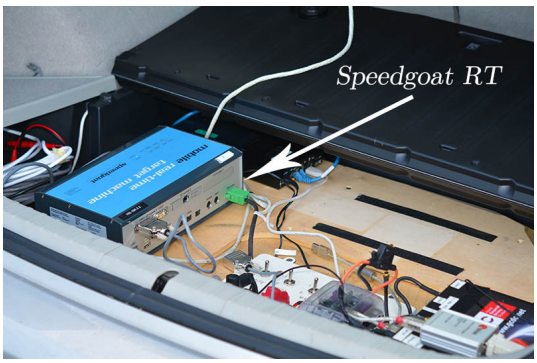

Figure 5-2: Controller platform of the vehicle.

The model outputs used in the design of the filter are either measured or estimated by the internal hardware of the vehicle and a Mobileye camera. The measurements and their sources are given as

- Yaw rate $\dot{\psi}$, measured internally by the vehicle using the original yaw-rate sensor of the vehicle,
- Longitudinal velocity V_x, estimated internally using the velocity of the non-driven rear wheels,
- Heading error with respect to the lane ψ_e, measured by the Mobileye camera,
- Lateral error with respect to the lane y_e, measured by the Mobileye camera,
- Controller setpoint δ_{set} before fault injection, provided as an output from the lateral controller,
- Ground truth of the injected faults f_a and f_m.

The accuracy and delay of the sensors introduce a few fundamental problems in the correct functioning of the FDI-Filter. These problems are solved using the methods from Section 5-2.

5-1-2 Testing location

Ideally, the tests are performed in a highway scenario. In such a scenario, the robustness of the filter can be tested at a high velocity with bank angle and curvature disturbances, although this could introduce dangerous scenarios. Not only are the lateral control methods of the vehicle not yet homologated for public road use, it would be irresponsible to deliberately introduce faults on the vehicle in these public scenarios. Therefore the tests have been performed at an isolated test area behind the VeHIL lab at TNO Automotive location

Helmond. A 100 meter long straight with ISO road lining is used such that the Mobileye lane measurements can be taken and thus lateral control can be applied. These conditions make the use of the FDI method slightly more complex as the maximum velocity during the tests is limited to $30\text{km} \cdot \text{h}^{-1}$ to $40\text{km} \cdot \text{h}^{-1}$. With respect to the design case (4.2) this results in a significantly lower excitation (i.e. lower $V_n\left[\delta_{set}\right](k)$) of the vehicle in a lateral control scenario, which could deteriorate not only the isolability of the FI-filter but also the measurement accuracy of the sensors. Moreover due to a limited distance and minimum required time for the Mobileye camera to detect the lanes, a limited distance is available to introduce and detect the fault. As a result of these last few remarks, the functioning of the filter is tested in challenging conditions.

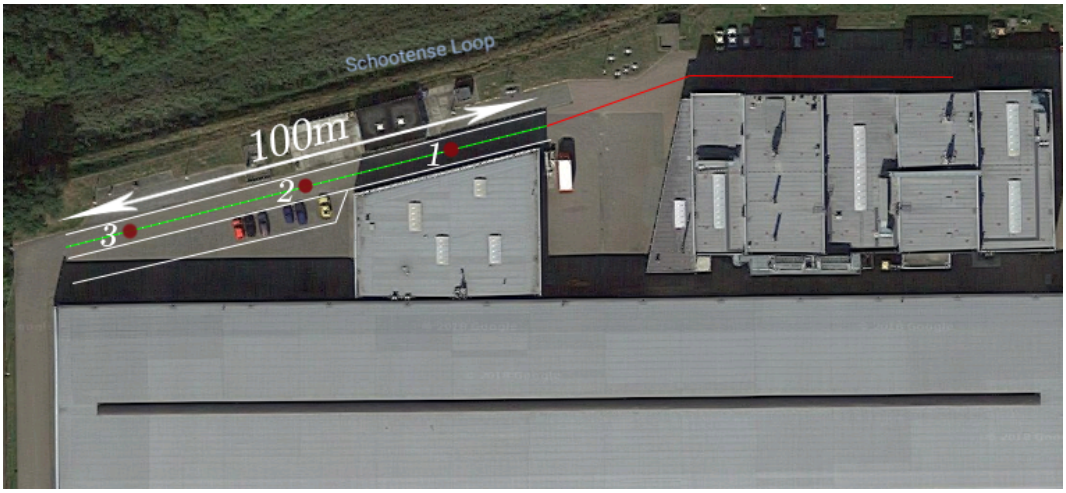

Figure 5-3: Test trajectory for the experimental tests (source: Google Maps).

Figure 5-3 shows the trajectory driven during the experimental test. The red line shows the trajectory without lane-marking, used to get the vehicle up to the desired starting velocity. The white line represents the side markings of the lane and the green line represents the center marking and thus the reference path for the vehicle. At point 1, the Mobileye module of the vehicle has detected the lanes and thus the vehicle can switch to autonomous lane-keeping through the HMI interface. At point 2, the fault is introduced in the reference steering angle of the vehicle through the Simulink interface. At point 3, the vehicle has to slow down to a halt as the end of the test-track is approaching. Under braking action the vehicle aborts the autonomous lane-keeping. As a result, controller setpoints are no longer given and therefore the fault estimatio algorithm is switched off.

5-2 Implementation, problems and solutions

In the experimental tests, it was found that real-life uncertainties such as sensor delay and inaccuracies caused poor results in the detection and isolation algorithms. As a result, in this section a systematic framework is proposed and applied to mitigate the effects of these uncertainties and take them in to account in the design of the filter itself. This section will cover systematic proposals for mitigating delays and for improving measurement quality.

5-2-1 Measurement delay

The camera measurements have been identified by TNO to have a measurement delay of 0.15s. On a sampling frequency of 100Hz this is a significant delay of 15 samples and thus it could cause inaccuracy in the residual signals, leading to poor isolation results. This delay is caused by the perception of the camera, i.e., converting the images of the road to physical distance or heading quantities. To mitigate the effect of measurement delay, a systematic approach is given to take into account the effect of this delay. The measurement delay is incorporated by modelling the effect in the state-space equations of the single-track model. To prevent clutter of the equations, the modeling approach is given using a scalar system with minimal realization $(a, b, c, 0)$ in the absence of disturbances and faults. The delay can be modeled as

$$\begin{bmatrix} X(k-w+1) \\ X(k-w+2) \\ \vdots \\ X(k-1) \\ X(k) \\ X(k+1) \end{bmatrix} = \begin{bmatrix} 0 & 1 & 0 & \dots & 0 & 0 \\ 0 & 0 & 1 & \dots & 0 & 0 \\ \vdots & \vdots & \vdots & \ddots & \vdots & \vdots \\ 0 & 0 & 0 & \dots & 1 & 0 \\ 0 & 0 & 0 & \dots & 0 & 1 \\ 0 & 0 & 0 & \dots & 0 & a \end{bmatrix} \begin{bmatrix} X(k-w) \\ X(k-w+1) \\ \vdots \\ X(k-2) \\ X(k-1) \\ X(k) \end{bmatrix} + \begin{bmatrix} 0 \\ 0 \\ 0 \\ \vdots \\ 0 \\ b \end{bmatrix} u(k),$$

$$y = \begin{bmatrix} c & 0 & 0 & \dots & 0 & 0 \end{bmatrix} \begin{bmatrix} X(k-w) \\ X(k-w+1) \\ \vdots \\ X(k-2) \\ X(k-1) \\ X(k) \end{bmatrix},$$

where w represents the total output delay in the system. The delay augmented state-space matrices can be used in the FD-Filter synthesis, resulting in a filter with a minimal order of $\deg(d^{-1}(q)N(q)L(q)) = 3+w$. The order of the filter increases since the relative degree of the disturbance κ to the output increases by t timesteps and thus requires a higher order filter to be rejected.

5-2-2 Measurement accuracy

The available measurements are assumed to have a perfect accuracy in Chapter 4. In the experimental scenario this assumption unfortunately does not apply. The camera measurements are logged at a sampling frequency of 10Hz and internally interpolated and resampled to a sampling frequency of 100Hz. The yaw rate sensor can be accurate for relatively high yaw rates, but in the low excitation scenario the magnitude the measurement is highly affected by amplitude quantization (see Figure 5-4). To condition the signals to better correspond to the true dynamics of the vehicle, a simple first-order low-pass filter is applied to the measurement data

$$G(q) = \frac{a_0}{q + a_1}, \tag{5.1}$$

where the DC-gain of this filter is set to 1 (such that $a_0 - a_1 = 1$). As a result, the original measurements and filtered measurements can be shown as in Figure 5-4.

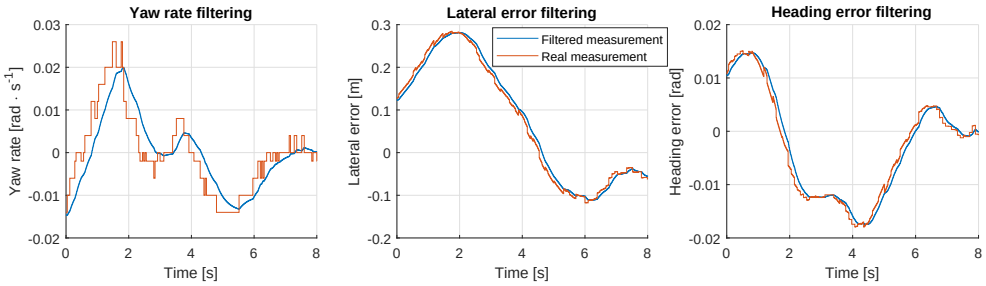

Figure 5-4: Original vehicle measurements and their filtered versions.

Group delay is an inherent effect of signal filtering. For this reason, the low-pass filter dynamics can be modeled in the FD-filter as well to take in to account these frequency dependent delays. A scalar system with minimal realization $(a, b, c, 0)$ in the absence of disturbances and faults is chosen to support these results. The low-pass filter from (5.1) is practically implemented using a series state-space representation as

$$\begin{bmatrix} X(k+1) \\ G(k+1) \end{bmatrix} = \begin{bmatrix} a & 0 \\ a_0 c & -a_1 \end{bmatrix} \begin{bmatrix} X(k) \\ G(k) \end{bmatrix} + \begin{bmatrix} b \\ 0 \end{bmatrix} u(k),$$
$$y = \begin{bmatrix} 0 & 1 \end{bmatrix} \begin{bmatrix} X(k) \\ G(k) \end{bmatrix},$$

where the signal $G \in \mathbb{R}$ represents the state of the low-pass filter $G(q)$. Incorporating the dynamical effects of the first-order low-pass filter increases the degree of the filter by one, as it requires an additional past measurement of the plant output to maintain causality of the filter.

5-2-3 Input delay

The third and final uncertainty to incorporate in the filter design is caused by the I/O behavior of the EPS of the Toyota Prius. As discussed in [38], the EPS system of the Toyota Prius has an input output delay of 0.1s. The delay can be modeled in the scalar minimal realization $(a, b, c, 0)$ as

$$\begin{bmatrix} X(k+1) \\ u(k-d+1) \\ u(k-d+2) \\ \vdots \\ u(k-1) \\ u(k) \end{bmatrix} = \begin{bmatrix} a & b & 0 & 0 & \dots & 0 \\ 0 & 0 & 1 & 0 & \dots & 0 \\ 0 & 0 & 0 & 1 & \dots & 0 \\ \vdots & \vdots & \vdots & \vdots & \ddots & \vdots \\ 0 & 0 & 0 & 0 & \dots & 1 \\ 0 & 0 & 0 & 0 & \dots & 0 \end{bmatrix} \begin{bmatrix} X(k) \\ u(k-d) \\ u(k-d+1) \\ \vdots \\ u(k-2) \\ u(k-1) \end{bmatrix} + \begin{bmatrix} 0 \\ 0 \\ 0 \\ \vdots \\ 0 \\ 1 \end{bmatrix} u(k).$$

Since the input at time instance k is modeled to be dependent on the fault at time instance k, a delay of the input results in the delay of the fault. An additional delay of the fault of 10 samples results in an increase relative degree of the fault to the output. Therefore, the minimal order of the filter increases by the number of sample delays added for the steering input. This final uncertainty augmentation gives us, combined with the other model techniques, a systematic methodology to adapt the FDI techniques to the experimental uncertainties.

5-3 Results

Following the results from Section 5-2, the uncertainty augmented vehicle model can be used to estimate the faults introduced in the steering control signal of the vehicle. Due to the many degrees of freedom for the filter design, it is chosen to freeze the model parameters and the FD-filter settings. The only remaining degrees of freedom are the pole locations for the first-order low-pass filters for the measurements of the vehicle. The settings for the filter, used for each experimental dataset, can be found in Appendix C. After evaluation of the experimental results, which were limited by the maximum time-span of the available measurements (imposed by the testing location as elaborated in Section 5-1-2), the FI-filter horizon is frozen at $n = 200$ steps. The FD-filter pole location is set to $q = 0.9$.

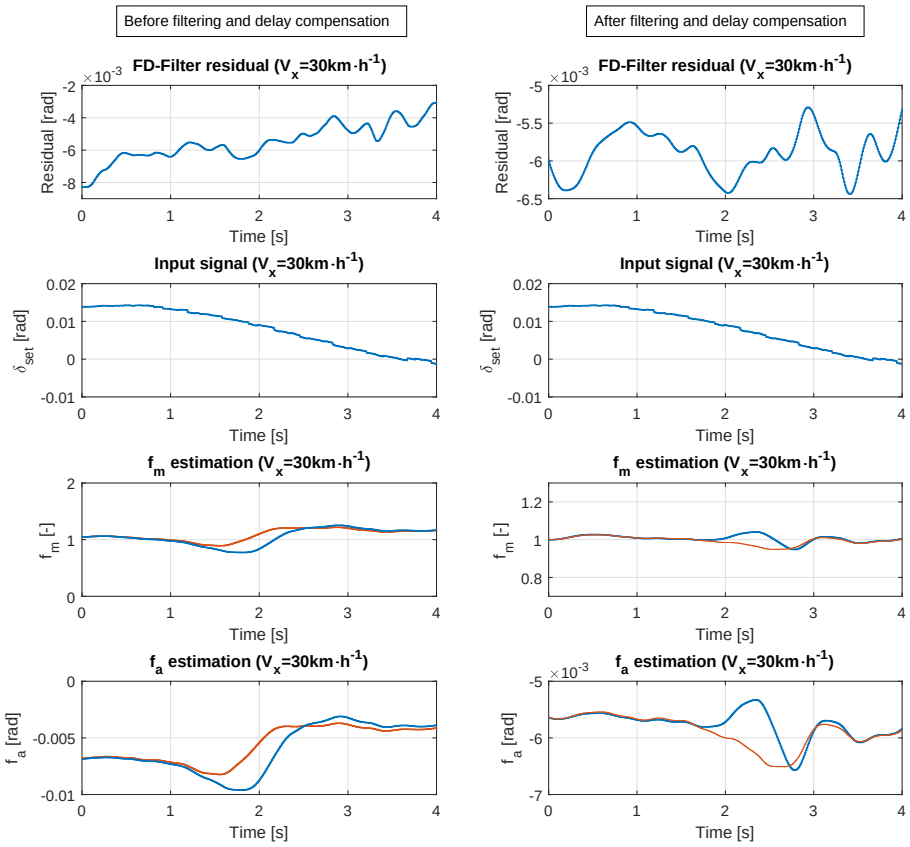

Figure 5-5: Experimental results for a testing velocity of $30\text{km} \cdot \text{h}^{-1}$ and no injected fault.

In the experimental tests it is assumed that the vehicle parameters from Table 4-1 correspond to the true parameters of the test vehicle. Furthermore, it is assumed that no physically related multiplicative fault is acting on the vehicle throughout the tests, though it can not be assumed that the additive fault is equal to zero. In previous tests done by TNO with the same testing vehicle, it has been found that the vehicle has a steering angle offset of around 0.36deg acting on the system. Calibration tests have been done with the vehicle at a constant

velocity. During this test, no external faults are introduced. As a result, the initial vehicle-related offset and multiplicative fault can be determined. The results of this test can be found in Figure 5-5. The results without measurement filtering and I/O delays do not give much of an insight as the residual drifts over the entire measurement. After compensation, it is found that there is an additive fault acting on the system wth a mean of 0.34deg (see f_a estimation in Figure 5-5). This value is fed back into the vehicle as a compensation to prevent this static offset from showing in the experimental results where the fault are artificially injected.

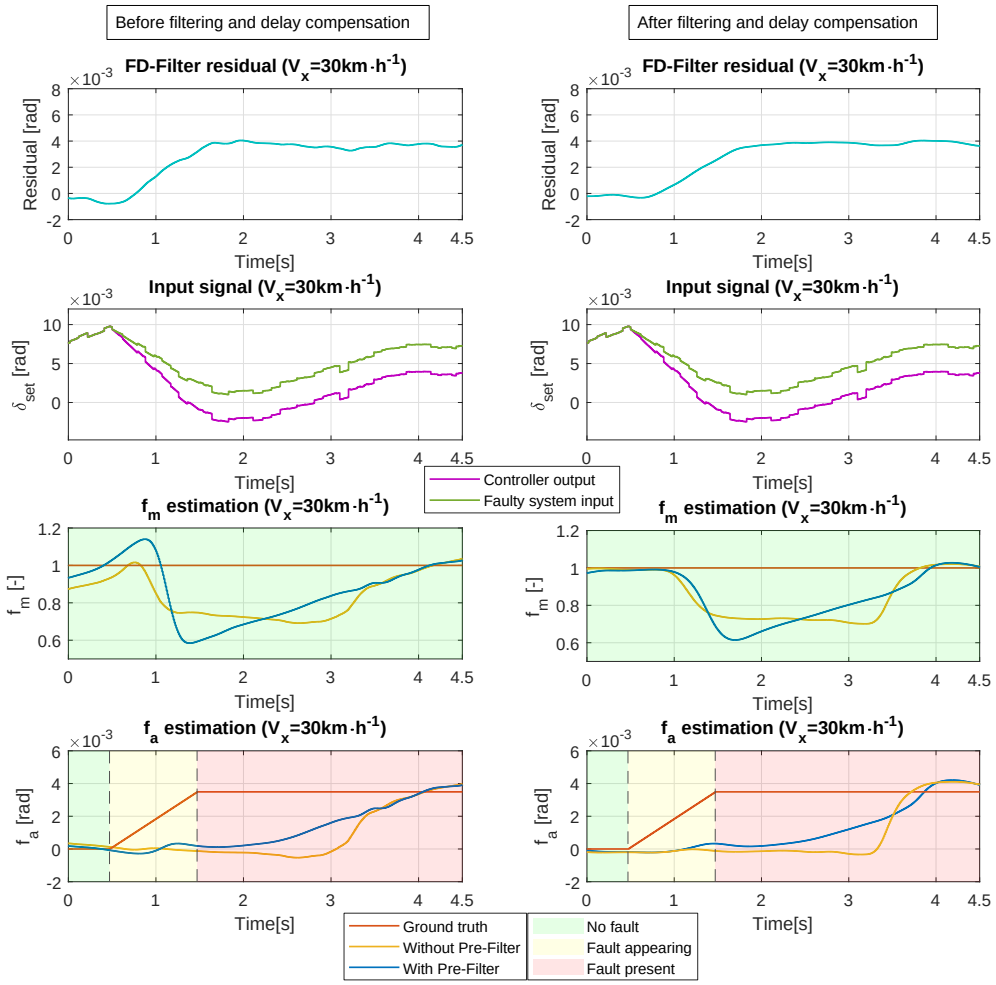

Figure 5-6: Experimental results for a testing velocity of $30\text{km} \cdot \text{h}^{-1}$ and an injected fault of $f_a = 0.2\text{deg}$.

Further remarks about the results can not be made as the fault is constant and the excitation is low. For this reason the non-linear isolation filter, with or without pre-filter, isolates the additive fault f_a. The first three experimental results are obtained at a longitudinal velocity of $30\text{km} \cdot \text{h}^{-1}$. The first test experimental test shows the introduction of an additive fault in the system during lane-keeping and is shown in Figure 5-6. The isolation result of the multiplicative fault from Figure 5-6 shows that without augmentation of the input-/output delays and signal filters the isolation performance is affected by disturbances. Despite the poor

estimation of f_m, the residuals provide a distinct detection signal of the additive fault and the isolation performance of the additive fault tracks the true additive fault. After modification of the single-track model with I/O delays and low-pass filters on the plant measurements, the isolation performance of the multiplicative fault is improved and only deviates from its true value once a change in the additive fault is detected. Once the estimation of the additive fault is complete, the multiplicative fault returns to its original value. It can be observed that due to a low excitation, the coupling between f_a and f_m is high in the transient behavior. Following the lessons learned in Chapter 4, this could be solved by increasing the variance of the input signal or increasing the estimation horizon. Although, neither of the two options were feasible in the experiment due to a limited distance to drive. Not many conclusions can be drawn regarding the performance of the pre-filter in this set of results, as the dynamical content of the input signal is very low and thus the error induced by the dynamics of the FD-filter is small. The next experimental data set shows the introduction of a multiplicative fault in Figure 5-7.

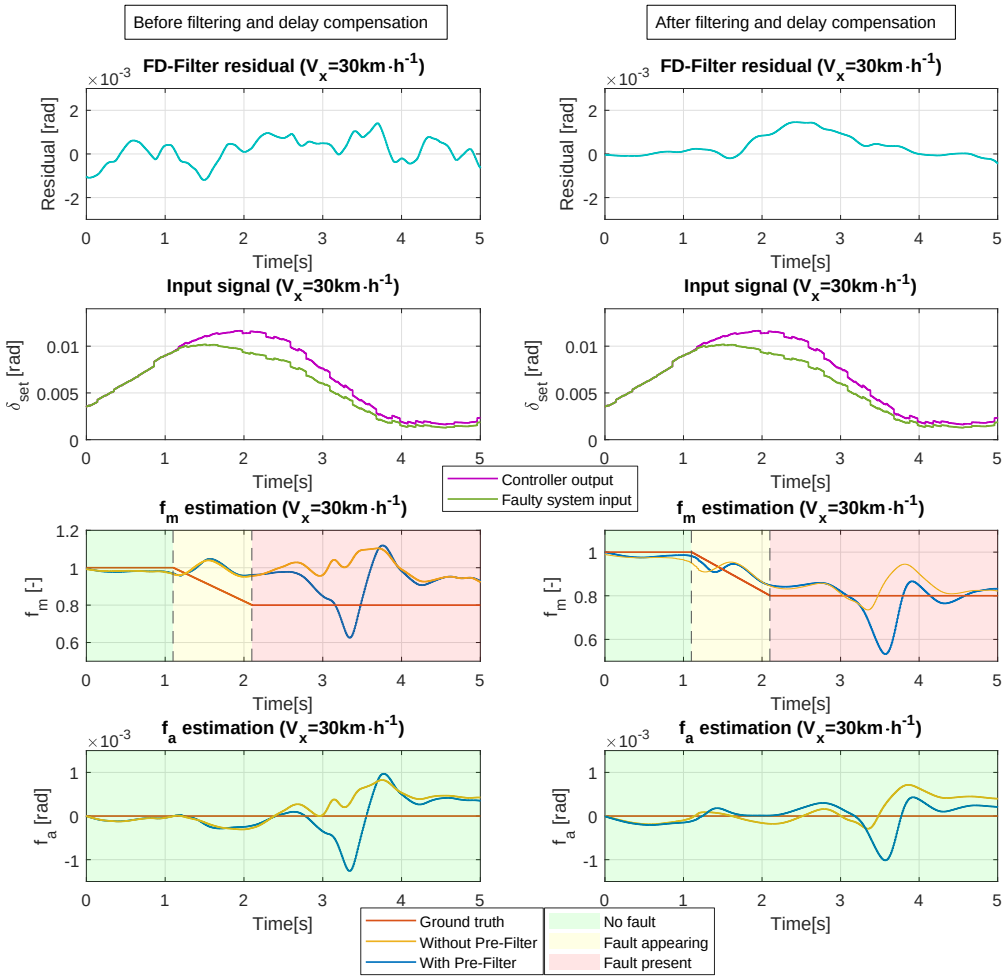

Figure 5-7: Experimental results for a testing velocity of $30\text{km}\cdot\text{h}^{-1}$ and an injected fault of $f_m = 0.8$.

A change of the multiplicative fault f_m is more difficult to observe dependent on the magnitude of the control input as is shown in Figure 5-7. Before the FD-filter modifications it seems no change of fault is detected at all. The unmodeled disturbances govern the residual and hence the FI-filter is unable to isolate a fault. After modifications to the FD-filter, the change in multiplicative fault is detected and the isolation filter converges to the true injected multiplicative fault. The additive fault returns to a value of 0.2rad or 0.0086deg, showing the fault is negligible with respect to the actual system input. Disturbances are still observed on the fault estimates between 3 and 4s. This can be explained by the decreasing excitation of the input, resulting in an amplificatication of unmodeled disturbances or model mismatch. Following the performance of the fault estimation of f_a and f_m separately, the next experimental set involves the estimation of both faults acting in the same set. The results of this experimental test are shown in Figure 5-8.

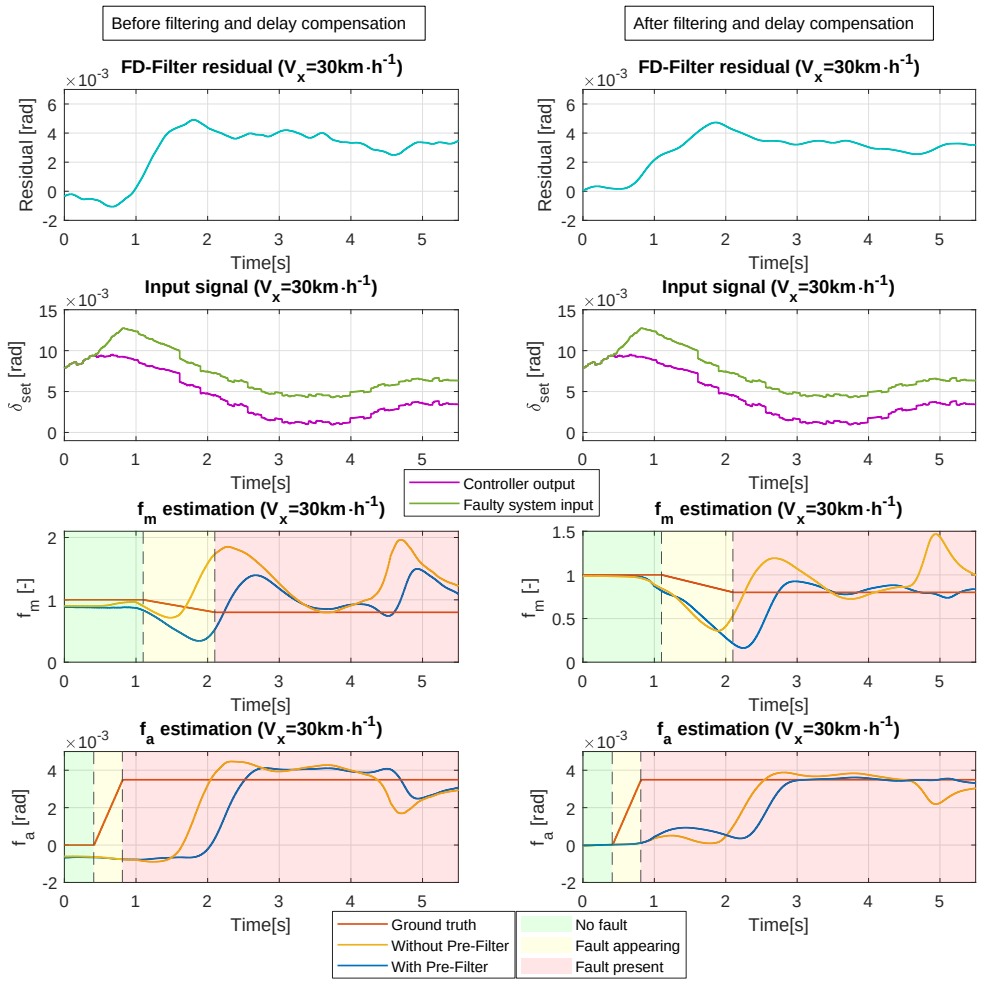

Figure 5-8: Experimental results for a testing velocity of $30\text{km} \cdot \text{h}^{-1}$ and injected faults of $f_m = 0.8$ and $f_a = 0.2$deg.

The detection of the additive fault is clear in both residuals in Figure 5-8, as well as showing a clear shape of the input caused by the multiplicative fault f_m. Without delay and filter

augmentation adjustments, the estimation of the multiplicative fault f_m oscillates around the true fault whereas the additive fault estimation seems more precise. After taking into account the I/O delays and filtering the measurements, the isolation results show different behavior for the filter with and without pre-filter. An increased dynamical content of the input combined with the relatively slow poles of the FD-filter introduce high disturbances in the non-linear isolation filter without pre-filter. With pre-filter, however, the estimates converge to the true faults f_a and f_m, showing that the non-linear filter with pre-filter performs best of the two, as expected. The final experimental result set is the testing of the LPV FD-filter with a time-varying velocity. After approaching the test-track and activating the lateral controller, the longitudinal velocity of the vehicle is increased through the HMI up to $40\text{km} \cdot \text{h}^{-1}$. The velocity trajectory for the next experimental dataset is shown in Figure 5-9.

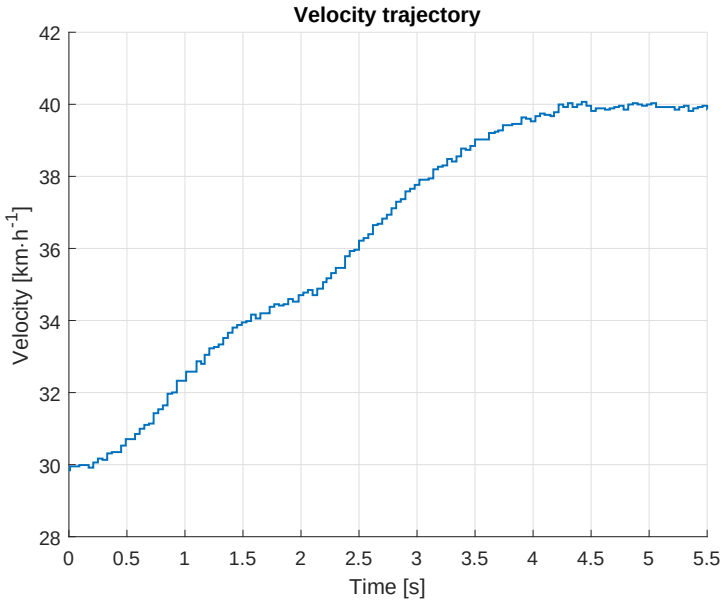

Figure 5-9: Velocity trajectory of the time-varying fault detection experiment, varying from a velocity of $30\text{km} \cdot \text{h}^{-1}$ to $40\text{km} \cdot \text{h}^{-1}$.

The results of detecting f_m and f_a for a time-varying velocity are shown in Figure 5-10. It can be observed that without I/O delay and filter augmentation the residual is again governed by noise. The isolation results show that the noise is captured in the multiplicative fault, although the magnitude of the additive fault is captured correctly. After adjusting the filter by adding low-pass filters to the output measurements and taking into account the I/O delays, the results improve significantly. It can be seen that the residual captures the magnitude of the faults f_m and f_a with a minimal effect of noise. This increase in estimation quality can be explained by the higher magnitude of the yaw-rate with respect to the previous measurements, resulting in more accurate measurements. Furthermore, the results show that the augmentation of the pre-filter results in a more steady convergence towards the true fault. Both the additive and multiplicative fault estimations converge to the ground truth faults in a time span of $2-3$s after the fault has been fully applied. Whether or not this is an acceptable time of convergence, is of course fully dependent on the magnitude of the fault and the state of the vehicle at that specific point in time. Too large offsets can result in steady-state errors

in the lane-keeping or path-following scenario. Too large multiplicative errors could result in unstable vehicle behavior due to for example actuator saturation.

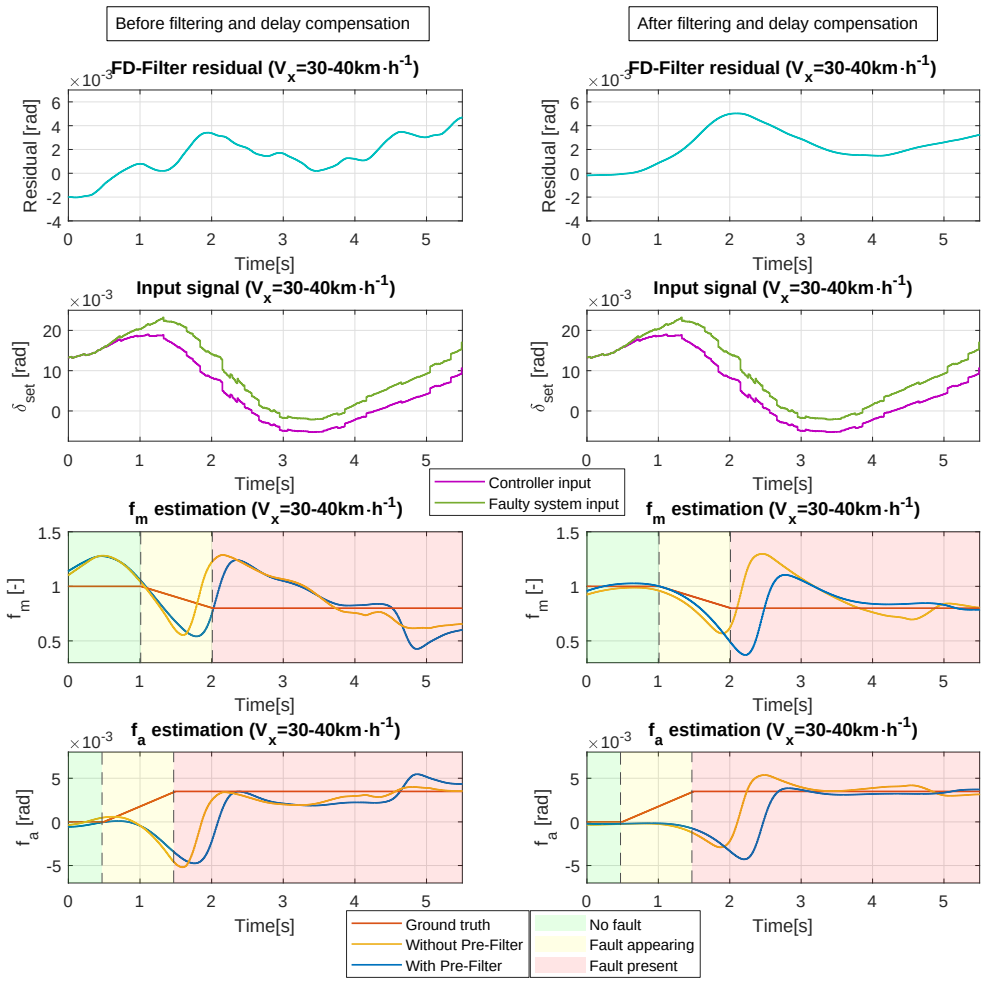

Figure 5-10: Experimental results at a time-varying testing velocity of $30\text{km} \cdot \text{h}^{-1}$ up to $40\text{km} \cdot \text{h}^{-1}$ and injected faults of $f_m = 0.8$ and $f_a = 0.2\text{deg}$.

In the previous set of experimental results it is ignored that the velocity is time-varying, since no different effects in the isolation behavior can be seen with respect to the previous results. The previous result set has been made by using the LPV FD-filter as detection filter. The following result set in Figure 5-11 shows a back to back comparison of the use of the LTI FD-filter (linearized at $30\text{km} \cdot \text{h}^{-1}$) compared to the use of a LPV FD-filter. Both of the experimental results have been obtained by implementing the I/O delay and low-pass filters.

From the results of Figure 5-11, combined with the velocity measurement in Figure 5-9, it can be seen that the LTI FD-filter has a poor robustness against the velocity change. Both the additive and the multiplicative fault estimation do not converge to the true faults, for both the non-linear isolation filter and the pre-filter augmented isolation filter. As is shown before, the LPV FD-filter does converge to the true faults and hence outperforms its LTI

alternative, showing that the results are as was expected.

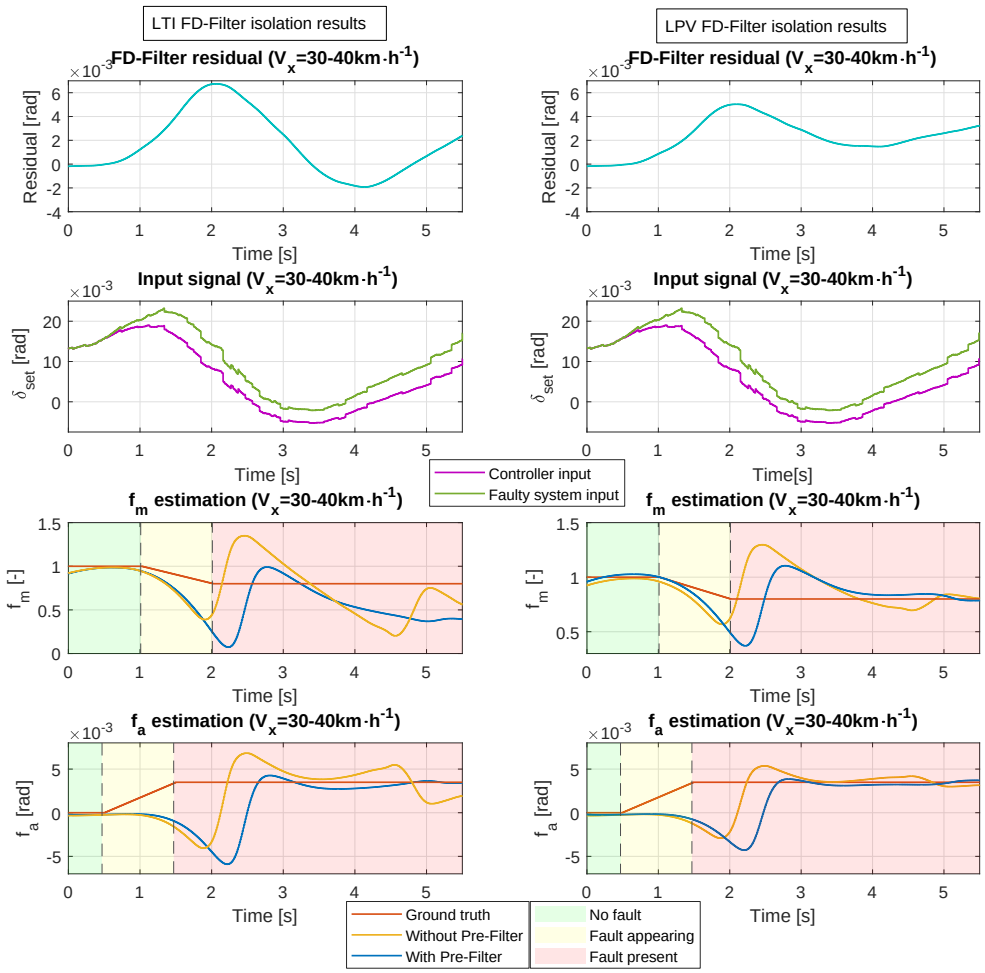

Figure 5-11: A comparison of the LTI FD-filter and LPV FD-filter performance at a time-varying testing velocity of $30\text{km} \cdot \text{h}^{-1}$ up to $40\text{km} \cdot \text{h}^{-1}$ and injected faults of $f_m = 0.8$ and $f_a = 0.2\text{deg}$.

5-4 Discussion on the experimental results

In this chapter, the developed theoretical methods have been applied in an experimental scenario. The experimental scenario, driving a real autonomous vehicle in a lane-keeping scenario, involved challenges that have first been identified and have subsequently been solved.

The first part of this chapter has introduced the experimental setup of the vehicle. In this part, the vehicle and its equipment has been shown and how the developed software can easily be implemented on this platform. Furthermore, it is shown that the testing area had a limited space for testing. This limited area imposed boundary conditions on the longitudinal velocity at which the vehicle could drive. Additionally, it shown which additional steps have been taken during the test sequence to actually be able to measure the vehicle states, i.e.,

waiting for valid camera measurements and activating the autonomous controller.

After analysis of the experimental setup, challenges were proposed that have been faced during the tests with the vehicle. The first source of error was proposed to be the delay of the camera measurements, caused by perception-processing steps that are taken after the camera images have been made. The second source of error was due to the accuracy of the measurements, particularly of the yaw-rate sensor. Quantization of the sensor measurements due to the low resolution of the sensors caused the measurements to be ill-conditioned. As a result, the measurements have been augmented with an extra low-pass filter. The third source of error was proposed to be an input delay, caused by the system dynamics of the electric power steering of the vehicle. All the aforementioned effects have been modeled and augmented in the vehicle model. Using this methodology, the developed framework could compensate for this effect and therefore increase the performance of the estimation methods.

Finally, the experimental results were shown. In these results, it was shown that the developed framework is able to estimate the faults acting on the system. Due to the low variance of the input signal (during lane-keeping at a relatively low velocity), the estimation horizon and the FD-filter poles had to be adjusted to reduce the performance bound and as a result the estimation error. As a result, reduced convergence times with respect to the case study have been observed. Furthermore, the transient behavior of especially a single time-varying additive fault acting on the system has shown interesting results. The transient behavior can be taken into account by further tuning of the framework, based on the results obtained in the case study. It is worth noting, that the results have been obtained on a velocity more than twice as low than the velocity proposed in the case study. It is expected that at a higher velocity, the excitation of the steering system is higher and as a result the estimation error would decrease further (as shown by the performance bounds).

Chapter 6

Conclusions and Future Directions

Following the work of this thesis, this chapter provides a brief overview of the conclusions that can be drawn from the theoretical framework, the simulation results on the automotive case study and experimental results of this thesis research. These conclusions are drawn in Section 6-1. Over the course of this research several different trajectories of extension have been found for the contributions of this thesis. These inspirations for future research will be briefly elaborated with a small theoretical and mathematical background in Section 6-2.

6-1 Conclusion

This thesis has proposed a set of novel methods for the fault detection and isolation of additive and multiplicative appearing faults in both discrete-time LTI and LPV systems. The research started by introduction of the research problem in the case study background (lateral control of an autonomous vehicle). Following this background a short state-of-the-art analysis showed a lack of a methodology for our specific research goals, i.e., the specific appearance of the additive and multiplicative fault combined with exogenous disturbances in a potentially LPV environment. Throughout the thesis research, it was found that developed methods were not only suitable for the case study, but for a wider set of applications. For this reason, the methodologies developed in this thesis research have been developed to accomodate more generalized set of models to which the case study belongs.

- In the first theoretical contribution, it was shown that the specific structure of the null-space computation based FD-filter combined with the non-linear isolation filter allowed us to decouple the additive and multiplicative fault by using information over a past measurement horizon. The main problem in this methodology was uncovered in the case study simulation, showing that the dynamical effects of the known signals combined with the dynamical content of the FD-filter could induce large asymptotic errors (even in constant fault scenarios).

- In the second theoretical contribution, the main source of error in the non-linear isolation filter was incorporated in the design of the isolation filter using the pre-filter, showing that the dynamical effect of the FD-filter could be fully decoupled in a constant fault scenario but also showed that the filter settles in finite time in case of a change in fault signals. Both the first and the second contribution were given a guaranteed performance bound which in linear simulations showed to be tight on top of the estimation error, hence providing a useful tool for finding the main sensitivities for error reduction.
- In the third theoretical contribution, a tractable synthesis approach for a LPV FD-filter was proposed. Given that the parameter measurements were measurable, simulations of this method showed that following the weak duality of the problem we could decouple the faults from the disturbances up to a numerical accuracy.

After development of the theoretical contributions, a systematic approach was devised to implement these methods on the fault detection in lateral control for autonomous vehicles. Based on a linearization of the lateral dynamics, the contributions were shown to fulfill the research goal. At least, in the linearized scenario which was assumed to approach the true non-linear model given a set of assumptions. The linearized approach was applied in an experimental setting, showing the systematic approach of adopting the filter to real-life effects such as measurement quantization and delays. The experimental results showed that the aforementioned methods of this thesis proved to be effective even in a low excitation scenario at a low longitudinal velocity.

As a result, the main objectives of this thesis research have been fulfilled. A generalized set of theorems has been developed that allows detection and isolation of the additive and multiplicative fault, while rejecting unmeasured exogenous disturbances in lateral control for autonomous vehicles for non-constant slowly time-varying longitudinal velocities. Furthermore, the suitabillity of the framework is proven in an experimental setting.

6-2 Proposals for future directions

Throughout the research, trajectories for future research that were outside of the scope of this thesis have been found as an extension to this research. These ideas find their purposes in the area of active fault isolation and fault tolerant control, as well as in the area of residual evaluation and threshold computation. The extensions are shortly introduced with a controller or filter schematic and if applicable a short mathematical background.

6-2-1 Proposals for extensions to fault tolerant control

Compensating for f_a in absence of f_m

Assuming there is no multiplicative fault acting on the system, the additive fault can be fully compensated using linear controller methods. This proposal shows that residual from the null space computation based parity-space filter from (2.6) can be used in a feedback law to fully compensate for this additive fault. Figure 6-1 shows the proposed schematic for feedback control of the additive fault using a Lyapunov stability-based FD-controller.

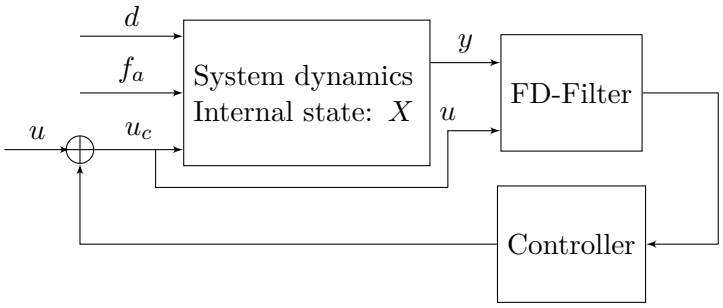

Figure 6-1: A visual representation of the proposed methodology for the Lyapunov stable additive fault feedback controller.

The following equations will provide a baseline in designing an additive fault feedback controller. Assume the FD-filter has already been created, the selection of polepairs for the transfer function $d(q)$ is not trivial; there can exist a stable FD-filter combined with a closed-loop stable plant resulting in an unstable system. Suppose the minimal realization of the plant is written as

$$\left[\begin{array}{c|c} A_1 & B_1 \\ \hline C_1 & D_1 \end{array}\right],$$

and the minimal realization of the filter dynamics (2.6) is written as

$$\left[\begin{array}{c|c} A_2 & B_2 \\ \hline C_2 & D_2 \end{array}\right].$$

By placing these two minimal realizations in series the total system description reads

$$\mathcal{A}_{series} = \begin{bmatrix} A_1 - B_1 D_2 C_1 & -B_1 C_2 \\ B_2 C_1 & A_2 \end{bmatrix}.$$

Therefore, a stable feedback controller can be found for closed-loop feedback if there exists a polepair $d(q)$ such that there exists a matrix P for the following feasibility problem

$$\begin{aligned} P &\succ 0, \\ P &= P^T, \\ \mathcal{A}_{series}^T P \mathcal{A}_{series} - P &\prec 0. \end{aligned}$$

Compensating for f_a in presence of f_m

Given that the linear system dynamics are fully known, following Theorem 3-1.3 and Theorem 3-2.1 it is given that we have full knowledge of the mapping $\|r(f_a, f_m)\|_{\mathscr{L}_{n2}}(k) \mapsto \left\| \left[(\widehat{f}_a(k) - \mu_n[f_a](k)) \quad (\widehat{f}_m(k) - \mu_n[f_m](k)) \right]^{\mathsf{T}} \right\|_2$. Following the proofs in Appendix A it is straightforward to find a guaranteed performance bound for the mapping $\|r\|_{\mathscr{L}_{n2}}(k) \mapsto \left\| \left[\widehat{f}_a(k) \quad \widehat{f}_m(k) \right]^{\mathsf{T}} \right\|_2$ which bounds the mapping $\|r\|_{\mathscr{L}_{n2}}(k) \mapsto \|\widehat{f}_a(k)\|_2$. By extending this bound to infinite horizon and combining it with a bound on the transfer function of the plant, closed-loop stability of the system in Figure 6-2 feeding back the additive fault can

be evaluated using the small-gain theorem [39]. It may require restrictive assumptions on the stochastical properties of signal $E(z)$ and hence should be investigated further to find feasibility and tractibility of this idea.

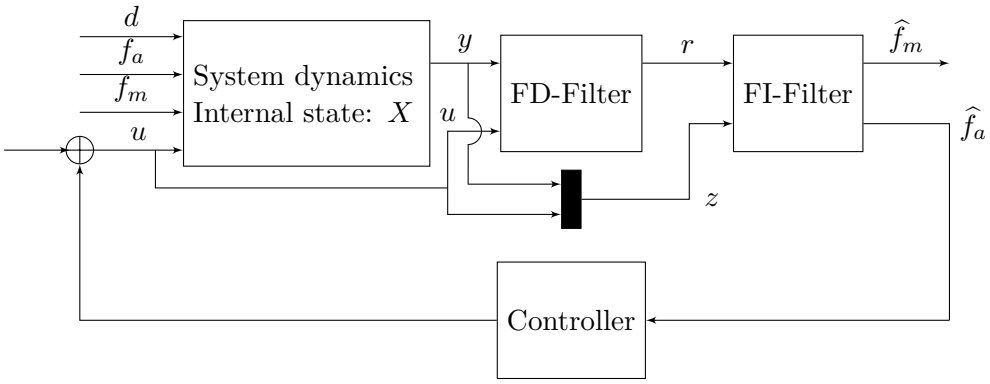

Figure 6-2: A visual representation of the proposed methodology for the small-gain controller.

6-2-2 Proposal for extension to active fault isolation

As emphasized in Remark 3-1.4, the estimation error from the non-linear isolation is highly dependent on some controllable and some uncontrollable factors. To briefly summarize, these factors are, for both the original algorithm and the extension to the pre-filter:

- The variance and mean of the known or filtered known signals $E(z)$ and $\widetilde{E}(z)$,
- The estimation horizon length n,
- The speed of the dynamics of the mapping $(f_a,\ f_m) \mapsto r$,
- The variance of the uncontrollable faults f_a and f_m.

The first three factors are in our control, although the last one, assuming it is an exogenous fault over which we do not have control, is not within our scope of influence. As has also been proposed in Section 3-1, adjusting the dynamical content of the mapping from the fault to the residual results in a difficult trade-off since it poses a direct compromise between reduction of the estimation error and a higher sensitivity for unknown disturbances and measurement noise. The estimation horizon n can be influenced, although this directly penalizes the convergence time of the estimates and could also deteriorate $V_n\left[E(z)\right](k)$, due to its dependence on the horizon. The variance of the known signals is a topic for which we have made large assumptions in for example (4.2). It is assumed that the system has a natural form of persistency of excitation due to measurement noise and the presence of exogenous disturbances and faults. In an ideal scenario (assuming no measurement noise or disturbances acting and assuming ideal camera measurements during lane-keeping for instance), there is a good chance that the lack of excitation deteriorates the estimation result. Referring back to Theorem 3-1.3 and Theorem 3-2.1, we find that for the non-linear isolation filter the estimation error upper-bounded with the multiplication factor

$$\sqrt{\frac{1+\left|\mu_n\left[E(z)\right]\right|}{nV_n\left[E(z)\right]}}. \tag{6.1}$$

Notice that this expression is very similar to the condition of persistence of excitation in the field of adaptive control [34], where the covariance of the regressor provides a leading condition in the decay rate of the estimation error. In theory, the bound is fully measurable, but having knowledge on how this bound affects the magnitude of the estimation error, this relation can be exploited in the field of active FDI. Since the magnitude of the upper-bound could speak for the conditioning of the estimation error, minimum and maximum thresholds for the bound can be set as a constraint for an optimization-based controller (e.g., Model Predictive Control (MPC)). Through this method, the estimation bound and thus the true estimation error lies underneath the performance bound while keeping the system under appropriate control.

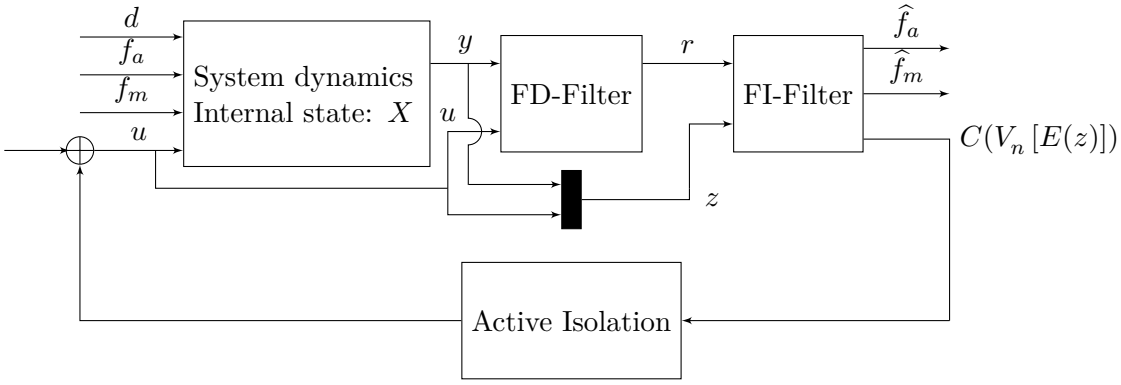

Figure 6-3: A visual representation of the proposed methodology for active isolation.

Figure 6-3 depicts the proposed schematic for such a controller where the Active Isolation controller block represents the MPC or other type controller exciting the system whenever the condition number $C(V_n\,[E(z)])$ of the estimation is below a certain threshold.

6-2-3 Proposal for extension to residual evaluation

As has been shown in the experimental results, it is unlikely that for model-based methods there is an availability of a perfect model. As a result, false positives or false negatives may occur, giving us a false idea of the presence or absence of a fault. Often systems implement a decision making process that as a consequence of the presence of a fault undertake action (for instance the autonomous vehicle case study), it would be highly undesirable to undertake this action as a result of false alarms, due to inaccurate model knowledge. To robustify the detection of the additive or multiplicative fault, further evaluation of the fault signals from the FI-filter is needed. A widely used approach (and therefore the proposed approach for future work) is the residual eveluation using the comparison with a threshold. If the fault surpasses this threshold, the fault is recorded as a detection and otherwise rejected. The general approach can be depicted as in Figure 6-4.

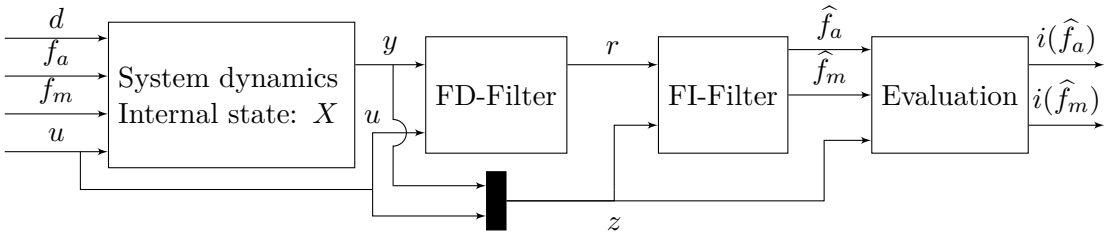

Figure 6-4: A visual representation of the proposed methodology for fault evaluation.

Where the binary signals $i(\widehat{f}_a)$ and $i(\widehat{f}_m)$ indicate the presence or absence of an alarm. In [40] several approaches are proposed that are given in more deterministic or more stochastic settings. Generally, the problem to be solved is to find a threshold, above this threshold it can be said with certainty that a fault is detected. Therefore, the challenge is to find two fault thresholds J_{th,f_a} and J_{th,f_m} such that

$$\begin{aligned}
\|\widehat{f}_a\|_{\mathscr{L}_{np}}(k) &> J_{th,f_a} \implies \text{Alarm, additive fault detected,}\\
\|\widehat{f}_a\|_{\mathscr{L}_{np}}(k) &\leq J_{th,f_a} \implies \text{No alarm, fault-free,}\\
\|\widehat{f}_m\|_{\mathscr{L}_{np}}(k) &> J_{th,f_m} \implies \text{Alarm, multiplicative fault detected,}\\
\|\widehat{f}_m\|_{\mathscr{L}_{np}}(k) &\leq J_{th,f_m} \implies \text{No alarm, fault-free,}
\end{aligned}$$

Given Section 4-4, it is shown that the uncertainty could be from a deterministic source, e.g., parameter uncertainty. By defining these parameter uncertainties as a polytopic set, i.e., a set of system matrices with minimum and maximum uncertainties according to [40] this information can then be used to find an optimal residual threshold given the deterministic uncertainties (using for instance an SDP based optimzation).

Appendix A

Technical Proofs

A-1 Proof of Theorem 3-1.3

Rewriting the non-linear input output filter in (3.4) leads to

$$\begin{aligned}\begin{bmatrix}\widehat{f}_a(k)\\ \widehat{f}_m(k)\end{bmatrix} =&\Phi_n[E(z)](k)r_n(k),\\ =&\Phi_n[E(z)](k)\Big(r_n(k)+\left(\mu_n\left[f_a\right](k)\mathbf{1}^\intercal+\mu_n\left[f_m\right](k)E_n(z(k))\right)\\ &-\left(\mu_n\left[f_a\right](k)\mathbf{1}^\intercal+\mu_n\left[f_m\right](k)E_n(z(k))\right)\Big),\end{aligned} \tag{A.1}$$

Note, that for the constant vectors of mean values of f_a and f_m, the following vector identity holds

$$\Phi_n[E(z)](k)\left(\mu_n\left[f_a\right](k)\mathbf{1}^\intercal+\mu_n\left[f_m\right](k)E_n(z(k))\right)=\begin{bmatrix}\mu_n\left[f_a\right](k)\\ \mu_n\left[f_m\right](k)\end{bmatrix},$$

which, in turn, for (A.1) results in:

$$\begin{bmatrix}\widehat{f}_a(k)-\mu_n\left[f_a\right](k)\\ \widehat{f}_m(k)-\mu_n\left[f_m\right](k)\end{bmatrix} =\Phi_n[E(z)](k)\underbrace{\left(r_n(k)-\mu_n\left[f_a\right](k)\mathbf{1}^\intercal-\mu_n\left[f_m\right](k)E_n(z(k))\right)}_{e_n(k)}. \tag{A.2}$$

Taking the 2-norm from both sides results in:

$$\left\|\begin{bmatrix}\widehat{f}_a(k)-\mu_n\left[f_a\right](k)\\ \widehat{f}_m(k)-\mu_n\left[f_m\right](k)\end{bmatrix}\right\|_2 =\|\Phi_n[E(z)](k)e_n(k)\|_2. \tag{A.3}$$

For the RHS we find, through the induced matrix 2-norm, that:

$$\|\Phi_n[E(z)](k)\|_2=\sup_{e_n(k)\neq 0}\frac{\|\Phi_n[E(z)](k)e_n(k)\|_2}{\|e_n(k)\|_2},$$

hence we find the condition:

$$\|\Phi_n[E(z)](k)e_n(k)\|_2 \leq \|\Phi_n[E(z)](k)\|_2 \cdot \|e_n(k)\|_2, \tag{A.4}$$
$$= \|\Phi_n[E(z)](k)\|_2 \cdot \|e\|_{\mathscr{L}_{n2}}(k). \tag{A.5}$$

This two part upper-bound for the combined estimation error in (A.3) can be reduced further to a more intuitive and useful upper-bound. The regressor-bound can be further reduced as described in the following lemma.

Lemma A-1.1 (Regressor upper-bound)**.** *The induced 2-norm of the regressor operator $\Phi_n[E(z)](k)$ is upper bounded by the following term defined for a time-horizon of n at time instance k:*

$$\|\Phi_n[E(z)](k)\|_2 \leq \sqrt{\frac{1 + |\mu_n\left[E(z)\right](k)|}{nV_n\left[E(z)\right](k)}},$$

Proof. The induced 2 norm of regressor pseudo-inverse $\Phi_n[E(z)](k)$ is defined by the spectral norm of matrix $\Phi_n[E(z)](k)$, i.e., its largest singular value:

$$\begin{aligned}
\|\Phi_n[E(z)](k)\|_2 =& \overline{\sigma}(\Phi_n[E(z)](k)), \\
=& \sqrt{\overline{\lambda}\left(\Phi_n[E(z)](k)\Phi_n^\intercal[E(z)](k)\right)}, \\
=& \sqrt{\overline{\lambda}\left(\left(\phi_n^\intercal[E(z)](k)\phi_n[E(z)](k)\right)^{-1}\phi_n^\intercal[E(z)](k)\phi_n[E(z)](k)\left(\phi_n^\intercal[E(z)](k)\phi_n[E(z)](k)\right)^{-1}\right)}, \\
=& \sqrt{\overline{\lambda}\left(\left(\phi_n^\intercal[E(z)](k)\phi_n[E(z)](k)\right)^{-1}\right)}.
\end{aligned}$$

The matrix $\phi_n^\intercal[E(z)](k)\phi_n[E(z)](k)$ can be rewritten in the following matrix form:

$$\begin{aligned}
\phi_n^\intercal[E(z)](k)\phi_n[E(z)](k) =& \begin{bmatrix} \sum_{i=0}^{n-1}(E(z)(k-i))^2 & \sum_{i=0}^{n-1}E(z)(k-i) \\ \sum_{i=0}^{n-1}E(z)(k-i) & n \end{bmatrix}, \\
=& n\begin{bmatrix} \sigma_n^2\left[E(z)\right](k) & \mu_n\left[E(z)\right](k) \\ \mu_n\left[E(z)\right](k) & 1 \end{bmatrix},
\end{aligned}$$

which is a symmetric positive definite matrix assuming that $\sigma_n^2\left[E(z)\right](k) \neq 0$ (an assumption made in Section 3-1). Hence, the spectral norm can be recast as:

$$\begin{aligned}
\|\phi_n[E(z)](k)\|_2 =& \sqrt{\left(\underline{\lambda}\left(\phi_n^\intercal[E(z)](k)\phi_n[E(z)](k)\right)\right)^{-1}}, \\
=& \sqrt{\frac{2}{n\left(\left(1+\sigma_n^2\left[E(z)\right](k)\right) - \sqrt{\left(1+\sigma_n^2\left[E(z)\right](k)\right)^2 - 4V_n\left[E(z)\right](k)}\right)}}, \\
=& \sqrt{\frac{2\left(\left(1+\sigma_n^2\left[E(z)\right](k)\right) + \sqrt{\left(1-\sigma_n^2\left[E(z)\right](k)\right)^2 - 4\mu_n^2\left[E(z)\right](k)}\right)}{n4V_n\left[E(z)\right](k)}},
\end{aligned}$$

which can be rewritten by the use of the Cauchy-Schwarz inequality as:

$$\|\Phi_n[E(z)](k)\|_2 \leq \sqrt{\frac{2\left(\left(1+\sigma_n^2\left[E(z)\right](k)\right) + \sqrt{\left(1-\sigma_n^2\left[E(z)\right](k)\right)^2} + \sqrt{4\mu_n^2\left[E(z)\right](k)}\right)}{n4V_n\left[E(z)\right](k)}},$$

$$=\sqrt{\frac{1+|\mu_n\left[E(z)\right](k)|}{nV_n\left[E(z)\right](k)}},$$

concluding the proof of Lemma A-1.1. □

The following lemma provides a proof for the upper bound of the error signal in (A.4), showing that it can be split up in three parts with three different dependencies (3.6a),(3.6b),(3.6c).

Lemma A-1.2 (Three-stage error bound)**.** *The total error term $e_n(k)$ (A.2) is upper-bounded by*

$$\|e\|_{\mathscr{L}_{n2}}(k) \leq e_1(k) + e_2(k) + e_3(k),$$

where the three error terms can be defined as

$$\begin{aligned}
e_1(k) =& \|\mathscr{T}_n(f_m E(z) + f_a) + \mathscr{O}_n x_F(k-n+1)\|_{\mathscr{L}_{n2}}(k),\\
e_2(k) =& \sqrt{nV_n\left[f_m\right](k)} \cdot \|E(z)\|_{\mathscr{L}_{n\infty}}(k),\\
e_3(k) =& \sqrt{nV_n\left[f_a\right](k)}.
\end{aligned}$$

Proof. The norm of the term $e_n(k)$ can be expanded as:

$$\begin{aligned}
\|e\|_{\mathscr{L}_{n2}}(k) =& \|(r - \mu_n\left[f_m\right]E(z) - \mu_n\left[f_a\right]\|_{\mathscr{L}_{n2}}(k)\\
=& \|r - (f_m E(z) + f_a) + (f_a - \mu_n\left[f_a\right]) + (f_m E(z) - \mu_n\left[f_m\right]E(z))\|_{\mathscr{L}_{n2}}(k)
\end{aligned}$$

Using the Cauchy-Schwarz inequality, we find:

$$\begin{aligned}
\|e\|_{\mathscr{L}_{n2}}(k) \leq& \|r - (f_m E(z) + f_a)\|_{\mathscr{L}_{n2}}(k) + \|f_a - \mu_n\left[f_a\right](k)\|_{\mathscr{L}_{n2}}(k)\\
&+ \|f_m E(z) - \mu_n\left[f_m\right]E(z)\|_{\mathscr{L}_{n2}}(k)
\end{aligned}$$

and using the Definition 3-1.2 for the restricted state and input transfer function, for the minimal realization of the mapping $G(q) - I$ (where $G(q)$ is defined in (2.7)), leads to

$$\begin{aligned}
\|r - (f_m E(z) + f_a)\|_{\mathscr{L}_{n2}}(k) =& \|\mathscr{T}_n(f_m E(z) + f_a) + \widetilde{\mathscr{O}}_n x_F(k-n+1)\|_{\mathscr{L}_{n2}}(k)\\
=& e_1(k)
\end{aligned}$$

Errors $e_2(k)$, $e_3(k)$ can be found by observing that the remaining terms are related to the variance of the faults:

$$\begin{aligned}
\|f_a - \mu_n\left[f_a\right]\|_{\mathscr{L}_{n2}}(k) =& \sqrt{nV_n\left[f_a\right](k)} && \text{(A.6)}\\
=& e_3(k)\\
\|E(z)(f_m - \mu_n\left[f_m\right])\|_{\mathscr{L}_{n2}}(k) \leq& \|E_n(z)^{\square}(k)\|_2 \cdot \sqrt{nV_n\left[f_m\right](k)} && \text{(A.7)}\\
& && \text{(A.8)}
\end{aligned}$$

where $E_n(z)^{\square}(k)$ is the diagonalized vector of n-steps for the signal $E(z)$ as defined in the notational section. By use of the induced 2-norm for a diagonal matrix it simply follows that

$$\begin{aligned}
\|E(z)(f_m - \mu_n\left[f_m\right])\|_{\mathscr{L}_{n2}}(k) \leq& \|E_n(z)^{\square}(k)\|_2 \cdot \sqrt{nV_n\left[f_m\right](k)} && \text{(A.9)}\\
\leq& \|E(z)\|_{\mathscr{L}_{n\infty}}(k) \cdot \sqrt{nV_n\left[f_m\right](k)}, && \text{(A.10)}\\
=& e_2(k),
\end{aligned}$$

concluding the proof of Lemma A-1.2. □

A-2 Proof of Theorem 3-2.1

The proof for Theorem 3-2.1 is partly analogous to the proof of Theorem 3-1.3. First, the filter equation (3.8) can be expanded as

$$\begin{aligned}\begin{bmatrix}\widehat{f}_a(k)\\ \widehat{f}_m(k)\end{bmatrix} =&\Phi_n[\widetilde{E}(z)](k)r_n(k),\\ =&\Phi_n[\widetilde{E}(z)](k)\Big(r_n(k)+\\ &\left(\mu_n\left[f_a\right](k)\mathbf{1}^\intercal+\mu_n\left[f_m\right](k)\widetilde{E}_n(z(k))\right)-\left(\mu_n\left[f_a\right](k)\mathbf{1}^\intercal+\mu_n\left[f_m\right](k)\widetilde{E}_n(z(k))\right)\Big),\end{aligned}$$

resulting in

$$\begin{bmatrix}\widehat{f}_a(k)-\mu_n\left[f_a\right](k)\\ \widehat{f}_m(k)-\mu_n\left[f_m\right](k)\end{bmatrix} =\Phi_n[\widetilde{E}(z)](k)\underbrace{\left(r_n(k)-\mu_n\left[f_a\right](k)\mathbf{1}^\intercal-\mu_n\left[f_m\right](k)\widetilde{E}_n(z(k))\right)}_{\widetilde{e}_n(k)}. \quad \text{(A.11)}$$

Analogous to (A.3), (A.4) and the results from Lemma A-1.1 it is found that the upper-bound of (A.11) can be written as

$$\left\|\begin{bmatrix}\widehat{f}_a(k)-\mu_n\left[f_a\right]\\ \widehat{f}_m(k)-\mu_n\left[f_m\right]\end{bmatrix}\right\|_2 \leq \sqrt{\frac{1+\left|\mu_n\left[\widetilde{E}(z)\right]\right|}{nV_n\left[\widetilde{E}(z)\right]}}\cdot\|\widetilde{e}\|_{\mathscr{L}_{n2}}(k), \quad \text{(A.12)}$$

Lemma A-2.1 (Three-stage error bound)**.** *The total error term* $\widetilde{e}_n(k)$ (A.11) *results in an upper-bound for the total estimation error which can be expressed by the following three terms:*

$$\begin{aligned}\widetilde{e}_1(k) =&\|\widetilde{\mathscr{O}}_nX_M(k-n+1)-f^{\square}_{m_n}(k)\widetilde{\mathscr{O}}_nX_E(k-n+1)\|_2+\|\widetilde{\mathscr{O}}_nX_A(k-n+1)+\widetilde{\mathscr{T}}_nf_{an}(k)-f_{an}(k)\|_2\\ &+\|(\widetilde{\mathscr{T}}_nf^{\square}_{m_n}(k)-f^{\square}_{m_n}(k)\widetilde{\mathscr{T}}_n)\|_2\|E_n(z(k))\|_{\mathscr{L}_{n\infty}}(k)\\ \widetilde{e}_2(k) =&\sqrt{nV_n\left[f_m\right](k)}\cdot\|\widetilde{E}(z)\|_{\mathscr{L}_{n\infty}}(k),\\ e_3(k) =&\sqrt{nV_n\left[f_a\right](k)}.\end{aligned}$$

Proof. The norm of the term $\widetilde{e}_n(k)$ can be expanded as:

$$\begin{aligned}\|\widetilde{e}\|_{\mathscr{L}_{n2}}(k) =&\|(r-\mu_n\left[f_m\right]\widetilde{E}(z)-\mu_n\left[f_a\right]\|_{\mathscr{L}_{n2}}(k)\\ =&\|r-(f_m\widetilde{E}(z)+f_a)+(f_a-\mu_n\left[f_a\right])+(f_m\widetilde{E}(z)-\mu_n\left[f_m\right]\widetilde{E}(z))\|_{\mathscr{L}_{n2}}(k)\end{aligned}$$

Using the Cauchy-Schwarz inequality, we find:

$$\begin{aligned}\|\widetilde{e}\|_{\mathscr{L}_{n2}}(k) \leq&\|r-(f_m\widetilde{E}(z)+f_a)\|_{\mathscr{L}_{n2}}(k)+\|f_a-\mu_n\left[f_a\right](k)\|_{\mathscr{L}_{n2}}(k)\\ &+\|f_m\widetilde{E}(z)-\mu_n\left[f_m\right]\widetilde{E}(z)\|_{\mathscr{L}_{n2}}(k)\end{aligned}$$

and using Definition 3-1.2 for the restricted state and input transfer function and the triangle inequality, we find

$$\|r-(f_m\widetilde{E}(z)+f_a)\|_{\mathscr{L}_{n2}}(k) =\|\widetilde{\mathscr{O}}_n(X_A(k-n+1)+X_M(k-n+1))+\widetilde{\mathscr{T}}_n(f^{\square}_{m_n}(k)E_n(z(k))+f_{an}(k))$$

$$
\begin{aligned}
&- f^{\square}_{m_n}(k)\widetilde{\mathscr{O}}_n X_E(k-n+1) - f_{an}(k) - f^{\square}_{m_n}(k)\widetilde{\mathscr{T}}_n\widetilde{E}_n(z(k))\|_2 \\
\leq &\|\widetilde{\mathscr{O}}_n X_M(k-n+1) - f^{\square}_{m_n}(k)\widetilde{\mathscr{O}}_n X_E(k-n+1)\|_2 \\
&+ \|(\widetilde{\mathscr{T}}_n f^{\square}_{m_n}(k) - f^{\square}_{m_n}(k)\widetilde{\mathscr{T}}_n)\|_2 \|E_n(z(k))\|_{\mathscr{L}_{n\infty}}(k) \\
&+ \|\widetilde{\mathscr{O}}_n X_A(k-n+1) + \widetilde{\mathscr{T}}_n f_{an}(k) - f_{an}(k)\|_2
\end{aligned}
$$

where the signals x_A and x_M represent the internal states of the systems with restricted state and input matrices $\widetilde{\mathscr{T}}_n$ and $\widetilde{\mathscr{O}}_n$ with inputs f_a and f_m respectively. The diagonal matrix $f^{\square}_{m_n}(k)$ represents the diagonalized vector of the sampled signal vector $f_{mn}(k)$ as defined in the notational section. Finally, X_E represents the initial condition for the pre-filter mapping of $E(z) \mapsto \widetilde{E}(z)$ (3.7). Error $\widetilde{e}_2(k)$ can be found analogously to (A.10) and the remaining term $\widetilde{e}_3(k)$ is exactly equal to (A.6), concluding the proof of Lemma A-2.1. □

A-3 Proof of Theorem 3-3.4

Recall the conditions for the linear parameter-varying filter $N_k(q)$ (3.12), given that the stable LTI filter $d(q)$ does not cancel the zeros of the filter equations, these conditions are equivalent to

$$N_k(q)H_k(q) = 0, \tag{A.13a}$$
$$N_k(q)F_k(q) \neq 0. \tag{A.13b}$$

This can be posed as a strongly convex quadratic optimization problem as in (3.16) given that the constraint

$$\|\bar{H}_k^\intercal \bar{N}_k^\intercal\|_2^2 = 0.$$

is equivalent to statement (A.13a). Furthermore, the objective function

$$\max_{\bar{N}_k} \bar{N}_k \bar{F}_{k_j},$$

is equivalent, if not more strict with respect to (A.13b). Finally, the constraint

$$\|\bar{N}_k^\intercal\|_2^2 \leq 1$$

ensures that the optimization variable $\bar{N}_k$ remains bounded. Without loss of optimality, this strongly convex and quadratic optimization problem can be recast as

$$\begin{cases} \min_{\bar{N}_k} & -\bar{N}_k \bar{F}_{k_j} + \|\bar{N}_k^\intercal\|_2^2, \\ s.t. & \|\bar{H}_k^\intercal \bar{N}_k^\intercal\|_2^2 = 0. \end{cases} \tag{A.14}$$

Additionally, the dual problem can be denoted as

$$\begin{cases} \max & g(\gamma), \\ s.t. & \gamma \geq 0, \end{cases}$$

where $\gamma \in \mathbb{R}$ represents a Lagrange multiplier and $g(\gamma)$ represents the dual function for (A.14)

$$g(\gamma) = \inf_{\bar{N}_k} \underbrace{\gamma \|\bar{H}_k^\intercal \bar{N}_k^\intercal\|_2^2 + \|\bar{N}_k^\intercal\|_2^2 - \bar{N}_k \bar{F}_{k_j}}_{L(\bar{N}_k, \gamma)},$$

such that $L(\bar{N}_k, \gamma)$ is the Lagrangian in the dual problem. The dual function can be rewritten by finding the infinum of the Lagrangian

$$\begin{aligned} \nabla L(\bar{N}_k, \gamma) &= 0, \\ -\bar{F}_{k_j}^\intercal + 2\bar{N}_k + 2\gamma \bar{N}_k \bar{H}_k \bar{H}_k^\intercal &= 0. \\ \bar{N}_k^* = \frac{1}{2} \bar{F}_{k_j}^\intercal (I + \gamma \bar{H}_k \bar{H}_k^\intercal)^{-1}. \end{aligned}$$

Substitution into the dual function yields

$$\begin{aligned} g(\lambda) &= \gamma \|\bar{H}_k^\intercal \bar{N}_k^{*\intercal}\|_2^2 + \|\bar{N}_k^{*\intercal}\|_2^2 - \bar{N}_k^* \bar{F}_{k_j}, \\ &= -\frac{1}{4} \bar{F}_{k_j}^\intercal (I + \gamma \bar{H}_k \bar{H}_k^\intercal)^{-1} \bar{F}_{k_j}, \end{aligned}$$

hence, the dual problem is rewritten as

$$\begin{cases} \max & -\frac{1}{4} \bar{F}_{k_j}^\intercal (I + \gamma \bar{H}_k \bar{H}_k^\intercal)^{-1} \bar{F}_{k_j}, \\ s.t. & \gamma \geq 0, \end{cases}$$

the quadratic objective is by definition negative definite, hence the duality gap goes to zero for $\lim_{\gamma \to \infty} \bar{N}^*$, thus concluding the proof.

Appendix B

Derivation of the Single-Track Model

This appendix describes the derivation of the single-track linear bicycle model. First, the equations of motion are formally derived, analogous to the approach proposed in [41]. Subsequently the single-track model is linearized. Finally the disturbance models used throughout this thesis are given and augmented to form a total state-space equation for the system.

B-1 Equations of motion

Figure B-1 provides a schematic overview of the single track model including the physical parameters.

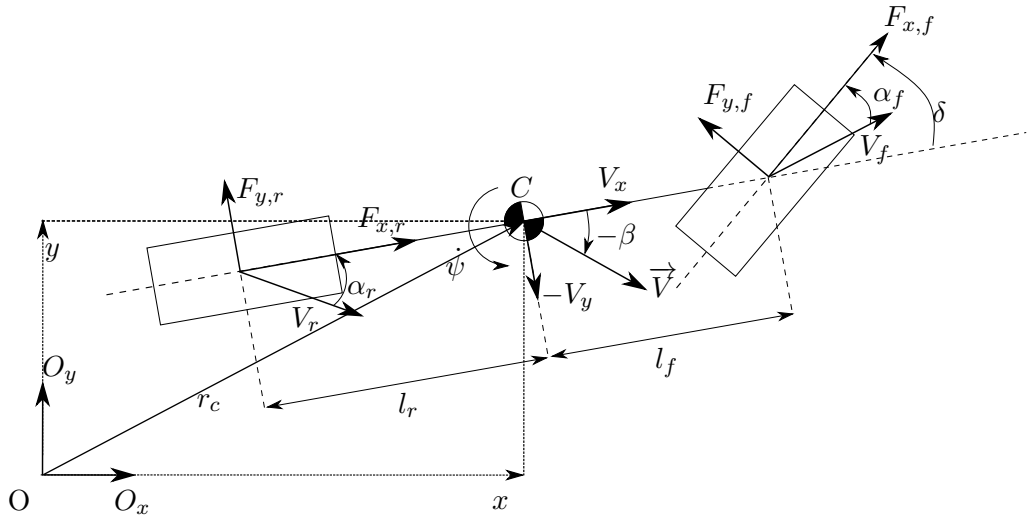

Figure B-1: Schematic diagram of the single-track bicycle model

The forces F_i, $i \in \{x_f, x_r, y_f, y_r\}$ represent the directional force vectors acting upon the front and rear tyres of the vehicle and thus acting on the center of gravity of the vehicle C. The

velocities V_x, V_y represent velocities of the center of gravity for which V represents the combined x, y velocity in its local coordinate frame, whereas the velocities V_f, V_r represent the magnitude and phase of the velocity of each tyre. The symbols α_f, α_r represent the front and rear sideslip angles of the tyres and the symbol β represents the bodyslip angle of the vehicle. The distances l_f, l_r represent the distance of the front and rear tyre with respect to the center of gravity location. Finally, the symbol δ represents the steering angle of the front wheel, we assume a purely front-wheel steered vehicle.

The symbol O represents the fixed reference frame and r_c represents the vector from the fixed frame O to the single-track center of gravity node C. Let O_x, O_y and C_x, C_y represent a set of unit vectors in the x and y direction of their respective coordinate frames O and C. The position of coordinate frame C with respect to frame O can be found with a rotation matrix $R(\psi)$ such that

$$\begin{aligned}\begin{bmatrix} C_x \\ C_y \end{bmatrix} =& R(\psi) \begin{bmatrix} O_x \\ O_y \end{bmatrix}, \\ =& \begin{bmatrix} \cos(\phi) & \sin(\phi) \\ -\sin(\phi) & \cos(\phi) \end{bmatrix} \begin{bmatrix} O_x \\ O_y \end{bmatrix}. \end{aligned} \tag{B.1}$$

where ψ represents the yaw angle around the z-axis. Additonally, the position of C can be defined as

$$r_c = \begin{bmatrix} x & y \end{bmatrix} \begin{bmatrix} O_x \\ O_y \end{bmatrix}.$$

Now, the velocity of frame C with respect to O can be found as

$$\begin{aligned}\dot{r}_c =& \begin{bmatrix} \dot{x} & \dot{y} \end{bmatrix} \begin{bmatrix} O_x \\ O_y \end{bmatrix}, \\ =& \begin{bmatrix} V_x & V_y \end{bmatrix} \begin{bmatrix} C_x \\ C_y \end{bmatrix}. \end{aligned}$$

The acceleration can subsequently be found as

$$\ddot{r}_c = \begin{bmatrix} V_x & V_y \end{bmatrix} \begin{bmatrix} \dot{C}_x \\ \dot{C}_y \end{bmatrix} + \begin{bmatrix} \dot{V}_x & \dot{V}_y \end{bmatrix} \begin{bmatrix} C_x \\ C_y \end{bmatrix}. \tag{B.2}$$

Using the rotation matrix in (B.1) it is found that

$$\begin{aligned}\begin{bmatrix} \dot{C}_x \\ \dot{C}_y \end{bmatrix} =& \dot{R}(\psi) \begin{bmatrix} O_x \\ O_y \end{bmatrix} + R(\psi) \begin{bmatrix} O_x \\ O_y \end{bmatrix} \\ =& \dot{\psi} \begin{bmatrix} 0 & 1 \\ -1 & 0 \end{bmatrix} \begin{bmatrix} \cos(\phi) & \sin(\phi) \\ -\sin(\phi) & \cos(\phi) \end{bmatrix} \begin{bmatrix} O_x \\ O_y \end{bmatrix} \\ =& \begin{bmatrix} 0 & \dot{\psi} \\ -\dot{\psi} & 0 \end{bmatrix} \begin{bmatrix} C_x \\ C_y \end{bmatrix} \end{aligned} \tag{B.3}$$

Hence, by substitution of (B.3) in (B.2) the final expression for the acceleration can be obtained

$$\ddot{r}_c = \begin{bmatrix} \dot{V}_x - \dot{\psi}V_y & \dot{V}_y + \dot{\psi}V_x \end{bmatrix} \begin{bmatrix} C_x \\ C_y \end{bmatrix}. \tag{B.4}$$

As a result of (B.4), the equations of motion can be derived using Newtons second law as

$$m\ddot{r}_c = \sum F_i.$$

Under the assumption that small steering angles δ are applied to the vehicle, it is found that this force equilibrium can be expanded in longitudinal and lateral force equilibria as

$$\begin{aligned} m(\dot{V}_x - \dot{\psi}V_y) =& F_{x,f} + F_{x,r}, \\ m(\dot{V}_y + \dot{\psi}V_x) =& F_{y,f} + F_{y,r}. \end{aligned}$$

These forces create a moment around the z-axis of the vehicle that can be calculated using the moment equilibrium again assuming a small steering angle δ)

$$I_z\ddot{\psi} = l_f F_{y,f} - l_r F_{y,r}.$$

Hence the equations of motion for a single track vehicle under low steering angles can be denoted as

$$\begin{aligned} m(\dot{V}_x - \dot{\psi}V_y) =& F_{x,f} + F_{x,r}, \\ m(\dot{V}_y + \dot{\psi}V_x) =& F_{y,f} + F_{y,r}, \\ I_z\ddot{\psi} =& l_f F_{y,f} - l_r F_{y,r}. \end{aligned}$$

B-2 Derivation of the linear model

In this section, the equations of motion derived from the previous section are linearized for use in a state-space equation. Subsequently the disturbances are modeled and augmented, resulting in the total model description as depicted in Figure B-2.

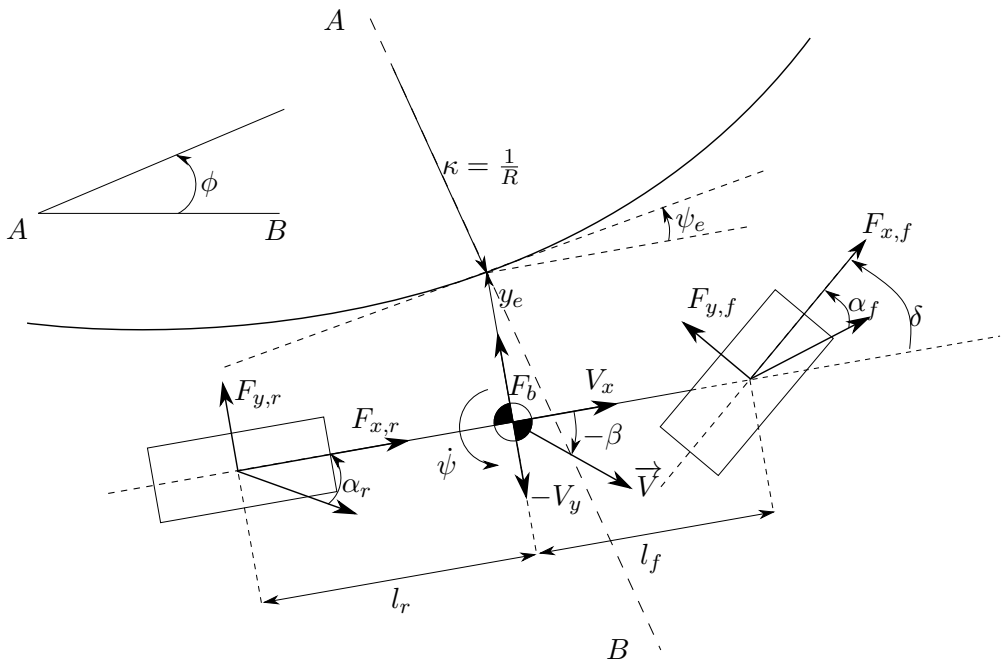

Figure B-2: Schematic diagram of the 2-DOF bicycle model with lane error dynamics

The following subsections show the derivation of the full model in terms of lateral dynamics, error dynamics of the camera and the faults and disturbances.

B-2-1 The linear single-track model

Following the previous section, the equations of motion for a single-track vehicle model can be denoted as

$$m(\dot{V}_x - \dot{\psi}V_y) = F_{x,f} + F_{x,r}, \tag{B.5a}$$
$$m(\dot{V}_y + \dot{\psi}V_x) = F_{y,f} + F_{y,r}, \tag{B.5b}$$
$$I_z\ddot{\psi} = l_f F_{y,f} - l_r F_{y,r}. \tag{B.5c}$$

The front and rear lumped lateral tire forces are assumed to have linear slip characteristics due to the low steering angle δ, hence the lateral force components can be written as

$$F_{y,f} = C_f \alpha_f, \tag{B.6a}$$
$$F_{y,r} = C_r \alpha_r, \tag{B.6b}$$

where $C_f \in \mathbb{R}_-$ and $C_r \in \mathbb{R}_-$ represent the lumped cornering stiffnesses of the front and rear axle respectively. From Figure B-2 the following expressions for the slip angles α_f, α_r can be found

$$\alpha_f = \delta - \arctan\left(\frac{V_{y,f}}{V_{x,f}}\right),$$

$$
\begin{aligned}
&= \delta - \arctan\left(\frac{V_y + l_f\dot{\psi}}{V_x}\right),\\
\alpha_r &= -\arctan\left(\frac{V_{y,r}}{V_{x,r}}\right),\\
&= -\arctan\left(\frac{V_y - l_r\dot{\psi}}{V_x}\right).
\end{aligned}
$$

Now, since we assume that $V_x \gg V_y$ and a small yaw-rate $\dot{\psi}$, the slip-angles can be approximated as

$$\alpha_f \approx \delta - \frac{V_y + l_f\dot{\psi}}{V_x}, \tag{B.7a}$$

$$\alpha_r \approx -\frac{V_y - l_r\dot{\psi}}{V_x}. \tag{B.7b}$$

Since the assumption of constant longitudinal velocity has been made, the assumption results in approximately zero longitudinal forces, i.e., the rolling friction and drag force is neglected. As a result of substituting (B.6) and (B.7) in (B.8), the linear single track model is derived

$$\begin{bmatrix}\dot{V}_y\\ \ddot{\psi}\end{bmatrix} = \begin{bmatrix}\frac{C_f+C_r}{mV_x} & \frac{C_f l_f - C_r l_r}{mV_x} - V_x\\ \frac{l_f C_f - l_r C_r}{V_x I_z} & \frac{l_f^2 C_f + l_r^2 C_r}{V_x I_z}\end{bmatrix}\begin{bmatrix}V_y\\ \dot{\psi}\end{bmatrix} + \begin{bmatrix}\frac{-C_f}{m}\\ \frac{-l_f C_f}{I_z}\end{bmatrix}. \tag{B.8}$$

For which the yawrate $\dot{\psi}$ is available for measurement.

B-2-2 Camera model, bank angle and fault modeling

For the autonomous vehicle in a lane-keeping scenario, measurements of the vehicle with respect to the lane are available. These measurements are then converted to error measurements of the vehicle with respect to the center of the lane. The objective of the lateral controller is then to control these variables to zero. Figure B-2 shows the error states (denoted as y_e and ψ_e) where the first represents the lateral error of the vehicle with respect to the center of the lane and the latter represents the heading error of the vehicle with respect to the direction of the lane. The lane is described using the notion of curvature [8] defined as a constant κ representing the inverse of the radius of the lane (defined as unit m^{-1}). Using the geometrical model of the vehicle from Figure B-2 the equations of motion of the error states can be defined [33]. Let the heading error be given as

$$\psi_e = \psi_L - \psi,$$

where ψ_L is the heading of the lane with respect to the global coordinate frame O. The time-derivative can therefore be defined as

$$
\begin{aligned}
\dot{\psi}_e &= \dot{\psi}_L - \dot{\psi},\\
&= V_x\kappa - \dot{\psi}.
\end{aligned} \tag{B.9}
$$

The second derivative of the lateral error y_e can be defined as

$$\ddot{y}_e = \dot{V}_{y,L} - \dot{V}_y,$$

$$\begin{aligned}&=V_x^2\kappa - (\dot{V}_y + V_x\dot{\psi}),\\ &=-\dot{V}_y + V_x(\dot{\psi}_L - \dot{\psi}).\end{aligned}$$

Assuming that the longitudinal velocity is constant, we find

$$\dot{y}_e = -V_y + V_x\psi_e, \tag{B.10}$$

hence giving a set of linear differential equations for the camera model. The bank angle as shown in Figure 4-2 introduces a lateral force on the center of gravity of the vehicle. Hence, in the lateral force equilibrium (B.5b), an additonal lateral force, F_b, is acting on the vehicle

$$\begin{aligned}m(\dot{V}_y + \dot{\psi}V_x) &= F_{y,f} + F_{y,r} + F_b,\\ &= F_{y,f} + F_{y,r} + mg\sin(\phi),\end{aligned} \tag{B.11}$$

where ϕ represents the banking angle of the road and thus of the vehicle and g represents the gravitational coefficient. Finally, recall the the fault model as introduced in (1.3)

$$\delta = f_m\delta_{set} + f_a.$$

Substitution of steering angle δ in (B.8) with the fault description shows the appearance of the faults in the lateral dynamics. Now, the new error states y_e (B.10) and ψ_e (B.9), the new found disturbances κ (B.9) and $\sin(\phi)$ (B.11) and the faults f_m and f_a can be augmented in (B.8) to form the total linear state-space form of the linearized system under investigation

$$\underbrace{\begin{bmatrix}\dot{V}_y\\ \ddot{\psi}\\ \dot{y}_e\\ \dot{\psi}_e\end{bmatrix}}_{\dot{X}} = \underbrace{\begin{bmatrix}\frac{C_f+C_r}{mV_x} & \frac{C_f l_f - C_r l_r}{mV_x} - V_x & 0 & 0\\ \frac{l_f C_f - l_r C_r}{V_x I_z} & \frac{l_f^2 C_f + l_r^2 C_r}{V_x I_z} & 0 & 0\\ -1 & 0 & 0 & V_x\\ 0 & -1 & 0 & 0\end{bmatrix}}_{A}\underbrace{\begin{bmatrix}V_y\\ \dot{\psi}\\ y_e\\ \psi_e\end{bmatrix}}_{X} + \underbrace{\begin{bmatrix}\frac{-C_f}{m}\\ \frac{-l_f C_f}{I_z}\\ 0\\ 0\end{bmatrix}}_{B}(f_m\delta_{set} + f_a) + \underbrace{\begin{bmatrix}0 & g\\ 0 & 0\\ 0 & 0\\ V_x & 0\end{bmatrix}}_{B_d}\underbrace{\begin{bmatrix}\kappa\\ \sin(\phi)\end{bmatrix}}_{d}, \tag{B.12a}$$

$$y = \underbrace{\begin{bmatrix}0 & 1 & 0 & 0\\ 0 & 0 & 1 & 0\\ 0 & 0 & 0 & 1\end{bmatrix}}_{C}\underbrace{\begin{bmatrix}V_y\\ \dot{\psi}\\ y_e\\ \psi_e\end{bmatrix}}_{X}. \tag{B.12b}$$

This vehicle model is an LTI state-space model. As proposed in [33], given that the longitudinal velocity is slowly time-varying, it can also be used as a LPV state-space model.

Appendix C

Experimental Validation Parameters

In this appendix the testing matrix and the model- and filter parameters for the experimental validation Chapter 5 are given. Using these parameters, the experimental results have been created. Table C-1 shows the testing matrix with the longitudinal velocities at which the vehicle is driven and the faults that are manually injected.

Test no.	Velocity $[\mathrm{km} \cdot \mathrm{h}^{-1}]$	f_a [deg]	f_m [-]
1	30	0	0
2	30	0.2	0
3	30	0	0.8
4	30	0.2	0.8
5	$30 \rightarrow 40$	0.2	0.8

Table C-1: Test matrix for the experimental results in Chapter 5.

Table C-2 shows the filter parameters used for each of the tests from Table C-1. The filter parameters include the pole location of the low-pass filter, the input delay and the output delay.

Test no.	a_0	a_1	b_0	b_1	c_0	c_1	δ_{set} delay	ψ_e, y_e delay	Filter degree
1	0.02	-0.98	0.05	-0.95	0.05	-0.95	$10 \cdot h$	$15 \cdot h$	31
2	0.03	-0.97	0.05	-0.95	0.05	-0.95	$10 \cdot h$	$15 \cdot h$	31
3	0.03	-0.97	0.05	-0.95	0.05	-0.95	$10 \cdot h$	$15 \cdot h$	31
4	0.03	-0.97	0.05	-0.95	0.05	-0.95	$10 \cdot h$	$15 \cdot h$	31
5	0.04	-0.96	0.05	-0.95	0.05	-0.95	$10 \cdot h$	$15 \cdot h$	31

Table C-2: Filter parameters for the experimental results in Chapter 5 (h=0.01).

The polynomial coefficients a_0, a_1 (5.1) belong to the filter of the yaw rate measurement $\dot{\psi}$, the coefficients b_0, b_1 belong to the filter of the measurement of ψ_e and finally the coefficients c_0, c_1 belong to filter on the measurement of y_e.

Bibliography

[1] M. Peden, R. Scurfield, D. Sleet, D. Mohan, and A. Hyder, "World report on road traffic injury prevention," World Health Organization Geneva, Tech. Rep., 2004.

[2] M. S. Young and N. A. Stanton, "What's skill got to do with it? Vehicle automation and driver mental workload," *Ergonomics*, vol. 50, no. 8, pp. 1324–1339, 2007.

[3] D. Adminaite, T. Calinescu, G. Jost, H. Stipdonk, and H. Ward, "Ranking EU progress 12th Road Safety Performance Index Report," no. June, 2018.

[4] S. Oncu, J. Ploeg, N. Van De Wouw, and H. Nijmeijer, "Cooperative adaptive cruise control: Network-aware analysis of string stability," *IEEE Transactions on Intelligent Transportation Systems*, vol. 15, no. 4, pp. 1527–1537, 2014.

[5] NHTSA, "Automated Vehicles for Safety." [Online]. Available: https://www.nhtsa.gov/technology-innovation/automated-vehicles-safety

[6] SAE, "J3016- Taxonomy and Definitions for Terms Related to Driving Automation Systems for On-Road Motor Vehicles." [Online]. Available: https://saemobilus.sae.org/content/j3016{_}201401

[7] J. Kosecka, R. Blasi, C. Taylor, and J. Malik, "A comparative study of vision-based lateral control strategies for autonomous highway driving," *Proceedings. 1998 IEEE International Conference on Robotics and Automation*, vol. 3, no. May, pp. 1903–1908, 1998.

[8] A. Schmeitz, J. Zegers, J. Ploeg, and M. Alirezaei, "Towards a generic lateral control concept for cooperative automated driving theoretical and experimental evaluation," *IEEE International Conference on Models and Technologies for Intelligent Transportation Systems*, pp. 134–139, 2017.

[9] G. Zhang, H. Zhang, X. Huang, J. Wang, H. Yu, and R. Graaf, "Active Fault-Tolerant Control for Electric Vehicles with Independently Driven Rear In-Wheel Motors Against Certain Actuator Faults," *IEEE Transactions on Control Systems Technology*, vol. 24, no. 5, pp. 1557–1572, 2016.

[10] H. Noura, D. Theilliol, J.-C. Ponsart, and A. Chamseddine, *Fault-tolerant Control System Design and Practial Applications*. Springer Science & Business Media, 2009.

[11] R. Isermann, "Supervision, fault-detection and fault-diagnosis methods: An introduction," *Control engineering practice*, vol. 5, no. 5, pp. 639–652, 1997.

[12] ——, "Model-based fault-detection and diagnosis, status and applications," *Annual Reviews in control*, vol. 29, pp. 71–85, 2005.

[13] B. Friedland, "Treatment of Bias in Recursive Filtering," *IEEE Transactions on Automatic Control*, vol. AC-14, no. 4, pp. 359–367, 1969.

[14] Z. Li, E. Mazars, Z. Zhang, and I. M. Jaimoukha, "State–space solution to the H-/H-infty fault-detection problem," *International Journal of Robust and Nonlinear Control*, vol. 22, no. 3, pp. 282–299, 2012.

[15] D. N. Shields, "Robust fault detection for generalized state space systems," in *Control, 1994. Control'94. International Conference on*, no. 389. IET, 1994, pp. 1335–1349.

[16] R. V. Beard, "Failure accomodation in linear systems through self-reorganization." Tech. Rep. Massachusetts Institute of Technology, 1971.

[17] T. Höfling and R. Isermann, "Fault detection based on adaptive parity equations and single-parameter tracking," *Control Engineering Practice*, vol. 4, no. 10, pp. 1361–1369, 1996.

[18] E. M. Cimpoesu, B. D. Ciubotaru, and D. Stefanoiu, "Fault Detection and Diagnosis Using Parameter Estimation with Recursive Least Squares," *2013 19th International Conference on Control Systems and Computer Science*, pp. 18–23, 2013.

[19] T. G. Park, K. S. Lee, and J. S. Ryu, "Actuator fault estimation with disturbance decoupling," *IEEE Proceedings - Control Theory and Applications*, vol. 147, no. 5, pp. 501–508, 2000.

[20] E. Frisk, M. Krysander, and J. Åslund, "Sensor placement for fault isolation in linear differential-algebraic systems," *Automatica*, vol. 45, no. 2, pp. 364–371, 2009.

[21] P. Mohajerin Esfahani and J. Lygeros, "A Tractable FDI Approach for Nonlinear Systems with Probabilistic Performance," *IEEE Transactions on Automatic Control*, vol. 9286, no. 257005, pp. 1–25, 2014.

[22] A. Varga, *Solving Fault Diagnosis Problems*. Springer, 2017, vol. 84.

[23] E. Frisk and M. Nyberg, "Residual generation for fault diagnosis of systems described by general linear differential-algebraic equations," *IFAC Proceedings Volumes (IFAC-PapersOnline)*, vol. 15, no. 1, pp. 137–142, 2002.

[24] P. A. Ioannou and J. Sun, "Robust Adaptive Control," *N/a*, vol. N/A, no. TFRT-1035, p. 825, 1996.

[25] G. Kreisselmeier, "Adaptive Observers with Exponential Rate of Convergence," *IEEE Transactions on Automatic Control*, vol. 22, no. 1, pp. 2–8, 1977.

[26] G. Zhang, H. Zhang, J. Wang, H. Yu, X. Wang, R. Graaf, and J. Doering, "Fault-type identification and fault estimation of the active steering system of an electric vehicle in normal driving conditions," vol. 231, no. 12, pp. 1679–1692, 2017.

[27] Y. Chen, K. L. Moore, J. Yu, and T. Zhang, "Iterative learning control and repetitive control in hard disk drive industry-a tutorial," *Decision and Control, 2006 45th IEEE Conference on Automatic Control*, vol. 22, no. 4, pp. 2338—-2351, 2006.

[28] J. S. Im, F. Ozaki, T. K. Yeu, and S. Kawaji, "Model-based fault detection and isolation in steer-by-wire vehicle using sliding mode observer," *Mechanical Science and Technology*, vol. 23, pp. 1991–1999, 2009.

[29] J. Zhang, Hui and Wang, "Active steering actuator fault detection for an automatically-steered electric ground vehicle," *IEEE Transactions on Vehicular Technology*, vol. 66, no. 5, pp. 3685–3702, 2017.

[30] R. Toth, H. S. Abbas, and H. Werner, "On the state-space realization of lpv input-output models: Practical approaches," *IEEE Transactions on Control Systems Technology*, vol. 20, no. 1, pp. 139–153, 2012.

[31] H. B. Pacejka, *Tire Characteristics and Vehicle Handling and Stability*. Elsevier, 2012.

[32] Rijkswaterstaat, "Richtlijn Ontwerp Autosnelwegen 2014," Tech. Rep., 2015.

[33] R. Rajamani, *Vehicle Dynamics and Control*. Springer Science & Business Media, 2011.

[34] R. R. Bitmead, "Persistence of Excitation Conditions and the Convergence of Adaptive Schemes," *IEEE Transactions on Information Theory*, vol. 30, no. 2, pp. 183–191, 1984.

[35] Gurobi Optimization LLC, "Gurobi Optimizer reference manual," 2018. [Online]. Available: www.Gurobi.com

[36] R. Toth, *Modeling and identification of linear parameter-varying systems*. Springer, 2010, vol. 403.

[37] M. Verhaegen and V. Verdult, *Filtering and System Identification, A Least Squares Approach*. Delft: Cambridge University Press, 2007.

[38] J. Craens and N. Das, "Taking over the steering of a toyota prius using the electric steering motor," Fontys, Tech. Rep., 2014.

[39] Hasan Khalil, "Nonlinear Systems - Third Edition," *Journal of Climate J Clim Vol 18*, 2002.

[40] S. X. Ding, *Model-based fault diagnosis techniques: design schemes, algorithms, and tools*. Springer Science & Business Media, 2008.

[41] I. O. M. A. E. E. Hassanain, "String-stable automated steering in cooperative driving applications," TU Delft, Tech. Rep.